MULTIPARTITE ENTANGLEMENT ENGINEERING FOR QUANTUM INFORMATION AND METROLOGY

A Dissertation

by

YUSEF MALEKI

Submitted to the Office of Graduate and Professional Studies of
Texas A&M University
in partial fulfillment of the requirements for the degree of

DOCTOR OF PHILOSOPHY

Chair of Committee,	Aleksei Zheltikov
Committee Members,	M. Suhail Zubairy
	Philip Hemmer
	Alexei Sokolov
Head of Department,	Girgory Rogachev

August 2020

Major Subject: Physics

ABSTRACT

Quantum entanglement is central to many quantum technologies and is an indispensable ingredient of quantum information theory. These facts make the generation, characterization and quantification of entangled states unavoidable tasks, beside all their fundamental significance. As a particular example of such applications one may consider quantum metrology in which quantum entanglement is shown to have a significant role for beating the classical limits. However, generation, characterization and quantification of suitable entangled states are challenging tasks, in general.

In this dissertation, we introduce new platforms for engineering multipartite entangled states that are shown to be useful for quantum information processing and quantum metrology applications. In particular, we introduce new methods which can be used for generating N00N states, as one of the most challenging states to generate, enabling realization of such states in both photonic and spintronic architectures. We sketch a rather generic quantum circuit, for the N00N state generation, that could be realized in various quantum systems. Furthermore, we extend the platform for the generation of states beyond the N00N state. Typical examples of such sates could be entangled coherent or squeezed states, for instance, that of specific importance for quantum information and metrology applications. Furthermore, we extend the protocol for the multipartite state scenario. Also, we demonstrate that attaining the ultimate sensitivity in phase estimation is not an exclusive property of the N00N states. As a result, we find a large class of entangled states that could provide us with the ultimate sensitivity achieved by the N00N state.

As a part of our effort for the N00N state generation, we develop a new scheme where N00N states could be realized in two ensembles of nitrogen–vacancy (NV) centers in diamond. This could be interesting by noting the fact that NV centers in diamonds provide a remarkably long coherence time, even at the room temperature. This opens up new possibilities for protecting N00N states against decoherence.

Moreover, having the long coherence time of the ensembles of the NV centers, we show that a

hybrid quantum system consisting of three ensembles of NV centers coupled to a superconducting device enables the generation of controllable macroscopic multipartite entangled states, which could be used as a building block for quantum networks.

Furthermore, we investigate entanglement of nonorthogonal states in details, and more specifically, we obtain a closed-form analytical expression for the entanglement degree of a multipartite qutrit state, that offers a quantitative measure for entanglement n-mode nonorthogonal qutrit states with an arbitrary n. Such higher dimensional entangled states could be useful in quantum communication protocols.

Finally, we introduce a new configuration where any pair of quantum states can perfectly be swapped between two quantum resonators enabling a realization of a universal swap operation in photonics systems. This can serve as a building block of various quantum information processors.

DEDICATION

To my mother and my father.

ACKNOWLEDGMENTS

First and foremost, I would like to thank my supervisor, Aleksei Zheltikov, for all of his support, guidance and help.

Special thanks to Suhail Zubairy, Philip Hemmer and Alexei Sokolov for accepting to be my committee members. I really appreciate their feedback on my work and the assistance they provided.

I am grateful to David Lee, Marlan Scully and Girish Agarwal for many discussions on various topics and for the insights they provided.

During my Ph.D. I had the privilege to enjoy discussions on physics and beyond with numerous colleagues and friends which I thank them all.

Last but not least, I would like to thank my family for their endless love. My parents always inspire me, give me hope and joy. My siblings have supported me, in many ways, for which I am deeply grateful. I also express my love to my beautiful nieces and nephews.

CONTRIBUTORS AND FUNDING SOURCES

Contributors

This work was supported by a dissertation committee consisting of Professor Aleksei Zheltikov, Professor M. Suhail Zubairy, Professor Philip Hemmer and Professor Alexei Sokolov of Texas A&M University.

All work conducted for the dissertation was completed by Yusef Maleki independently.

Funding Sources

Graduate study was supported by a fellowship and funding from Texas A&M University and funding from Welch Foundation.

TABLE OF CONTENTS

Page

LIST OF FIGURES

FIGURE Page

1. INTRODUCTION

1.1 Introduction

Quantum entanglement is a peculiar characteristics of quantum mechanics, whereby a quantum system can manifest very perplexing physical effects which cannot be observed in the classical systems [1–3]. Since quantum entanglement has been found to be a vital resource for employing quantum applications [1–6], there has been a lot of interest in the study of entanglement and its characteristics. In fact, it is considered as the cornerstone of various quantum information processing applications such as quantum cryptography and quantum computing [2, 3, 7, 8]. Considering the fact that these applications mainly require entangled states, detection, classification and quantification of entanglement of the quantum states are not only interesting from the fundamental perspective, but also of profound practical importance [9–14]. Quantification of entanglement is also important for characterization of a successful preparation of a quantum state in the experiments [15, 16]. However, this is still an arduous task in general, and entanglement of the states involving higher-dimensional multi-partite system states are not fully understood yet, and a physically motivated measure that could be utilized in order for quantifying entanglement of a generic quantum system is not known yet [9, 11–13, 17].

One of the most interesting areas that quantum entanglement could be found useful is the notion of quantum metrology. In fact, quantum entanglement can provide profound implications on metrology and parameter estimations, from both fundamental and practical perspectives. It is quite well-known that estimating an unknown parameter is central in many areas of science and is of utmost importance in improvements in technology [18]. Therefore, it is not surprising that attaining the best possible accuracy of a target parameter is an important goal of parameter estimation [19–21]. One way of improving the accuracy of an estimation is by repeating the experiment and collecting more and more information on the parameter. More precisely, using N independent resources, for measuring the parameter φ, the optimal sensitivity of the parameter is

determined by the central limit theorem and scales as $\Delta\varphi \propto \frac{1}{\sqrt{N}}$. This is called the shot-noise limit or the standard quantum limit [19].

In the parameter estimation scenario, quantum physics provides an intriguing capability that cannot be realized in the classical realm [22–24]. In fact, using quantum resouses the precision limit can be significantly improved such that it can saturate the fundamental limit that is allowed by the quantum mechanics, enabling the estimation error of $\Delta\varphi \propto \frac{1}{N}$. This fundamental limit is known as the Heisenberg Limit (HL). This limit provides the best acheveable precision that is permitted by the quantum mechanics for a given N [25].

It is quite well-known that the entangled state of the form $\frac{1}{\sqrt{2}}(|N\rangle \otimes |0\rangle + |0\rangle \otimes |N\rangle)$, which is called N00N state, can fulfill the Heisenberg limit precision. This state, however, is extremely difficult to generate and is fragile to decoherence [25]. These difficulties are apparent by noting the fact that generation of the photonic N00N state has not been exceeded $N = 5$, which was realized in a microwave photons in a circuit QED based structure [26]. Hence, developing new platforms where the robustness of the N00N state generations could be improved is a very important task; albeit, it seems to be anything but trivial.

Throughout this dissertation, we are going to provide ways to generate various entangled states for quantum metrology and quantum information applications. We shall generate states in photonic systems based on cavity QED schemes and in ensembles of nitrogen–vacancy centers in diamonds.

One important feature of NV ensembles is the capability for being integrated with different physical systems which allows manipulation of various hybrid systems with desired applications [27, 28], as the spins in NV centers are capable of being coherently coupled to both optical and microwave fields [27, 28]. Recently, various hybrid systems including NV centers in diamonds and superconducting devices such as flux qubits and resonator have attracted a remarkable interest due to their promising potential for quantum information and computation applications as well as considering the fundamental futures of quantum mechanics [27, 29]. Such a hybrid architecture is capable of utilizing the advantages of both NV centers and superconducting elements.

We show that a hybrid quantum system consisting of three ensembles of NV centers coupled

to a superconducting device enables the generation of controllable macroscopic multipartite entangled states, which could be used as a building block for quantum networks. The key feature in using NV ensemble rather than a single NV center is that the coupling strength of an individual NV center coupled to a superconducting coplanar waveguide resonator (CPWR) is at the range just few a few Hz [30], which is far below the dissipation rate of CPWR; however, the collective coupling strength between an NV centers ensemble of N_0 spins enhances by a factor of $\sqrt{N_0}$ compared to the coupling strength of a single spin [30, 31], that overcomes the undesirability of a single NV center for the coherent exchange of quantum information.

Furthermore, we investigate entanglement of nonorthogonal states in details, and more specifically, we obtain a closed-form analytical expression for the entanglement degree of a multipartite qutrit state, that offers a quantitative measure for entanglement n-mode nonorthogonal qutrit states with an arbitrary n. Such higher dimensional entangled states could be useful in quantum communication protocols.

Finally, we introduce a new configuration where any pair of quantum states can perfectly be swapped between two quantum resonators enabling a realization of a universal swap operation in photonics systems. This can serve as a building block of various quantum information processors.

2. ENTANGLED STATE GENERATION FOR QUANTUM METROLOGY AND PHASE ESTIMATION: N00N STATE AND BEYOND [1]

2.1 Introduction

In the parameter estimation scenario, quantum physics provides an intriguing capability that cannot be realized in the classical realm [22–24]. In fact, using quantum resources the precision limit can be significantly improved such that it can saturate the fundamental limit that is allowed by the quantum mechanics, enabling the estimation error of $\Delta\varphi \propto \frac{1}{N}$, with N as the number of the available resources, such as number of the photons. This fundamental limit is known as the Heisenberg Limit (HL). This limit provides the best achievable precision that is permitted by the quantum mechanics for a given N [25]. It is quite well-known that the entangled state of the form

$$\frac{1}{\sqrt{2}}(|N\rangle \otimes |0\rangle + |0\rangle \otimes |N\rangle),$$

which is called N00N state, can fulfill the Heisenberg limit precision. This state, however, is extremely difficult to generate and is fragile to decoherence [25].

One of the simplest methods to generate photon entanglement is simply feeding the photon to a beam splitter (BS). If we feed one port of the beam splitter with a single photon having the state $|1\rangle$ and the other port of it with the vacuum state $|0\rangle$, we immediately get a N00N state with $N = 1$ (1001 state) [see Fig. 2.1 (a)]. Now, it is natural to think of replacing the single photon in the input state of the beam splitter with N photons given by $|N\rangle$. However, the resultant state

[1] This chapter is partly based on the following journal publications with the permission: (i) Reprinted with permission from "Generating maximally-path-entangled number states in two spin ensembles coupled to a superconducting flux qubit" by Yusef Maleki, Aleksei Zheltikov, 2018 *Phys. Rev. A* **97** 012312, Copyright [2020] by The American Physical Society. (ii) Reprinted with permission from "A high-N00N output of harmonically driven cavity QED" by Yusef Maleki, Aleksei Zheltikov, 2019 *Scientific Reports* **9** 16780, Copyright [2020] by The SpringerNatur, licensed under the Creative Commons Attribution 4.0 International License http://creativecommons.org/licenses/by/4.0/ . (iii) Reprinted with permission from "Spin cat-state family for Heisenberg-limit metrology" by Yusef Maleki, Aleksei Zheltikov, 2020 *J. Opt. Soc. Am. B* **37** 1021-1026, Copyright [2020] by The Optical Society (OSA). (iv) Reprinted with permission from "Recovery of maximally entangled quantum states by weak-measurement reversal" by Yusef Maleki, Aleksei Zheltikov, 2018 *Laser Physics Letters* **15** 056201, Copyright [2020] by Astro Ltd. .

is not a N00N state anymore, and it contains a superposition of other possibilities in the output state. The, N00N state with $N = 2$ is also easy to generate with the use of beam splitter. In this case, we need to feed both ports of the beam splitter with a single photon having the state $|1\rangle$, where the output of this process immediately provides the $N = 2$, N00N state of the form $\frac{1}{\sqrt{2}}(|2\rangle \otimes |0\rangle + |0\rangle \otimes |2\rangle)$. However, it turns out that generation of N00N states for $N > 2$, becomes a challenging problem. Generation of such an state is fundamentally important for not only practical applications but also for understanding the underlying quantum nature and capability of the system. That being said, engineering other types of entangled states which can break the shot noise limit is also of paramount importance. This importance is stimulated by the difficulty of the N00N state generation, where such states can be used for quantum metrology instead of N00N states. Examples of such states could be entangled coherent states, entangled squeezed states, two-mode squeezed states, etc. One could only consider the recent application of the squeezed light for gravitational wave detection by LIGO [32], to appreciate the importance of such non-classical states.

In this chapter, we are going to introduce new methods for generation of high-N00N states. We will develop novel schemes and techniques that enables the generation of N00N states in a variety of the contexts.

Central to our approach to the high-N00N state generation, is the realization of the effective Hamiltonian of the form

$$H_{\text{eff}} = i\kappa(a_1 a_2^\dagger - a_2 a_1^\dagger)\sigma_z, \tag{2.1}$$

in which the boson annihilation and creation operators of the first and the second modes are $a_1, a_1^\dagger$ and $a_2, a_2^\dagger$, respectively. These operators could be associated to any harmonic oscillator systems such as photons in the cavity. The qubit operators in this equation, $\sigma_z = |1\rangle\langle 1| - |0\rangle\langle 0|$, $\sigma_+ = |1\rangle\langle 0|$ and $\sigma_- = |0\rangle\langle 1|$ are the Pauli operators, that obey su(2) Lei algebra. Therefore, this Hamiltonian can be considered as a two-level system (qubit) interacting with two bosonic modes such as two modes of the light fields.

As a particular case that will be investigated in this chapter, we are going to demonstrate the

possibility of the generation of a high number N00N state which can be realized using quantum memories of nitrogen-vacancy ensembles (NVE) interacting with a superconducting flux qubit. The prepared state can be stored for a longer time since NVEs have long decoherence time. The lifetime of NV centers has been experimentally realized to exceed $1s$ even at room temperature [33], in contrasts microwave photons in superconducting cavities have lifetimes on the order of $\sim 1ms$ [34]. Therefore, NVEs have the advantage of being used as quantum memories [35]. In contrary to recent approaches [36, 37], our approach does not require step by step operations to increase of the number of excitation in the entangled state. In such treatments, the system is subjected to the decoherence during every single operation step, therefore, the fidelity of large number N00N state creation decreases drastically, by increasing the photon number N [37]. In contrast, we first prepare a large number Fock state and then create entanglement between the NVE memories. It is remarkable that the coupling between the flux qubit and the NV centers is about a factor of 1000 larger than the coupling obtained via cold atoms which is significantly strong [38, 39].

Furthermore, we extend the discussion for generation of entangled states beyond the N00N state. More specifically, we show that integration of a specific configuration of resonator–qubit system followed by a beam splitter can indeed produce a N00N state from the input state. Thus, our scheme mimics the so-called Magic Beam Splitter (MBS) [40] where the injection of N photons from one port of the MBS and keeping the other port in the vacuum state gives a N00N state [see Fig.2.1(b)]. In this platform, the state can be generated fast and efficiently with only a few operational steps. As was mentioned, this quantum beam splitter can generate states beyond the N00N state where it enables us to generate mesoscopic and macroscopic entangled states, such as entangled coherent and squeezed states. We shall show that a large class of maximally entangled states can be achieved in this architecture. Also, we shall show that this approach can be used to generate a wide variety of multi-mode entangled states, including multi-N00N states which can be very important for quantum metrology applications.

Furthermore, we will demonstrate that the ability to attain the HL precision is not an exclusive

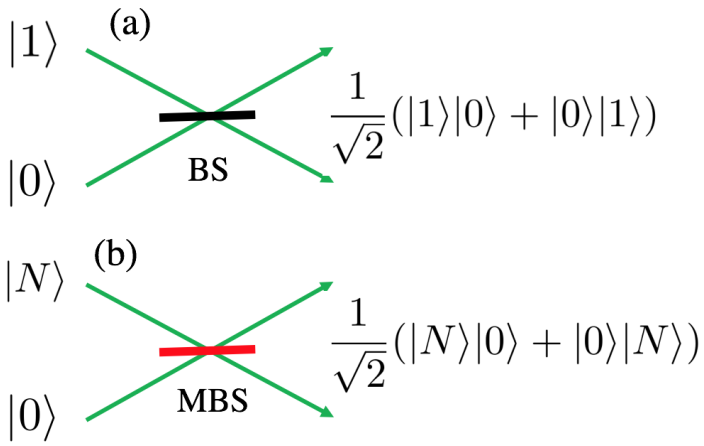

Figure 2.1: Generation of single photon N00N state by injecting the single photon input state from one of the ports to a beam splitter (a), and generation of multiphoton N00N state by injecting the input state N photons from one of the ports to a magic beam splitter (b).

property of N00N states. In fact, we will show that a large class of spin cat states consisting of a superposition of spin coherent states that can result in Heisenberg limit precision measurement. We prove that superposition of any two antipodal points on the Bloch sphere (two antipodal spin coherent state) results in the Heisenberg limit precision which is well known for the so-called N00N state. Therefore, this generalizes the states with Heisenberg limit precision from restricted class of N00N state to a large class of spin cat states (we call spin antipodal cat states). The generalization allows more general ways to produce the states for Heisenberg limit metrology than the restrictive case of N00N state. And clarifies the connection between Heisenberg limit precision and two-mode cat states. We show that some antipodal cat states can be generated in cavity QED structure.

2.2 Quantum circuit for N00N state generation

As was mentioned earlier, central to our approach for the high-N00N state generation, will be derivation of the effective Hamiltonian in Eq. (2.1). For simplicity one can consider two cavity fields interacting with a single qubit. We will provide a detailed derivation of this effective Hamiltonian later; however, it is stimulating to see how such a Hamiltonian results in a generation

of N00N state, starting from N photons in one of the resonators. In fact, we are going to show that, starting from this interaction Hamiltonian one can generate a N00N state in the two modes. To this aim, we consider the qubit to be in the logical superposition state $\frac{1}{\sqrt{2}}(|0\rangle + |1\rangle)$. The first and the second field modes are prepared in the $|0\rangle_1$ and $|N\rangle_2$ Fock states, respectively. Therefore, the initial state of the composed system including the atom and the cavities is thus given by [23]

$$|\psi(0)\rangle = \frac{1}{\sqrt{2}}(|0\rangle + |1\rangle)|0\rangle_1|N\rangle_2.$$

Starting from this initial state we consider the time evolution of the entire system with the effective Hamiltonian above. This implies that, the time evolution operator

$$U(t) = e^{-iH_{\text{eff}}\Delta t/\hbar}$$

should be applied to this initial state, from which we find [23]

$$|\psi(t)\rangle = \frac{1}{\sqrt{2}}(e^{-iH_{\text{eff}}\Delta t/\hbar}|0,N\rangle|0\rangle + e^{-iH_{\text{eff}}\Delta t/\hbar}|0,N\rangle|1\rangle), \tag{2.2}$$

where $|0,N\rangle \equiv |0\rangle_1|N\rangle_2$.

We let the system evolve for the time interval $\Delta t_1 = \pi/(4\Omega)$. This entails the time evolved state $|\psi(t)\rangle$ to degenerate into

$$|\psi\rangle_1 = \frac{1}{\sqrt{2^N}}\sum_{k=1}^{N}\binom{N}{k}^{\frac{1}{2}}|k,N-k\rangle(|0\rangle + (-1)^k|1\rangle). \tag{2.3}$$

We note that in this state, the two fields and the qubit become entangled. The measurement of the first resonator in the state $|k\rangle$ projects the qubit in two orthogonal superposition of the computational basis. Namely, detecting the first resonator in the state with an even k projects the qubit into the state $\frac{1}{\sqrt{2}}(|0\rangle + |1\rangle)$, and with odd k projects the qubit into the state $\frac{1}{\sqrt{2}}(|0\rangle - |1\rangle)$. These two basis are orthogonal. Alternatively, detecting the qubit in these two orthogonal basis provides

information about the k. Similar argument can be made for the second mode.

Next, we apply the Hadamard gate to this state. The Hadamard gate is given by a 2×2 matrix acting on the Hilbert space of a single qubit which is given by

$$\mathcal{H} = \frac{1}{\sqrt{2}} \begin{pmatrix} 1 & 1 \\ 1 & -1 \end{pmatrix}. \tag{2.4}$$

The role of this gate is to rotate the basis of the Hilbert space of the qubit. Hence, applying this gate translates into a local transformation of the qubit basis such that $|0\rangle \rightarrow \frac{1}{\sqrt{2}}(|0\rangle + |1\rangle)$, and $|1\rangle \rightarrow \frac{1}{\sqrt{2}}(|0\rangle - |1\rangle)$. Once the qubit is subjected to the Hadamard gate, we let the system to undergo the time evolution again within the time interval $\Delta t_2 = \pi/(4\Omega)$. With this time evolution the quantum state of the system reduces to $|\psi\rangle_2$, which is explicitly given by

$$|\psi\rangle_2 = \frac{1}{\sqrt{2^N}} \sum_{k=1}^{N} \binom{N}{k}^{\frac{1}{2}} [1 + (-1)^k]|k, N-k\rangle|0\rangle + \frac{1}{\sqrt{2^N}} \sum_{k=1}^{N} \binom{N}{k}^{\frac{1}{2}} [1 - (-1)^k]|k, N-k\rangle|1\rangle. \tag{2.5}$$

Next, we measure the qubit in its computational basis, which projects the field modes into the superposition of the number states. If the outcome of the measurement performed on the qubit gives $|0\rangle$, the wave function of the system collapses to

$$|\psi\rangle_3 = \frac{1}{\sqrt{2^N}} \sum_{k=1}^{N} \binom{N}{k}^{\frac{1}{2}} [1 + (-1)^k]|k, N-k\rangle|0\rangle. \tag{2.6}$$

Clearly, the qubit becomes disentangled from the rest of the system due to the wave function collapse.

Alternatively, if the outcome of the measurement gives $|1\rangle$, then the wave function of the system

collapses to

$$|\psi\rangle_3 = \frac{1}{\sqrt{2^N}} \sum_{k=1}^{N} \binom{N}{k}^{\frac{1}{2}} [1-(-1)^k]|k, N-k\rangle|1\rangle \tag{2.7}$$

Once we measure the state of the qubit, regardless of the outcome of the measurement, we apply the time evolution operator one more time on the collapsed wave function of the system. First, let us assume the outcome of the measurement to be $|0\rangle$. Applying the time evolution operator on the corresponding collapsed wave function, for a time interval $\Delta t = \pi/(4\Omega)$ following the measurement step results in the N00N state

$$|\text{N00N}\rangle = \frac{1}{\sqrt{2}}((-1)^N|N\rangle_1 \otimes |0\rangle_2 + |0\rangle_1 \otimes |N\rangle_2). \tag{2.8}$$

Alternatively, if the outcome of the measurement of the qubit gives $|1\rangle$, then, once we let the system to evolve for a time interval $3\pi/(4\Omega)$, one arrives at the N00N state of the form

$$|\text{N00N}\rangle = \frac{1}{\sqrt{2}}(|N\rangle_1 \otimes |0\rangle_2 - |0\rangle_1 \otimes |N\rangle_2). \tag{2.9}$$

It is worth to note that, regardless of what the outcome of the measurement of the qubit state be, the N00N state can be obtained at the final step of this protocol. This implies the fact that, considering the ideal scenario where, no decoherence is involved and the measurement is perfect, we arrive at the 100% fidelity of N00N state generation from $|\psi\rangle_2$. Therefore, the N00N state generated with this protocol is deterministic. If the measurement yields $|0\rangle$, it takes the system less time to evolve to the N00N state.

It is interesting to note that, once the Fock state $|N\rangle$ is provided, the number of the steps that is needed to arrive at the N00N state is independent of the number of the photons N. Most of the N00N state generation schemes starts from $N = 1$ N00N state and increases the N in several steps. In these schemes, the number of the operations is directly related to the number N, however, in the architecture given in this chapter this may not be the case. This is important as it can provide a better control on decoherence. In fact, once we prepare a high-fidelity Fock state $|N\rangle$, in one of

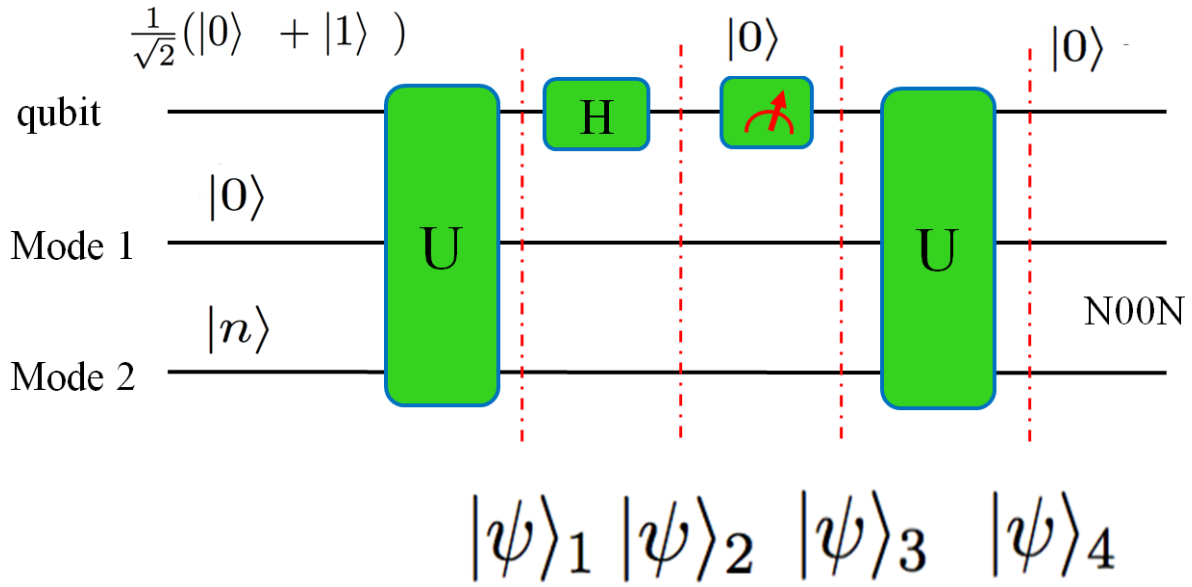

Figure 2.2: N00N state generation circuit: U represents the time evolution of a quantum state, governed by the time-evolution operator with the effective Hamiltonian H_{eff}. $\mathcal{H}$ is the Hadamard gate acting locally on the qubit. For the time interval $\Delta t_1 = \pi/(4\Omega)$, the system evolves from its initial state to $|\psi\rangle_1$. The Hadamard gate yields the state $|\psi\rangle_2$. Once a measurement on the state of the flux qubit is performed, the total wave function of the systems collapses to $|\psi\rangle_3$. finally, time evolution $U(t)$ provides the desired N00N state. (Yusef Maleki and Aleksei M. Zheltikov, 2018)

the modes, without getting the rest of the system involved in the process, we can translate that into a N00N state in just a few operational steps. Thus, this scheme is more robust to decoherence. On the other hand, contrary to most of the proposed protocols, this scheme is simpler and requires less devices. We only need a single qubit which interacts with two modes. The architecture described above, is schematically given in Fig. (2.2) [see [23]].

2.3 Derivation of the effective Hamiltonian

2.3.1 Modulating the coupling between the qubit and the resonators:

We consider a setup of two resonators interacting with a same two-level atom, where the Hamiltonian can be written as a summation of the free part and the interaction part $H = H_0 + H_1$ [40]. We assume that the coupling parameter of the cavity fields and the qubit is periodically modulated.

Therefore, the free part of the Hamiltonian is

$$H_0 = \hbar\frac{\omega_0}{2}\sigma_z + \hbar\omega_1 a_1^\dagger a_1 + \hbar\omega_2 a_2^\dagger a_2,$$

and the interaction part reads

$$H_1 = 2\hbar g_0 \sum_{j=0}^{2} \cos(\upsilon_j t + \varphi_j)(\sigma^+ a_j + a_j^\dagger \sigma^-).$$

Here, ω_0 is the frequency of the two-level energy splitting between its ground and exited levels. ω_1 and ω_2 are the frequencies of the first and the second cavities, respectively. g_0 is the coupling strength of the resonators and the qubit. υ_j is the modulating frequency and φ_j is the modulating phase of the resonator j, with $j = 1, 2$. We consider the resonant case where $\omega_1 = \omega_2 = \omega$ and take $\hbar = 1$, for simplicity. Now, with this Hamiltonian, we are going to extract the effective Hamiltonian of the N00N state that we already discussed. To this aim we define the unitary evolution $U_0(t) = \exp[-iH_0 t]$, using the free part of the the Hamiltonian. Consequently, in the rotating frame the interaction Hamiltonian can be given as

$$H_I = U_0(t) H U_0^{-1}(t) - H_0.$$

The explicit form of the interaction Hamiltonian, thus, reads

$$H_I = \delta\sigma_z/2 + 2g_0 \sum_{j=1}^{2} \cos(\upsilon_j t + \varphi_j)(\sigma^+ a_j + a_j^\dagger \sigma^-),$$

where we have $\delta = \omega_0 - \omega$. If we express the $\cos(\upsilon_j t + \varphi_j)$ term as an exponential form, the Hamiltonian equivalently can be expressed as

$$H_I = \delta\sigma_z/2 + g_0 \sum_{j=1}^{2} [(\sigma^+ a_j + a_j^\dagger \sigma^-)e^{i\varphi_j}]e^{i\upsilon_j t} + [(\sigma^+ a_j + a_j^\dagger \sigma^-)e^{-i\varphi_j}]e^{-i\upsilon_j t}.$$

This Hamiltonian has two parts which is related to the time dependent terms $e^{i\upsilon_j t}$ and $e^{-i\upsilon_j t}$, re-

spectively. Therefore, we define the operator h_j such that

$$h_j = g_0(\sigma^+ a_j + a_j^\dagger \sigma^-)e^{i\varphi_j}.$$

With this definition the Hamiltonian reduces to

$$H_I = \delta\sigma_z/2 + \sum_{j=1}^{2} h_j^\dagger e^{i\upsilon_j t} + h_j e^{-i\upsilon_j t}.$$

This is a Floquet Hamiltonian [44–47], which will enable us to further reduce the Hamiltonian to attain the effective Hamiltonian of the desire.

Without loss of generality, we consider the same modulation frequencies $\upsilon_j = \upsilon$ in the following. Also we note that h_j commutes with its Hermitian conjugate part, such that $[h_j, h_j^\dagger] = 0$. With these considerations, the effective Hamiltonian reduces to

$$H_{\text{eff}} = \delta\sigma_z/2 + i\frac{2g_0^2}{\upsilon}\sin(\varphi_1 - \varphi_2)(a_1 a_2^\dagger - a_2 a_1^\dagger)\sigma_z.$$

Thus, the coupling strength of the Hamiltonian can be directly controlled by the modulation phase factor of each cavity. To maximize the coupling strength in the Hamiltonian we take $\varphi_1 - \varphi_2 = \pi/2$, and define $\kappa = \dfrac{2g_0^2}{\upsilon}$, where the Hamiltonian can be expressed as

$$H_{\text{eff}} = \delta\sigma_z/2 + i\kappa\sigma_z(a_1 a_2^\dagger - a_2 a_1^\dagger). \tag{2.10}$$

Taking the resonance case $\delta = 0$, we attain the desired Hamiltonian of the system as

$$H_{\text{eff}} = i\kappa\sigma_z(a_1 a_2^\dagger - a_2 a_1^\dagger). \tag{2.11}$$

It is remarkable that, the term $\sin(\varphi_1 - \varphi_2)$ controls the coupling strength of the scheme, here. Therefore, it is highly important to have a precise control on the modulation of the system in practical scenarios. It is clear that when the modulation phases are identical, the term $\sin(\varphi_1 - \varphi_2)$

becomes zero, and no effective Hamiltonian can be attained in this case.

The maximum coupling is determined by the term $\kappa = \frac{2g_0^2}{\upsilon}$. Therefore, even though the modulation frequency υ, must be larger enough compared to the parameter g_0, however, if we choose it to be very large, the coupling constant of the effective Hamiltonian may be small. Hence, we need to be careful to satisfy the strong coupling regime when choosing the modulation frequency. Specifically, if we take $\upsilon = 2g_0$, the coupling strength of about $\kappa = g_0/2$, can be achieved.

2.3.2 Modulating the frequencies of the resonators:

We showed that the effective Hamiltonian of our system can be realized in setup of two resonators interacting with the same two level qubit by an specific modulation of the coupling of the system. Now, we are going to show that such a Hamiltonian can be achieved with an slightly different approach. In this case, we are going to consider the same setup of two resonators interacting with the same qubit, where, alternatively the resonators are modulated with the frequencies given by [23, 40, 41]

$$\nu_j(t) = \nu + \Delta \sin(\nu_d t - \varphi_j).$$

In this scenario, the frequencies of the resonators are modulated, with the same frequencies but different phases. The frequency of the qubit is constant and no modulation is applied on that. Therefore, we can express the Hamitonian of the system as

$$H \;=\; \hbar\frac{\omega_0}{2}\sigma_z \;+\; \hbar\nu_1(t)a_1^\dagger a_1 \;+\; \hbar\nu_2(t)a_2^\dagger a_2 \;+\; \hbar g_\nu \;(\sigma^+ a_1 \;+\; a_1^\dagger\sigma^- \;+\; \sigma^+ a_2 \;+\; a_2^\dagger\sigma^-). \quad (2.12)$$

Here, g_ν is the coupling constant of the atom to the resonators. Also, $\nu_1(t)$ and $\nu_2(t)$ are the frequencies of the resonators which are time dependent through the modulation term above. From this Hamiltonian one can derive the interaction Hamiltonian of the system. Thus, in the framework of the rotating wave approximate when $\omega_0 = \nu$ the total Hamiltonian of the system above can be simplified as

$$H_I = \hbar g_\nu \sigma^+ (\hat{a}_1 e^{i\zeta\cos(\nu_d t - \varphi_1)} + \hat{a}_2 e^{i\zeta\cos(\nu_d t - \varphi_2)}) + h.c.,$$

where $\zeta = \Delta/\nu_d$.

This Hamiltonian can be reduced to a Floquet Hamiltonian by using the identity [44, 45]

$$e^{i\zeta\cos(\nu_d t+\varphi_j)} = \sum_{n=-\infty}^{\infty} J_n(\zeta)e^{in(\nu_d t+\varphi_j)},$$

where $J_n(\zeta)$ is the nth-order Bessel function of the first kind. Inserting this in the Hamiltonian above enables us to write the Hamiltonian in the form of a Floquet Hamiltonian which can be expressed as

$$H_I = H_0 + \sum_{n=1}^{\infty} H_n e^{in\nu_d t},$$

where the time-independent part of the Hamiltonian is expressed in terms of the 0th-order Bessel function of the first kind in the above expansion which reads

$$H_0 = \hbar g J_0(\zeta)(\sigma^+(\hat{a}_1 + \hat{a}_2) + (\hat{a}_1^\dagger + \hat{a}_2^\dagger)\sigma^-)$$

and the time-dependent part of the Hamiltonian is expressed in terms of the nth-order Bessel function where we can write

$$H_n = \hbar g i^n J_n(\zeta)[(\sigma^+\hat{a}_1 + (-1)^n\hat{a}_1^\dagger\sigma^-)e^{in\varphi_1} + (\sigma^+\hat{a}_2 + (-1)^n\hat{a}_2^\dagger\sigma^-)e^{in\varphi_2}].$$

The interaction Hamiltonian of this form can be reduced to the effective Hamiltonian, for which we have

$$H_{\text{eff}} = H_0 + \sum_{n=1}^{\infty}[H_n, H_{-n}]/(n\hbar\nu),$$

This is key to obtain the desired effective Hamiltonian that we seek for. Therefore, with an straightforward calculation the Hamiltonian can be written as

$$H_{\text{eff}} = \hbar g J_0(\zeta)(\sigma^+(\hat{a}_1 + \hat{a}_2) + h.c.) + i\hbar\Omega(\hat{a}_1^\dagger\hat{a}_2 - \hat{a}_1\hat{a}_2^\dagger)\sigma_z.$$

In this equation, $\Omega = g^2\chi/\nu$ is the coupling coefficient which depends on g^2 and ν similar to the

previous scheme. In this relation the parameter χ is determined through

$$\chi = \sum_{n=1}^{\infty} 2J_n(\zeta)^2 \sin(n(\varphi_1 - \varphi_2))/n.$$

It is evident that when the modulation phases are identical, this parameter becomes zero and we cannot attain the desired Hamiltonian, hence the modulation phases play a crucial role in this scenario. To improve the coupling of the system, we need to optimize the parameter χ, which provides a direct strategy to control the overall coupling of the system.

We specifically choose $\zeta = 2.40$ ($J_0(2.40) = 0$) and $\varphi_2 \neq \varphi_1$ to derive the effective Hamiltonian [23, 40, 41]

$$H_{\text{eff}} = i\hbar\Omega(\hat{a}_1^\dagger \hat{a}_2 - \hat{a}_1 \hat{a}_2^\dagger)\sigma_z \tag{2.13}$$

To maximize the effective coupling coefficient of the Hamiltonian Ω, one can maximize χ through controlling the phase difference $\varphi_1 - \varphi_2$. If we choose $\varphi_1 - \varphi_2 = \pi/3$, we will obtain $\chi \approx 0.628$.

The effective Hamiltonian can be realized in different quantum platforms. In particular, one can couple two superconductor resonators to the same qubit. In this case the coupling strength between the the resonators and the qubit can be hundreds of MHz. With such a strategy, one is able to strongly couple the resonators to the qubit and obtain the desired Hamiltonian. Therefore, in such a setup, one can effectively realize N00N state shared within the two resonators following the quantum circuit which was already discussed in a great details. As was already noted such an strategy provides a robust platform for realizing N00N states, with a high number of photons. Since Fock state with 15 microwave photons has already been generated in the lab, and generation of the Fock states with about 20 photons seems quite feasible, the platform described here can be useful for breaking the existing limitations of the N00N state generation.

Even though generation of such a N00N state with the method that has already investigated above, seems quite pleasing, we show that the main Hamiltonian can be realized in spin systems as well. In particular, we are interested in generation of the N00N state in nitrogen vacancy centers in diamond. This can provide many advantages considering the long coherence time of the diamonds,

which enables to overcome the decoherence problem of the N00N state generation as the main challenge of this state. Furthermore, since NVEs are very good candidates for quantum memories, generation of such states can be of particular importance as it enables us to preserve the generated N00N states for the sufficiently long period of time. Therefore, in the following we are going to describe this architecture in details.

2.3.3 N00N state in nitrogen vacancy centers in diamond

Now, we are going to show that N00N states can be generated in NVEs in diamond, based on the Ref. [23]. The scheme of the N00N state generation is following the same N00N state generation circuit. Thus, we are going to sketch a scenario where a similar effective Hamiltonian can be extracted for NVEs interacting with a qubit.

In this platform, we investigate a quantum architecture consisting of two separate noninteracting NVEs in diamond coupled to a common superconducting qubit. As a part of this architecture, we consider a large and gap-tunable flux qubit [Fig.2.3(a)] [38, 48]. Such a hybrid scheme combines the long coherence time of spins in NV centers, the advantage of controlling NV centers by microwave and optical fields [42, 43], the tunability property of superconducting devices, the circuit scalability, and the remarkable compatibility with the cutting-edge nanotechnologies [38, 48]. It is notable that, even though microwave photons in superconducting resonators provide a unique platform for N00N state generation which was mentioned earlier, unlike microwave photons in superconducting resonators, which have lifetimes of the order of 1 ms [34], the coherence time of NV centers in diamond can approach 1 s even at relatively high temperatures [33]. Thus, combining the advantages from both devices seems to be more desirable for the quantum state preparation purposes.

Now, we describe the quantum characteristics of the flux qubit. To this aim we note that we need to choose the biasing in the main loop of the flux qubit close to half the flux quantum, $\Phi_0 = h/(2e)$. Therefore, the flux qubit could be described [48] in terms of a Hamiltonian in a two-dimensional Hilbert space. The Hamiltonian describing this system could explicitly be given

by

$$H = -[\epsilon(\Phi_{ext})\sigma_z + \Delta(\Phi'_{ext})\sigma_x]/2$$

where σ_x and σ_z are the well-known Pauli operators in the basis of flux qubit. The parameter $\Delta(\Phi'_{ext})$ is the flux qubit tunneling splitting energy, and finally $\epsilon(\Phi_{ext})$ is the energy bias of the flux qubit. These parameters provide a platform for controlling the qubit Hamiltonian of the system.

When a static magnetic field of half the flux quantum is applied perpendicular to the main loop of the flux qubit, the clockwise and counterclockwise persistent current states in the system become almost degenerate [27,29]. These clockwise and counterclockwise states provide us with the capability to define the logical basis states $|0\rangle_f$ and $|1\rangle_f$. In this setting, $|0\rangle_f$ and $|1\rangle_f$ represent the states of the clockwise and counterclockwise persistent current, respectively. Noting the fact that $\epsilon(\Phi_{ext})$ and $\Delta(\Phi'_{ext})$ can be adjusted independently by external magnetic fluxes through the main and the α loops, one can set $\epsilon(\Phi_{ext}) = 0$. Therefore, by preparing the system in one of its computational basis $|0\rangle_f$ or $|1\rangle_f$, one can perform a single qubit operation on the system considering the Hamiltonian given above. In the following, we will show that such a flux qubit can be combined with NVEs to construct an interesting hybrid architecture for information processing and entangled state generation. To this aim we first need to consider the NVEs Hamiltonian in details.

For the NV centers in diamond architecture, we only are interested in the ground state of such a system. Interestingly, the ground state of an NV center in diamond is a spin triplet state with zero-magnetic-field splitting of about $D_{gs} \approx 2.87$ GHz between the $m_s = 0$ sublevel and the degenerate $m_s = \pm 1$ sublevels [Fig.2.3(b,c)]. To get rid of the degeneracy in the $m_s = \pm 1$ sublevels, we can apply an external magnetic field to induce Zeeman splitting. Therefore. we apply the external magnetic field B_{ext} along the [100] direction of the diamond crystal lattice, to remove the degeneracy of $|m_s = \pm 1\rangle$ sublevels [Fig.2.3(c)]. Hence, one can focus on the two sublevels $m_s = 0$ and $m_s = -1$, to reduce the system into a two-level system. This enables us to reduce the Hilbert space of the system into a two-dimensional space in which one can define the computational basis for the information processing operations. With this description, the spin

operators of the jth NV center can be defined though Pauli operators. Hence, we explicitly define

$$s_{zj} = |-1_j\rangle\langle -1_j| - |0_j\rangle\langle 0_j|,$$

$$s_{+j} = |-1_j\rangle\langle 0_j|,$$

$$s_{-} = |0_j\rangle\langle -1_j|.$$

The definition of the Pauli matrices for a single NV, enables one to define a generic scenario for the situation which includes N_0 nitrogen vacancy centers. More precisely, if an NVE contains N_0 NV spin, collective spin operators can easily be expressed through summing the spins of the system which can be written as

$$S_\tau = \sum_{k=1}^{N_0} s_{\tau k}(\tau = z, \pm).$$

It is quite notable that qubits based on nitrogen vacancy centers with an external magnetic field B_{ext} applied to induce splitting between the $m = 1$ and $m = -1$ sublevels have been investigated extensively in the literature (see, e.g., [27, 29]). One main difference of what we are going to present here with the earlier works is that we apply additional time-dependent B_j fields, to NVEs beside with B_{ext} to provide a periodic modulation of the $m = 0$ – $m = -1$ splitting. This interestingly provides us with the capability of generating N00N states which is the main goal of our discussion in this chapter. To obtain the desired effective Hamiltonian, we are going to apply the Holstein–Primakoff (HP) transformation [49] to the spin operators of NV centers. Such a strategy enables mapping of the collective spin behavior of a quantum system to a harmonics oscillator. Therefore, by applying HP transformation on the time-dependent $m = 0$ and $m = -1$ splitting we show that the transformation leads to a closed-form Hamiltonian that we are seeking for.

To be able to apply the HP transformation, we need to restrict ourselves in the regime of weak excitation, where the spin operators of an NVE with a large N_0 can be mapped onto bosonic operators via an HP transformation [49]. Thus, we assume the the the number of the excitation

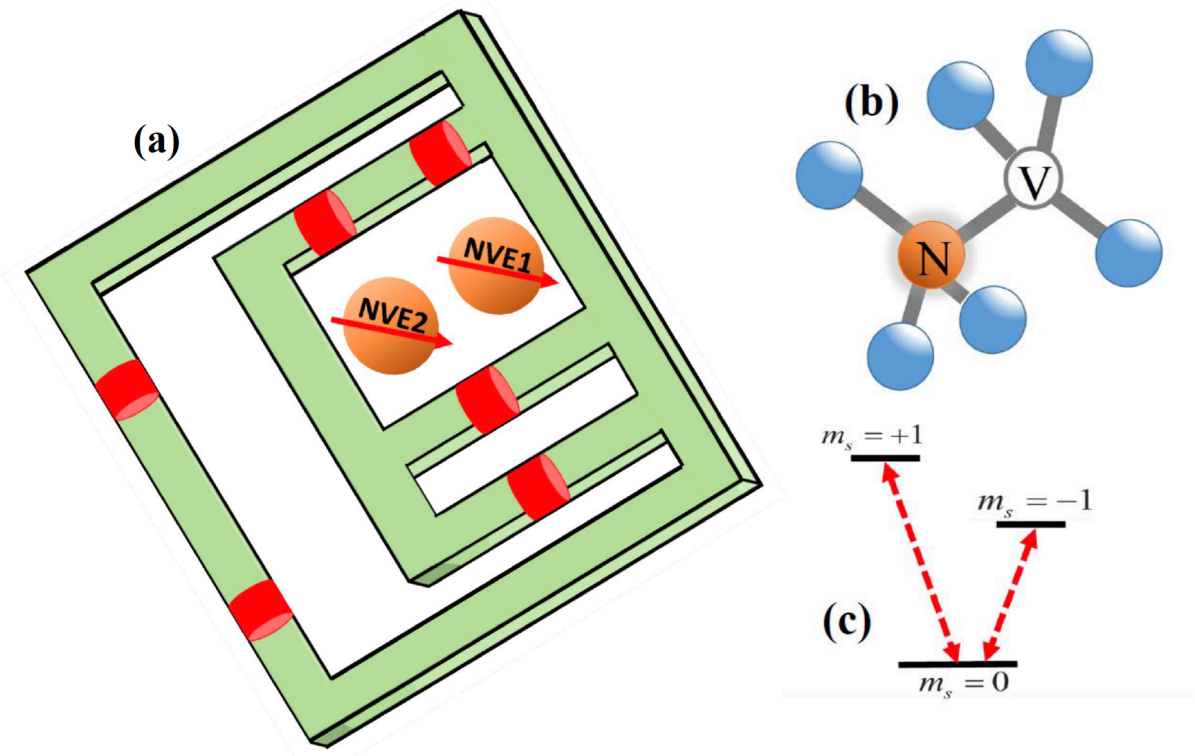

Figure 2.3: (a) Two ensembles of NV centers coupled to a superconducting flux qubit consisting of four Josephson junctions forming the main loop and an α loop. (b,c) Crystal-lattice (b) and energy (c) diagrams of an NV center in diamond. (Yusef Maleki and Aleksei M. Zheltikov,2018)

is very small compared to N_0. With such an assumption, one can perform the HP transformation resulting in

$$\sum_{k=1}^{N_0} s_{+k}^j = c_j^\dagger \sqrt{N_0 - c_j^\dagger c_j} \backsimeq \sqrt{N_0} c_j^\dagger,$$

and

$$\sum_{k=1}^{N_0} s_{-k}^j = c_j \sqrt{N_0 - c_j^\dagger c_j} \backsimeq \sqrt{N_0} c_j,$$

also

$$\sum_{k=1}^{N_0} s_{zk}^j = 2c_j^\dagger c_j - N_0.$$

In the relations above $j = 1, 2$ for the first and the second NVEs, respectively. In this manner,one has $[c_j, c_j^\dagger] = 1$.

We note that once we have a collective spin system, the coupling of the system enhances drastically compared to the single spin coupling. More precisely, the collective coupling strength of an ensemble of N_0 spins enhances by a factor of $\sqrt{N_0}$ compared to coupling strength of a single spin [31]. Therefore, increasing N_0 seems to to be favorable from this perspective as it is much easier to fulfill the requirements of the strong coupling regime. Furthermore, the weak-excitation requirement mentioned above is necessary for the validity of HP mapping, could be satisfied via the conditions $c_1^\dagger c_1 << N_0$ and $c_2^\dagger c_2 << N_0$. This in turn limits the N number in attainable N00N states, $N << N_0$. However, N_0 can be sufficiently large in a realistic scenario. For instance, $N_0 \sim 10^7$ has been used in the practicle experiments [39], which is sufficiently higher than what we expect for the N00N state generations.

The total Hamiltonian of the NVE-flux-qubit hybrid system considered here can now be written as

$$H = -\hbar \frac{\Delta(\Phi'_{ext})}{2} \sigma_x + \hbar \sum_{j=1}^{2} \omega_j c_j^\dagger c_j + \hbar \sum_{j=1}^{2} g(c_j^\dagger + c_j)\sigma_z, \tag{2.14}$$

where

$$\omega_j = D_{gs} - g_e \mu_B B_z - g_e \mu_B B_j,$$

g_e is the ground-state Lande factor and μ_B is the Bohr magneton and B_z is the magnetic field sensed by the spins due to the applied external magnetic filed B_{ext} and the magnetic field produced by the flux qubit. Also, the parameter g is the coupling constant between the NVE esnenbles and the flux qubit.

We Further assume that the sizes of the NVEs are sufficiently small to neglect spatial variations of the magnetic field induced by the flux qubit. Furthermore, the magnetic fields are chosen such that

$$\omega_j = \Delta(\Phi'_{ext})/2 + \delta \sin(\nu t + \varphi_j),$$

where $\delta \sin(\nu t + \varphi_j)$ is controlled by the ac magnetic field. Choosing large ν and small δ, so that $\Delta(\Phi'_{ext}) \gg \zeta = \delta/\nu$, we apply the rotating-wave approximation (RWA) and use the basis of flux qubit eigenstates to reduce the interaction Hamiltonian of the considered system to

$$H_I = \hbar g \sigma^+ (\hat{c}_1 e^{i\zeta \cos(\nu t + \varphi_1)} + \hat{c}_2 e^{i\zeta \cos(\nu t + \varphi_2)}) + H.c. \tag{2.15}$$

This Hamiltonian can be reduced to a Floquet Hamiltonian by using the identity $e^{i\zeta \cos(\nu t + \varphi_j)} = \sum_{n=-\infty}^{\infty} J_n(\zeta) e^{in(\nu t + \varphi_j)}$, where $J_n(\zeta)$ is the nth-order Bessel function of the first kind, which gives $H_I = H_0 + \sum_{n=1}^{\infty} H_n e^{in\nu t}$, where $H_0 = \hbar g J_0(\zeta)(\sigma^+(\hat{c}_1 + \hat{c}_2) + (\hat{c}_1^\dagger + \hat{c}_2^\dagger)\sigma^-)$ and $H_n = \hbar g \sum_{j=1}^{2} i^n J_n(\zeta)(\sigma^+ \hat{c}_j + (-1)^n \hat{c}_j^\dagger \sigma^-) e^{in\varphi_j}$. The interaction Hamiltonian of this form can be replaced by the effective Hamiltonian $H_{\text{eff}} = H_0 + \sum_{n=1}^{\infty} [H_n, H_{-n}]/(n\hbar\nu)$, which can be written as $H_{\text{eff}} = \hbar g J_0(\zeta)(\sigma^+(\hat{c}_1 + \hat{c}_2) + h.c.) + i\hbar\Omega(\hat{c}_1^\dagger \hat{c}_2 - \hat{c}_1 \hat{c}_2^\dagger)\sigma_z$. Here, $\Omega = g^2\chi/\nu$ is the coupling coefficient with $\chi = \sum_{n=1}^{\infty} 2J_n(\zeta)^2 \sin(n(\varphi_1 - \varphi_2))/n$.

We set $\zeta = 2.40$ ($J_0(2.40) = 0$) and $\varphi_2 \neq \varphi_1$ to find the effective interaction Hamiltonian:

$$H_{\text{eff}} = i\hbar\Omega(\hat{c}_1^\dagger \hat{c}_2 - \hat{c}_2^\dagger \hat{c}_1)\sigma_z. \tag{2.16}$$

It is straightforward to see now that the coupling coefficient can be tuned by varying the B_j fields. In particular, with $\varphi_1 - \varphi_2 = \pi/3$ and $\nu = 5\chi g \simeq 3.14g$, we have $\Omega/2\pi \approx 14$ MHz.

Such coupling strengths have been recently demonstrated for a system of a flux qubit and an NVE with $N_0 \approx 3 \times 10^7$ [39]. With the decay rates of NVEs and the flux qubit estimated as $\gamma_{NV} \sim 1$ Hz [33] and $\gamma_{FQ} \sim 1$ MHz [50], we find that the requirement of strong coupling, $\Omega \gg \gamma_{FQ}, \gamma_{NV}$, is fulfilled.

As one of its interesting features, our protocol of N00N-state generation requires only local operations on the flux qubit at the second and third steps, where the state $|\psi\rangle_1$ is degenerated into $|\psi\rangle_3$. Consequently, the operation time for each of these two steps reduces to the single-qubit operation time, Δt_2, $\Delta t_3 \sim 1$ ns [29]. This fact allows the overall time $\Delta\tau = \sum_{i=1}^{4} \Delta t_i$ of N00N-state generation to be sufficiently shortened. This is useful for avoiding decoherence buildup in the system. With our earlier estimate of $\Omega/2\pi \simeq 14$ MHz, the system could be in a strong-coupling regime, for which we have $\Delta t_1 \approx 9$ ns. Hence, we find for the total time required to create a N00N state through the considered process to be $\Delta\tau \approx 20$ ns when the $|0\rangle_f$ state is found at the measurement step and $\Delta\tau \approx 38$ ns if the measurement yields $|1\rangle_f$. In both situations, the time that is needed for N00N-state generation is much shorter than the dephasing times of both the flux qubit, ~ 1 μs [50] and the NVEs ~ 350 μs [28].

The architecture for the N00N state generation proposed here is robust against the buildup of decoherence. This, could one advantage of such a state generation scheme compared to the ones in which entangled states are generated first and then step-by-step increase in N are performed in the state. In order for quantifying the behavior of the system against the buildup of decoherence in the generated N00N state in our scheme, we need to analyse the density matrix elements and fidelity of the system for the generated N00N state. To this aim we need to solve the evolution equation for the density operator $\hat{\rho}$ [51, 52],

$$\frac{\partial\hat{\rho}}{\partial t} = \sum_j -\frac{\gamma_j}{2}(1+\bar{n}_{th})(2\hat{c}_j\hat{\rho}\hat{c}_j^\dagger - \hat{c}_j{}^\dagger\hat{c}_j\hat{\rho} - \hat{\rho}\hat{c}_j^\dagger\hat{c}_j) - \frac{\gamma_j}{2}\bar{n}_{th}(2\hat{c}_j^\dagger\hat{\rho}\hat{c}_j - \hat{c}_j\hat{c}_j^\dagger\hat{\rho} - \hat{\rho}\hat{c}_j\hat{c}_j^\dagger), \qquad (2.17)$$

where j = 1, 2, and γ_i is the decoherence rate of the ith NVE, and

$$\bar{n}_{th} = [\exp(-\hbar\omega/k_B T) - 1]^{-1}.$$

is the thermal phonon number at temperature T.

In this study, we take $\gamma_1 = \gamma_2 = \gamma$ and choose T = 20 mK. Since the temperature is sufficiently low, the coherence time for the NV centers could be sufficiently long. Thus, we choose $1/\gamma \approx 1$ s as an achieveable coherence time for NV centers [33]. In Fig. 2.4(a), we demonstrate the density matrix elements $\rho_{ij,kl} = \langle ik|\hat{\rho}(t)|jl\rangle$ (in which $|jl\rangle = |j\rangle_1 \otimes |l\rangle_2$) are obtained by numerically solving Eq. 2.17 for the initial conditions which correspond to the $N = 2$ N00N state stored in the two spin ensembles at $t = 0$. The system decay is captured by the density matrix elements evolution shows that the system is remarkably robust to the decoherence as was expected for the NVEs.

It is also insightful to consider the fidelity of the N00N state as the system evolves in time through decoherence. This is shown in Fig. 2.4(b), where we demonstrate the fidelity carried out as $F = \langle N00N|\hat{\rho}(t)|N00N\rangle$. As a result of these calculations, at t = 1 ms, the fidelity F is still higher than 0.99. This is a sufficiently long time for many quantum operations demonstrating the unique characteristics of the NVEs. Furthermore, we can see that it remains above 0.97 for as long as $t \approx 3.5$ ms [the inset in Fig. 2.4(b)]. Thus, N00N states in NVEs seem to have a long survival time which make them a good candidate for such a task.

It is remarkable that that at T = 20 mK the average thermal excitation number is about $\bar{n}_{th} = 0.001$. It is also possible to sufficiently cool down the system below 10 mK using the current technologies for which the thermal excitation number as small as $\bar{n}_{th} \lesssim 10^{-6}$ can be attained. This implies that we can ignore the effects of the thermal excitation when the system is cooled down sufficiently. Thus, without the thermal effects (at $T = 0$ K), the analytic solution of the master

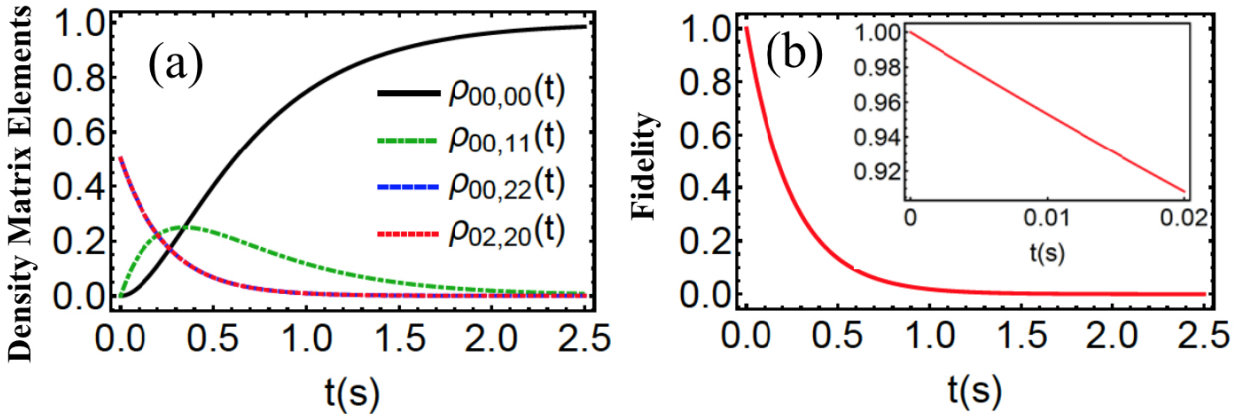

Figure 2.4: Time evolution of the density matrix elements $\rho_{ij,kl}$ (a) and the fidelity (b) calculated by solving Eq. (12) for the NVE–flux-qubit source of N00N states with an $N = 2$ N00N state prepared in a system at $t = 0$ (Yusef Maleki and Aleksei M. Zheltikov,2018).

equation for N00N state at time t reads

$$\hat{\rho}(t) = \frac{1}{2}[\sum_{n=0}^{N} e^{-\gamma n t} \begin{pmatrix} N \\ n \end{pmatrix} (1-e^{-\gamma n t})^{N-n}(|n0\rangle\langle n0|+|0n\rangle\langle 0n|)+e^{-\gamma N t}(|N0\rangle\langle 0N|+|0N\rangle\langle N0|)]. \tag{2.18}$$

This exact solution of the master equation provides the phase sensitivity which can be obtained in such a damping process could thus be obtained as $\Delta\phi \geq e^{\gamma N t}/N$. This shows that damping effects result in an exponential decrease in the precision of phase measurements.

Moreover, to have a better insight into the robustness of the scheme against decoherence we find the fidelity of the state in this scenario, which is found to be $F = e^{-\gamma N t}$. The N00N-state fidelity decreases exponentially. Since the decoherence rate in the system is determined in terms of the coherence time of it, i.e., $\gamma = \frac{1}{\tau}$, we can arrive at the conclusion that the long coherence time of the NVE demonstrates an exponential advantage compared to the physical systems which have shorter coherence time. For a given N, the fidelity decreases to $\sim e^{-1}$ at $\gamma N t = 1$, for which the state is effectively relaxed to the ground state.

2.4 Entangled state generations beyond the N00N state

Here, we are going to consider generation of entangled state beyond the N00N state. These entangled states could be very useful for various quantum information processing tasks. We are going to show that a vast class of entangled states could be generated with the scheme that will be provided here. More interestingly, various maximally entangled states could be engineered with the protocol we shall lay out in what follows. We are going to follow [40] in doing so. The starting point to our system is still the same effective Hamiltonian that we have already focused on. In this platform, we consider two cavities which interact with a common qubit. Using the Hamiltonian in Eq. (2.1) we can derive the dynamics of the field operators as

$$\dot{a}_1 = \kappa a_2(t)\sigma_z,$$
$$\dot{a}_2 = -\kappa a_1(t)\sigma_z.$$

The solution to these equations can be found to be

$$a_1 = a_1(0)\cos(\kappa t) - a_2(0)\sin(\kappa t)\sigma_z,$$
$$a_2 = a_2(0)\cos(\kappa t) + a_1(0)\sin(\kappa t)\sigma_z.$$

At $\kappa t = \pi/4$, we have

$$a_1 = \frac{1}{\sqrt{2}}(a_1(0) - a_2(0)\sigma_z),$$
$$a_2 = \frac{1}{\sqrt{2}}(a_2(0) + a_1(0)\sigma_z).$$

Next, we let the photons to go through a 50/50 beam splitter given by the two–mode unitary operation

$$U = \exp[-\pi/4(a_1^\dagger(0)a_2(0) - a_2^\dagger(0)a_1(0))].$$

This process results in the following transformation of the field operators

$$a_1(0) = \frac{1}{\sqrt{2}}(a_1(0) + a_2(0)),$$
$$a_2(0) = \frac{1}{\sqrt{2}}(a_2(0) - a_1(0)).$$

Thus, the total transformation, after passing through the beam splitter can be given by

$$a_1 \rightarrow a_1(0)|e\rangle\langle e| + a_2(0)|g\rangle\langle g|, \tag{2.19}$$

$$a_2 \rightarrow a_2(0)|e\rangle\langle e| - a_1(0)|g\rangle\langle g| \tag{2.20}$$

These transformations are central to generation of entangled states which will become clear soon. Note that these are conditional photon transformation subjected to the state of the qubit. We will see that such a transformation maps various initial states into interesting entangled states which could be useful for various tasks. Now, to see the power of such a transformation, let us consider an specific example as the input state

$$|\psi\rangle = |N\rangle|0\rangle\frac{1}{\sqrt{2}}(|g\rangle + |e\rangle).$$

The above transformation, acting upon this initial state, gives rise into

$$|\psi\rangle \longrightarrow \frac{1}{\sqrt{2}}(|N\rangle|0\rangle|e\rangle + |0\rangle|N\rangle|g\rangle).$$

By applying an external $\pi/2$ pulse (Hadamard gate) to the atom in the state above the overall state of the system degenerates into

$$[(|N\rangle|0\rangle + |0\rangle|N\rangle)|e\rangle + (|N\rangle|0\rangle - |0\rangle|N\rangle)|g\rangle]/2.$$

Therefore, the measurement on the state of the atom provides different N00N states. Namely,

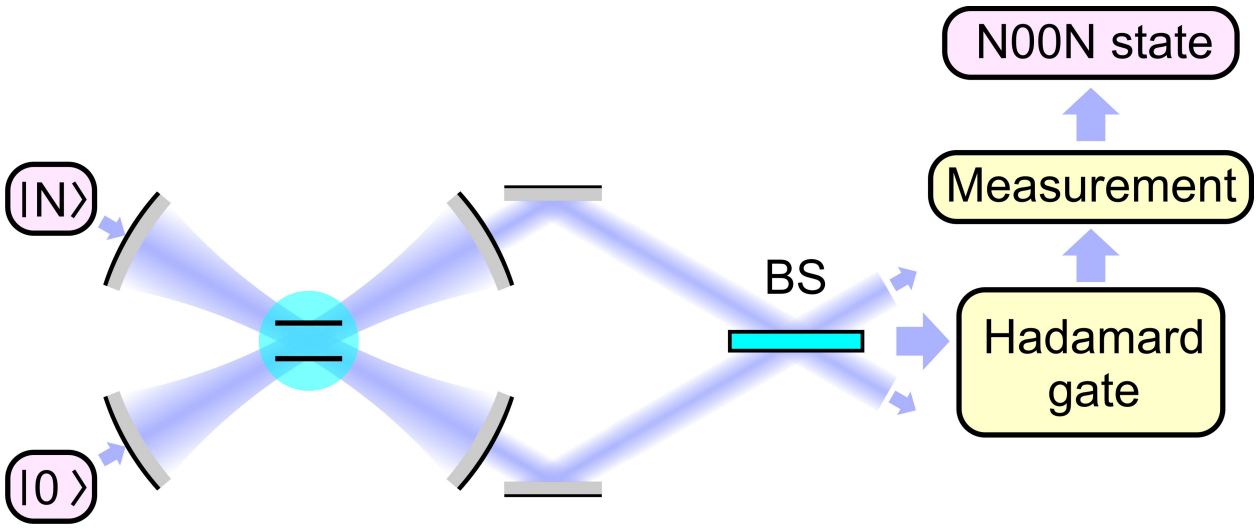

Figure 2.5: Architecture of the magic beam splitter in our approach. The input state first interacts with the system of the two resonators interacting with a qubit for as long as $\kappa t = \pi/4$. Then the photons in the resonators are sent to a beam splitter. Finally, by applying a Hadamard gate and performing a measurement on the qubit we attain a N00N state. (Yusef Maleki and Aleksei M. Zheltikov,2019)

detection of the atom in the exited state results in the N00N state

$$\frac{1}{\sqrt{2}}(|N\rangle|0\rangle + |0\rangle|N\rangle),$$

and detection of the atom in its ground state gives

$$\frac{1}{\sqrt{2}}(|N\rangle|0\rangle - |0\rangle|N\rangle).$$

Regardless of the sign differences, both of the states give the same result in the phase estimation scenario, and both are N00N states. We summarize the transformation presented here in Fig. 2.5. Accordingly, the input state first interacts with the resonators–qubit system, then goes through a beam splitter. Finally, a Hadamard gate followed by a measurement is performed on the qubit which gives the desired N00N states.

As was mentioned earlier, the usefulness of our architecture can even be extended beyond the N00N state generation. For instance, let us consider the case where we prepare the initial state of

the first cavity in a coherent state

$$|\alpha\rangle = e^{-\frac{|\alpha|^2}{2}} \sum_{n=0}^{\infty} \frac{\alpha^n}{\sqrt{n!}} |n\rangle,$$

where α is an arbitrary complex number. To this aim, we consider the initial state of the system to be expressed as

$$|\psi\rangle = |\alpha\rangle|0\rangle \frac{1}{\sqrt{2}}(|g\rangle + |e\rangle),$$

where we could generate the superposed state of the form

$$|\psi\rangle \longrightarrow \frac{1}{\sqrt{2}}(|\alpha\rangle|0\rangle|e\rangle + |0\rangle|\alpha\rangle|g\rangle)$$

This is a micro-macro entangled state where an atom is entangled with a shared coherent state in the cavities. Thus, one can generate entangled state of the form

$$|\varphi^{\pm}\rangle = \frac{1}{\sqrt{2 \pm 2e^{-|\alpha|^2}}}(|\alpha\rangle|0\rangle \pm |0\rangle|\alpha\rangle).$$

The state $|\varphi^{+}\rangle$ is proven to be very usefull in quantum merology [53]. If we start with a squeezed state at the input stage, we could entangle the squeezed state with the vacuum.

Our approach can generate states even beyond such a superposition. In general, we take the quantum states

$$|\psi_1\rangle = \sum_{n=0}^{d_1} b_n |n\rangle,$$

and

$$|\psi_2\rangle = \sum_{n=0}^{d_2} c_n |n\rangle.$$

Hence, we prepare the initial state in

$$|\psi\rangle = |\psi_1\rangle|\psi_2\rangle \frac{1}{\sqrt{2}}(|g\rangle + |e\rangle).$$

Then, given the detection of the atom in its exited state, we can generate the symmetric entangled state

$$|\psi^{+}\rangle = \frac{1}{\sqrt{2+2|\langle\psi_1|\psi_2\rangle|^2}}(|\psi_1\rangle|\psi_2\rangle + |\psi_2\rangle|\psi_1\rangle), \tag{2.21}$$

alternatively, if we detect the atom in its ground state, we attain the anti-symmetric entangled state

$$|\psi^{-}\rangle = \frac{1}{\sqrt{2-2|\langle\psi_1|\psi_2\rangle|^2}}(|\psi_1\rangle|\psi_2\rangle - |\psi_2\rangle|\psi_1\rangle). \tag{2.22}$$

Thus, we can generate several interesting states in our architecture such as superposition of two coherent states $|\alpha\rangle$ and $|\beta\rangle$

$$\frac{1}{\sqrt{2\pm2|\langle\alpha|\beta\rangle|^2}}(|\alpha\rangle|\beta\rangle \pm |\beta\rangle|\alpha\rangle),$$

or superposition of two squeezed states $|\xi_1\rangle$ and $|\xi_2\rangle$

$$\frac{1}{\sqrt{2\pm2|\langle\xi_1|\xi_2\rangle|^2}}(|\xi_1\rangle|\xi_2\rangle \pm |\xi_2\rangle|\xi_1\rangle),$$

or even hybrid entangled states of the forms

$$\frac{1}{\sqrt{2\pm2|\langle\xi_1|\alpha\rangle|^2}}(|\alpha\rangle|\xi_1\rangle \pm |\xi_1\rangle|\alpha\rangle),$$

$$\frac{1}{\sqrt{2\pm2|\langle N|\alpha\rangle|^2}}(|\alpha\rangle|N\rangle \pm |N\rangle|\alpha\rangle),$$

$$\frac{1}{\sqrt{2\pm2|\langle N|\xi_1\rangle|^2}}(|\xi_1\rangle|N\rangle \pm |N\rangle|\xi_1\rangle).$$

Such states are of paramount importance in beating the shot noise limit in quantum metrology and have a vast application in quantum information processing.

In principle, quantum entanglement emerges from the tensor product property of the Hilbert space of a quantum system in which two or more subsystems share a single state which can be represented based on the superposition of the bases of these Hilbert spaces [9,17]. In the framework

of pure quantum state of two subsystems, the state $|\psi\rangle$ is said to be separable (not-entangled) if we can write it as the product of the states of each subsystems ($|\psi\rangle = |\psi\rangle_1 \otimes |\psi\rangle_2$. Here 1 and 2 represent the state of the first and the second subsystems); otherwise, the state is called entangled [9, 17]. A similar definition can be developed for the case of a mixed quantum state. In fact, entanglement is a purely quantum correlation with no classical description which is responsible for many interesting physical phenomena in the quantum regime [2, 3]. Once we are given a quantum state of two (or more) subsystems, a natural question is whether the subsystems are entangled or not. However, the amount of entanglement and quantum correlation of the subsystems can depend on many factors in a system. The two subsystems can present maximum entanglement (or maximum quantum correlation of any type) or no entanglement at all. They can also present quantum entanglement ranging between these two extreme cases of maximum and minimum. This entails a formalism to quantify the degree of quantum correlations and more importantly quantum entanglement. In other words, precise measures of entanglement is found to be necessary for this aim [2, 3, 9, 11, 17, 54]. For a system of two two-level subsystems, such as two spin-1/2 particles, Wootters introduced an elegant measure of entanglement called concurrence [54], that quantifies the degree of entanglement in such a scenario.

In this work, we are interested in the entanglement between the electron and the proton of the hydrogen atom. Since each spin space of the subsystems (electron and proton) provide a two-dimensional Hilbert space, the total system could be considered as a two-qubit quantum state. Therefore, one can use concurrence as a measure of entanglement in a bipartite system of the electron–proton. The entanglement of a two-qubit system can be characterized by the concurrence [54]

$$C = \max\{0, \lambda_1 - \lambda_2 - \lambda_3 - \lambda_4\}, \tag{2.23}$$

where λ_i are the eigenvalues of the Hermitian matrix

$$R = \sqrt{\sqrt{\rho}\tilde{\rho}\sqrt{\rho}}.$$

The operator $\tilde{\rho}$ is defined as

$$\tilde{\rho} = (\sigma_y \otimes \sigma_y)\rho^*(\sigma_y \otimes \sigma_y).$$

Here, ρ^* is the complex conjugate of ρ, and σ_y is the spin flip operator (y component of the Pauli matrices).

In the definition of the concurrence C, the eigenvalues are given in non-increasing order expressed as

$$\lambda_1 \geq \lambda_2 \geq \lambda_3 \geq \lambda_4.$$

Concurrence, ranges between 0 and 1. For a maximally entangled state we have $C = 1$ and for a separable state $C = 0$.

Using concurrence to quantify entanglement of the H atom, we find its explicit form to be

To quantify the entanglement degree of the generated states $|\psi^{\pm}\rangle$ we can use concurrence as the measure of entanglement [54], which is defined as

$$C = |\langle\psi|\sigma_y \otimes \sigma_y|\psi^*\rangle|, \tag{2.24}$$

where σ_y is the spin flip operator and $|\psi^*\rangle$ is the complex conjugate of $|\psi\rangle$. With some straightforward calculation, we find the concurrence as

$$C = \frac{1 - |\langle\psi_1|\psi_2\rangle|^2}{1 \pm |\langle\psi_1|\psi_2\rangle|^2}. \tag{2.25}$$

Where, the plus(minus) sign in the denominator shows the concurrence of the state $|\psi^+\rangle(|\psi^-\rangle)$. Interestingly, $|\psi^-\rangle$ is maximally entangled for any input states. However, $|\psi^+\rangle$ is maximally entangled if and only if the input states in the modes are orthogonal states, i.e., $\langle\psi_1|\psi_2\rangle = 0$. For instance, considering the input state $|N\rangle|M\rangle$, one can generate maximally entangled states

$$|\psi\rangle \longrightarrow \frac{1}{\sqrt{2}}(|N\rangle|M\rangle + |M\rangle|N\rangle),$$

in this class of states. This reduces to the N00N states when $M = 0$.

Considering the maximal entanglement of $|\psi^-\rangle$, a wast class of maximally entangled states can be generated in this setup. It is notable that, having maximally entangled states are extremely important in many quantum protocols. This scheme can be useful in a vast span of quantum disciplines and can provide a new platform for information processing tasks.

2.5 Eantangled state generation beyond the two-mode states

As was shown earlier, it is quite possible to generate a large class of entangled states, such as N00N state and entangled coherent states in the architecture that we have described earlier. It would be quite interesting to extend the scheme to a miltimode scenario. Generation of entangled states with more than two modes could be very important for various applications as well. However, generation of multimode quantum states is one of the most challenging tasks in most of the practical applications of quantum science. Thus, what will be presented here could be found useful in various quantum disciplines.

Now, we would like to show how the scheme that we investigated earlier, can be used to generate a multimode state. To do so. we first prepare an array of two-cavity system where, the array consists of pairs of cavities and a single qubit(see Fig. 2.6). Furthermore, we prepare the initial state of the entire system in some specific state of the interest. For instance, let us examine the following initial state as an input of the scheme

$$|\psi\rangle = |N,0\rangle \otimes |N,0\rangle \otimes ... \otimes |N,0\rangle \frac{1}{\sqrt{2}}(|g\rangle + |e\rangle).$$

Then, we send the qubit through the two-resonator network, where it interacts for the time length of $\kappa t = \pi/4$ with each resonator pair. Once the qubit is interacted with each pair, the photons go though the beam splitters after that. Consequently, the initial state of the system degenerates into

$$|\psi\rangle \longrightarrow \frac{1}{\sqrt{2}}(|N,0\rangle ... |N,0\rangle |e\rangle + |0,N\rangle ... |0,N\rangle |g\rangle).$$

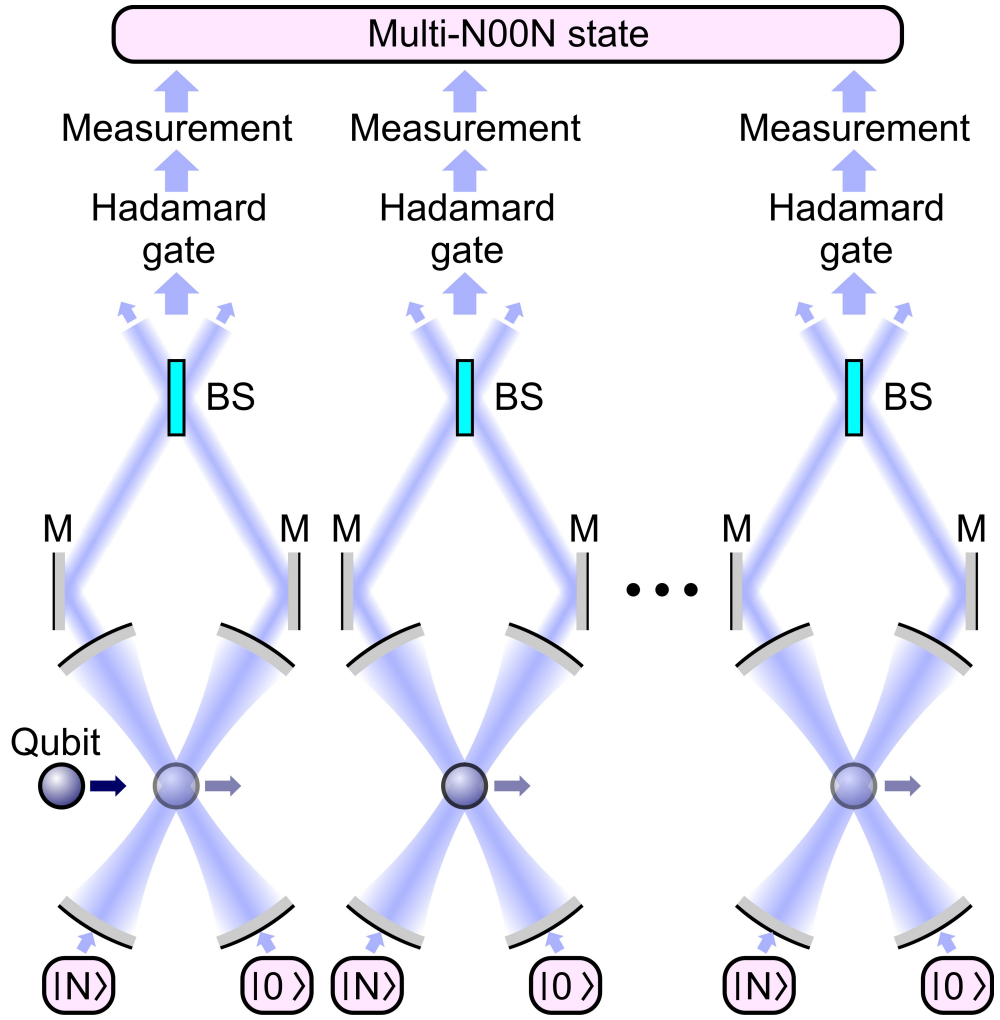

Figure 2.6: The network of multi-N00N state generation architecture. The qubit is sent through the resonator network to interact with each resonator pair. Then the photons inside the each pair is sent to a beam splitter. (Yusef Maleki and Aleksei M. Zheltikov,2019)

Now, by applying a $\pi/2$ pulse on the qubit and performing a measurement we get the multi-N00N state

$$|\psi\rangle \longrightarrow \frac{1}{\sqrt{2}}(|N,0\rangle...|N,0\rangle \pm |0,N\rangle...|0,N\rangle).$$

It is interesting that for an array of M resonator pairs, the phase resolution of the system reduces to $\Delta\varphi \propto \frac{1}{MN}$. To achieve this value through a N00N state we should be able to increase the number of phtons to MN in each of the entangled modes which is a very hard task for relatively large M and N.

Recently, a scheme to generate double N00N states was proposed [55]. To appreciate, the approach we introduce here, we restrict ourselves to $M = 2$ and compare the proposal of our work with the approach of [55]. In their setup they need $N + 2$ operational steps to generate a double N00N state; however, in our system we can generate a N00N state in just a few operational steps, which is independent of the number of the photons. This is a big advantage of our approach. Furthermore, our structure is even capable of generating multi-N00N states that can facilitate the quantum phase estimation techniques. That being said, we can generate a vast class of multi-mode entangled state by preparing each resonator in our specific state of interest.

2.6 Heisenberg-Limit metrology beyond N00N states

It was already discussed that N00N states have the specific capabilities to reach the Heisenberg-Limit for the phase estimation sensitivity. The question we want to answer here is whether this HL sensitivity is an exclusive property of N00N states. In what follows, we demonstrate that this is not the case in general. In fact, what we are going to show is that there is a large class of Fock state superposition which can reach the HL sensitivity. To lay out a rather general formalism for such states we will consider the relation between N00N state and spin coherent state superposition based on [41]. To this aim, we note that for such a two-mode Fock state representation, one may introduce the Schwinger realization of the su(2) algebra in terms of the field operators as

$$J_+ = a^\dagger b, \qquad J_- = b^\dagger a, \qquad J_z = \frac{1}{2}(a^\dagger a - b^\dagger b).$$

Hence, J_- and J_+ are the lowering and raising operators of the spin states, respectively. The generators of su(2) Lie Algebra $J_\pm$ and J_z satisfy the commutation relations

$$[J_+, J_-] = 2J_z, \qquad [J_z, J_\pm] = \pm J_\pm.$$

Taking $j = \frac{n}{2}$, and $m = \frac{n_a - n_b}{2}$, one can define

$$|n_a\rangle_a |n_b\rangle_b \equiv |j, m\rangle, \qquad (n = n_a + n_b).$$

This relation maps all the basis of the Hilbert space of the entire system from Fock state products to the Dicke state basis described by the su(2) algebra. The two special cases which are interesting to note are given by

$$|0\rangle_a \otimes |2j\rangle_b \equiv |j, -j\rangle, \quad \text{and} \quad |2j\rangle_a \otimes |0\rangle_b \equiv |j, j\rangle.$$

With this definition, the generators of the spin operators act on the basis as

$$J_\pm |j, m\rangle = \sqrt{(j \pm m)(j \pm m + 1)}|j, m \pm 1\rangle, \quad \text{and} \quad J_z|j, m\rangle = m|j, m\rangle.$$

Therefore, given N photons in one of the two modes, the two special cases could be expressed as

$$|0\rangle_a \otimes |N\rangle_b \equiv |j, -j\rangle_z, \quad \text{and} \quad |N\rangle_a \otimes |0\rangle_b \equiv |j, j\rangle_z.$$

These realizations in hand, one can rewrite the N00N state in Dicke basis as [56]

$$|\text{N00N}\rangle = \frac{1}{\sqrt{2}}(|j, j\rangle_z + |j, -j\rangle_z).$$

Thus, the N00N state is the superposition of the two north and the south poles of the Bloch sphere in the Dicke state basis. We note that, the superposition of the states with other principle numbers,

i.e.,

$$\frac{1}{\sqrt{2}}(|j,m\rangle_z + |j,-m\rangle_z),$$

cannot give raise to the N00N state since in the Fock basis it is equivalence to the state

$$\frac{1}{\sqrt{2}}(|\frac{n}{2}+m\rangle_a|\frac{n}{2}-m\rangle_b + |\frac{n}{2}-m\rangle_a|\frac{n}{2}+m\rangle_b).$$

Clearly, such state could not reproduce the HL sensitivity that is achievable with N00N state. However, considering the fact that N00N state are the two extreme points on the z direction, one might think of considering the states in some other extreme points such as points in the x direction. In fact, the superposition of the two extreme points in x direction could be expressed as

$$|j,\pm j\rangle_x = \frac{1}{2^j}\sum_{m=-j}^{j}\begin{pmatrix} 2j \\ j+m \end{pmatrix}^{\frac{1}{2}}(\pm 1)^{j+m}|j,m\rangle_z,$$

Noting that $|j,m\rangle_z = |\frac{n}{2}+m\rangle_a|\frac{n}{2}-m\rangle_b$, the superposition of such states is not equal to the N00N state. In fact, the normalized superposition of the two extreme points in x direction is

$$|\psi\rangle = \frac{1}{\sqrt{2}}(|j,j\rangle_x + |j,-j\rangle_x).$$

Now, we show that this state could be equivalent to the N00N state in phase estimation scenario if we perform an specific strategy that will become clear soon. To see this, we need to show that this state can indeed give Heisenberg limit precision. For this purpose, let us apply the unitary operator around x-axis $\exp(i\theta_x j_x)$ on the state $|\psi\rangle$. With this operator applied, the state $|\psi\rangle$ becomes

$$|\psi(\theta_x)\rangle_= \frac{1}{\sqrt{2}}(e^{i\theta_x j}|j,j\rangle_x + e^{-i\theta_x j}|j,-j\rangle_x).$$

Therefore, we can calculate the phase uncertainty as $\Delta\theta_x = \frac{1}{2j} = \frac{1}{N}$. Thus, the phase estimation is exactly equal to the HL as the N00N state. From this result one can easily realize that the

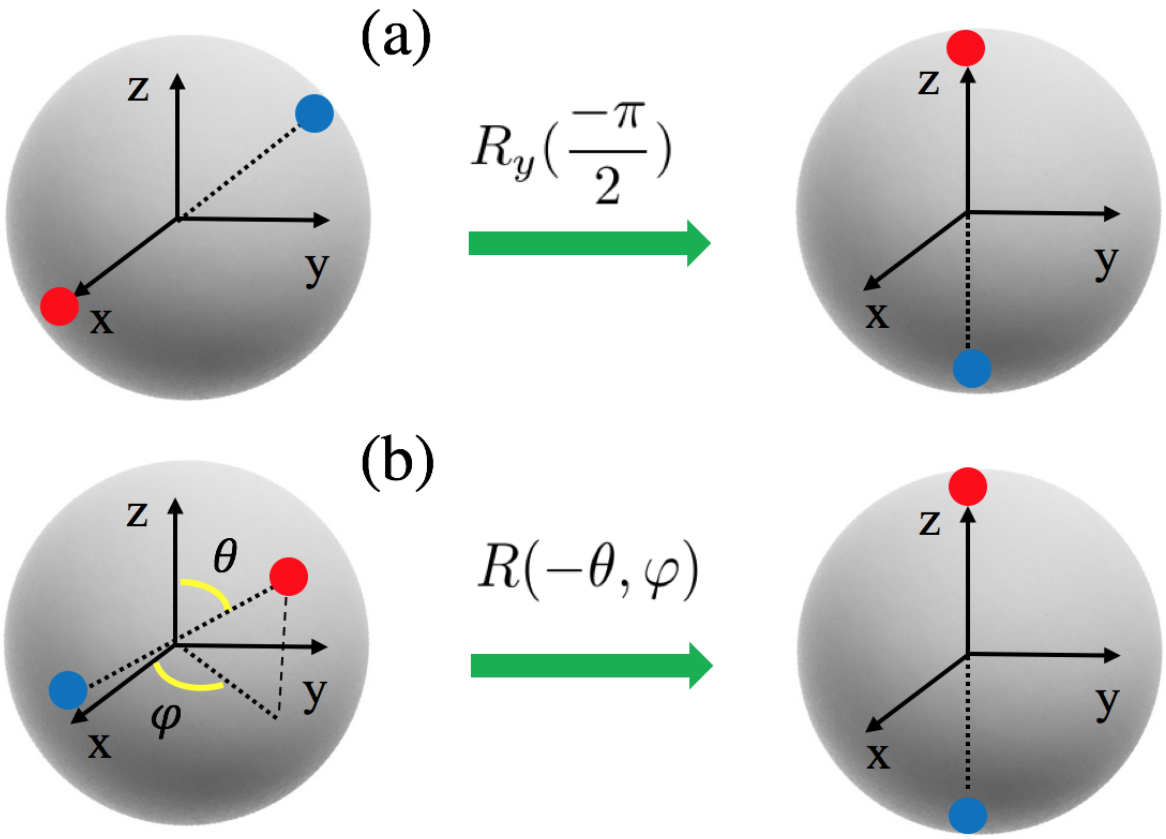

Figure 2.7: Rotation of the $|j, \pm j\rangle_x$ about y-axis on the Bloch sphere. (Yusef Maleki and Aleksei M. Zheltikov,2020)

superposition of the two lowest and highest states in the y direction, i.e., $|j, \pm j\rangle_y$ can reach the HL as well. These considerations through the extreme points in the x and the y directions was clearly pointed investigated in Ref. [56].

Now, it is tempting to ask that if there is any other superposed state that can reach this limit, or are these three states the only ones that can fulfill the N00N state property for the precise measurement? If there are some other states what are these states? Also, how we can generate such superposition states of the Dicke basis say in x, y and z directions? We shall address the generation scheme later; however, we first are going to discuss the first questions.

It is remarkable that in such a cat state the two superposed points are antipodals on the Bloch sphere. In general, an element of the Bloch sphere can be obtained by applying a rotation operator

on a reference point (such as $|j,-j\rangle_z$). Such rotation can be given based on the generators of the su(2) algebra of the spin system. The most general form of the rotation operator then can be expressed as

$$R(\theta,\varphi)e^{i\vartheta J_z} = \exp\{\frac{-\theta}{2}(J_+e^{-i\varphi} - J_-e^{i\varphi})\}e^{i\vartheta J_z}.$$

On the z direction basis, the term $e^{-i\vartheta J_z}$ give rise to an overall phase, that dose not effect the precision measurement. Since, The state

$$\frac{1}{\sqrt{2}}(e^{i\vartheta_1}|N\rangle_a \otimes |0\rangle_b + e^{-i\vartheta_1}|0\rangle_a \otimes |N\rangle_b),$$

is as good as the N00N state, for precise measurement purposes (this extra phase degree of freedom was introduced in Ref. [56] to facilitate the generation of N00N state). However, the first term displaces the ground state of the Dicke basis to a coherent state as

$$|\theta,\varphi,j\rangle = \exp[\frac{\theta}{2}(J_+e^{-i\varphi} - J_-e^{i\varphi})]|j,-j\rangle = \frac{1}{(1+|\gamma|^2)^j}\sum_{m=-j}^{j}\begin{pmatrix}2j\\ j+m\end{pmatrix}^{\frac{1}{2}}\gamma^{j+m}|j,m\rangle, \quad (2.26)$$

where $\gamma = e^{-i\varphi}\tan(\frac{\theta}{2})$. The overlap of two spin coherent states is given by

$$\langle\delta,j|\gamma,j\rangle = \frac{(1+\bar{\delta}\gamma)^{2j}}{(1+|\delta|^2)^j(1+|\gamma|^2)^j}.$$

Now, we examine the superposition of two antipodal coherent states on the Bloch sphere. We consider, with out loss of generality, a superposition given by

$$\frac{1}{\sqrt{2}}(|\theta,\varphi,j\rangle + |\pi-\theta,\pi+\varphi,j\rangle),$$

In order for to investigate the phase shift and sensitivity obtained through this superposition, we

consider the following Hermitian operator.

$$J_\gamma = J_z \cos\theta - \frac{1}{2}(J_+ e^{-i\varphi} + J_- e^{i\varphi}) \sin\theta.$$

In fact, with such a Hermitian operator, we can define the unitary phase shift operator $U = e^{-i\xi J_\gamma}$, such that

$$e^{-i\xi J_\gamma} \frac{1}{\sqrt{2}}(|\theta, \varphi, j\rangle + |\pi - \theta, \pi + \varphi, j\rangle) = \frac{1}{\sqrt{2}}(e^{i\xi j}|\theta, \varphi, j\rangle + e^{-i\xi j}|\pi - \theta, \pi + \varphi, j\rangle). \quad (2.27)$$

Thus, the phase uncertainty can be obtained as $\Delta\xi = \frac{1}{2j}$. Therefore, we can get HL phase uncertainty using the superposition of the two orthogonal spin coherent states as above. This shows that the HL phase uncertainty is not an exclusive property of the N00N states, and it can indeed be extracted with a large class of quantum states.

Now, one may ask whether it is possible to get such HL precision via superposition of two non-orthogonal spin coherent states which are not antipodal points or is this just limited to the antipodal orthogonal coherent state superposition? To have a better insight into such superposition we show the relation between the N00N state and such superposition states. To this aim we note that the two extreme points of the x direction are related to the diagonal z component of the spin coherent state in Eq. 2.26 by the $\frac{\pi}{2}$ rotation $R_y(\frac{\pi}{2}) = \exp(-i\frac{\pi}{2}j_y)$ about the y-axis, i.e.,

$$R_y(\frac{-\pi}{2})|j, \pm j\rangle_x = |j, \pm j\rangle_z.$$

This is shown in Fig. 2.7. Thus, by rotating the cat state about y-axis and noting that $|0\rangle_a|N\rangle_b \equiv |j, -j\rangle_z$, and $|N\rangle_a|0\rangle_b \equiv |j, j\rangle_z$ we create the N00N state

$$|\text{N00N}\rangle = \frac{1}{\sqrt{2}}(|2j\rangle_a \otimes |0\rangle_b + |0\rangle_a \otimes |2j\rangle_b).$$

This result clearly shows that a N00N state, is in fact a typical type of spin cat state [56]. A

coherent state can be expressed as an action of the rotation operator on the ground state such that $|\theta, \varphi, j\rangle = R(\theta, \varphi)|j, -j\rangle$. It is also remarkable that the antipodal point of this coherent state is

$$|\pi - \theta, \pi + \varphi, j\rangle = R(\theta, \varphi)R(\pi, \varphi)|j, -j\rangle = R(\theta, \varphi)|j, j\rangle.$$

Therefore, by applying the rotation operator $R^{-1}(\theta, \varphi) = R(-\theta, \varphi)$, we can get the N00N state. Thus, the spin cat states of antipodal points can be converted to the N00N state by some global unitary transformation. It is notable that such transformations change the states entirely and may transform it to a completely different state. With this description, now consider a superposition of two spin coherent state as $|\theta_1, \varphi_1, j\rangle + |\theta_2, \varphi_2, j\rangle$. We apply the operator $R(-\theta_1, \varphi_1)$ on the state and noting that the product of two rotation operators gives a rotation operator, up to a phase factor, we may express the state as

$$|j, -j\rangle + R(-\theta_1, \varphi_1)R(\theta_2, \varphi_2)R(\pi, 0)|j, j\rangle.$$

This can be fulfilled for $R(\theta_2, \varphi_2) = e^{i\beta}R(\theta_1, \varphi_1)R(\pi, \varphi')$. Where we have used the fact that $|j, -j\rangle = R(\pi, 0)|j, j\rangle$. Now considering the fact that multiplication of two rotation operators gives rise to a rotation operator, up to a phase factor

$$R(\gamma_1)R(\gamma_2) = R(\gamma_3)e^{i\Phi(\gamma_1,\gamma_2)J_z}$$

where

$$\gamma_3 = \frac{\gamma_1 + \gamma_2}{1 - \gamma_1^*\gamma_2}, \qquad \Phi(\gamma_1, \gamma_2) = -i\ln(\frac{1 - \gamma_1^*\gamma_2}{1 - \gamma_1\gamma_2^*})$$

with $\gamma_1 = e^{-i\varphi_1}\tan(\frac{\theta_1}{2})$, and $\gamma_2 = e^{-i\varphi_2}\tan(\frac{\theta_1}{2})$. Thus, to have a N00N state one needs to have

$$R(-\theta_1, \varphi_1)R(\theta_2, \varphi_2)R(\pi, 0) = Ie^{i\Theta J_z}$$

Where, Θ is some phase determined by the variables of $R(\theta_1, \varphi_1)$ and $R(\theta_2, \varphi_2)$. Thus, with this

description the states $|\theta_1, \varphi_1, j\rangle$, and $|\theta_2, \varphi_2, j\rangle$ need to be antipodals. In other cases the action of the operator $e^{i\phi J_z}$ shall not result in the HL metrology. We may express this in Fock basis as

$$\frac{1}{(1+|\gamma|^2)^{\frac{n}{2}}} \sum_{m=0}^{n} \binom{n}{m}^{\frac{1}{2}} \{\gamma^m + e^{i\psi}(-\frac{1}{\bar{\gamma}})^m\}|m\rangle_a|n-m\rangle_b, \tag{2.28}$$

where n is the number of the total photons. It is quite evident that this state is completely different from the N00N state, however, it can give the HL precision as N00N state. Therefore, such a two-mode superposition of the photon number states can give the set of the states satisfying this limit. This may allow us to circumvent the difficulty of generating of the N00N state and permits more general ways to produce the state that may reach HL precision.

The interaction Hamiltonian of the two-mode field and the two-level atom reads

$$H_1 = i\hbar\Omega(a^\dagger b - b^\dagger a)\sigma_z \tag{2.29}$$

Now if the atomic state is initially prepared at $\frac{1}{\sqrt{2}}(|g\rangle + |e\rangle)$ and one of the fields in the Fock state $|n\rangle_b$, and the other is prepared in the vacuum state $|0\rangle_a$, then

$$|\psi(0)\rangle = \frac{1}{\sqrt{2}}(|g\rangle + |e\rangle)|0\rangle_a|n\rangle_b.$$

Therefore, defining $\xi(t) = e^{i\varphi}\tan(\Omega t)$ the initial state evolves to

$$|\psi(t)\rangle = \frac{1}{\sqrt{2}}(|e\rangle \otimes |\xi(t), j\rangle + |g\rangle \otimes |-\xi(t), j\rangle).$$

This, in fact, is a type of micro-macro entanglement between the electronic state of the atom and the cavity fields. We apply a $\frac{\pi}{2}$ pulse on the atomic state which transforms $|e\rangle \rightarrow \frac{1}{\sqrt{2}}(|g\rangle + |e\rangle)$ then make a measurement on the ground state of the electronic state that projects the state to $\frac{1}{\sqrt{2}}(|\xi(t), j\rangle + |-\xi(t), j\rangle)$, which is a spin cat state. Therefore, there is a large class of spin cat states that can give HL metrology.

2.7 Recovery of amplitude damped N00N states

Once created, N00N states are highly prone to decoherence and eventually lose their phase super-resolving power when they couple to the environment or a detector, e.g., as a part of measurement process.

In most of the measurement processes, a quantum system collapses to one of its eigenstates. However, within a special class of physical measurements referred to as weak measurements [57–61], the system does not completely collapse by the measurement process and it is described as the superposition of its eigenstates. In this type of measurements the input state can be retrieved with a nonzero success probability by reversing the weak measurement process.

As was recently shown weak-measurement reversal can protect quantum state from amplitude damping [58, 59]. This approach provides a powerful tool for information processing by enabling a high-fidelity restoration of two-qubit quantum states [61]. Here, we show that the weak-measurement reversal procedure can be useful for protecting N00N states, enabling the HL phase super-resolution provided by such states to be recovered in spite of the damping induced by weak measurements [22].

To demonstrate the recovery of sub-SNL precision in N00N-state-based phase measurements, we consider a N00N state subject to amplitude damping [62]

$$|\Psi\rangle = \frac{1}{\sqrt{1+e^{-2N\gamma t}}}(|N\rangle \otimes |0\rangle + e^{-N\gamma t}|0\rangle \otimes |N\rangle). \tag{2.30}$$

The unbiased quantum Cramér-Rao bound (QCRB), setting a limit on the precision with which the phase ϕ of the density matrix $\rho(\phi)$ can be measured is [18, 24] $\Delta\phi \geq \Delta\phi_{QCB} \equiv 1/\sqrt{N_m F_Q}$. Here, N_m is the number of measurements and F_Q is the quantum Fisher information [18,24], $F_Q = Tr[\rho(\phi)L_\phi^2]$. The symmetric logarithmic derivative L_ϕ is defined by $\partial_\phi \rho(\phi) = (1/2)[\rho(\phi)L_\phi + L_\phi\rho(\phi)]$.

For the amplitude-damped N00N state above, the precision of phase estimation is thus limited by $\Delta\phi \geq [\cosh(N\gamma t)]/N$, showing that amplitude damping leads to an exponentially decreasing

sensitivity of N00N-state-based phase measurements. Since $\gamma = 1/\tau$, τ being the coherence time, it is straightforward to see, that NV-based N00N states ($\tau \cong 1$ s) maintain their phase-superresolving ability within much longer periods of time compared to photonic N00N states ($\tau \cong$ 1 ms).

The optimal phase sensitivity of the state versus γt for different N is given in Fig.4.5. The sensitivity of the state degrades by the weak measurement process. Even though the sensitivity gets far from the LH but for small enough time one expects that it still is below the shot noise limit. In fact the condition that the state provides below SNL sensitivity is determined by

$$\gamma t < \frac{\cosh^{-1}(\sqrt{N})}{N}. \tag{2.31}$$

We further analyze the parity operator measurement sensitivity in the weak measurement scenario. For the NOON state the sensitivity of the phase estimation in the interfrometer is of vital importance. For the measured operator $\hat{O}$ the variance is limited by [18, 24]

$$\Delta\phi = \Delta\hat{O}/|\frac{\partial\hat{O}}{\partial\phi}| \tag{2.32}$$

The operator used for N00N state phase estimation can be $P = |0N\rangle\langle N0| + |N0\rangle\langle 0N|$, which results in phase error

$$\Delta\phi_p = \frac{\sqrt{\cosh^2(N\gamma t) - \cos^2(N\varphi t)}}{N|\sin(N\varphi t)|} \tag{2.33}$$

It is notable that $\Delta\phi_p$ obtained here is larger than the one we obtained from CRB. The phase sensitivity of the state for the parity measurement is depicted in Fig.2.8. The sensitivity of the state drastically degrades by the weak measurement process.

Since controlling the weak measurement is important for quantum metrological applications it would be interesting if we could reverse the weak measurement and partial collapse process. In fact, reversing the weak measurement and protecting entangled qubit systems from such decoherence has been experimentally demostrated [58]. Such process can be fully or partially reversed

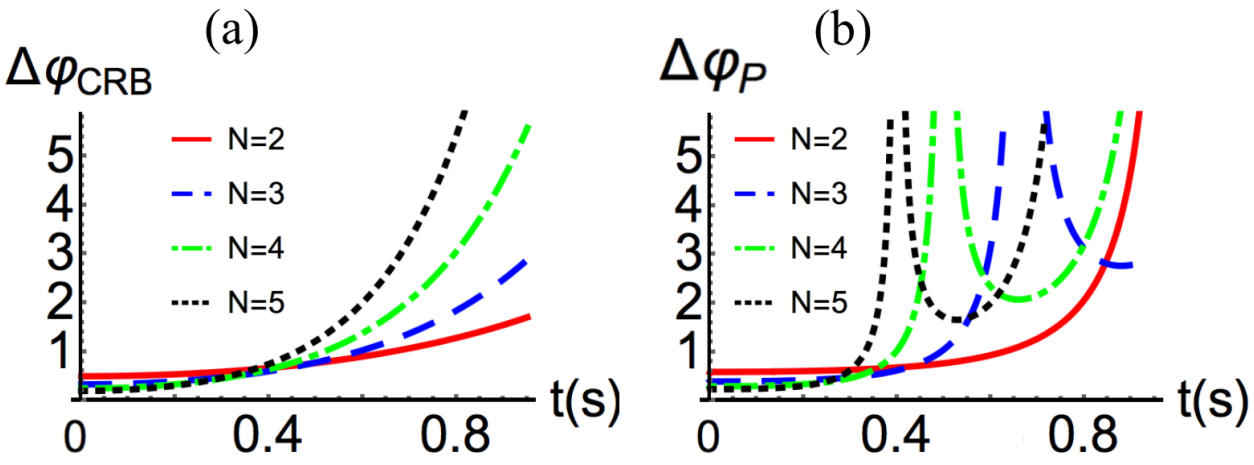

Figure 2.8: (a) Time evolution of the Cramér–Rao bound φ_{CRB} and (b) the phase error $\Delta\varphi_P$ (with $\varphi = \pi/2$) for a N00N-state phase estimator subjected to a weak measurement with $\gamma = 1$ Hz. (Yusef Maleki and Aleksei M. Zheltikov,2018)

from the amplitude damping via an ancilla assisted protocol containing a series of CNOT and generalized Hadamard gates [58]

To demonstrate entanglement recovery in an amplitude-damped N00N state, we set an ancilla qubit such that $\tan\theta = e^{N\gamma t}$ and define a generalized Hadamard gate as

$$\mathcal{H} = \begin{pmatrix} \cos\theta & \sin\theta \\ \sin\theta & -\cos\theta \end{pmatrix}. \tag{2.34}$$

With the generalized Hadamard transform applied to an ancilla qubit, the state of the system consisting of the amplitude-damped N00N state and the ancilla qubit (up to a normalization factor) is

$$(|N\rangle_{c_1}|0\rangle_{c_2} + e^{-N\gamma t}|0\rangle_{c_1}|N\rangle_{c_2}) \otimes (\cos\theta|\Downarrow\rangle + \sin\theta|\Uparrow\rangle) \tag{2.35}$$

The N00N state basis consists of the orthonormal Fock states $\{|0\rangle, |N\rangle\}$ in each subsystem. Since each subsystem contains two basis they can mapped to the qubit basis, and hence, We also consider a CNOT gate acting on the subsystem containing the state of the second NVE (considered as the two-level system with the basis $|0\rangle_{c_2}, |N\rangle_{c_2}$) and the ancilla qubit.

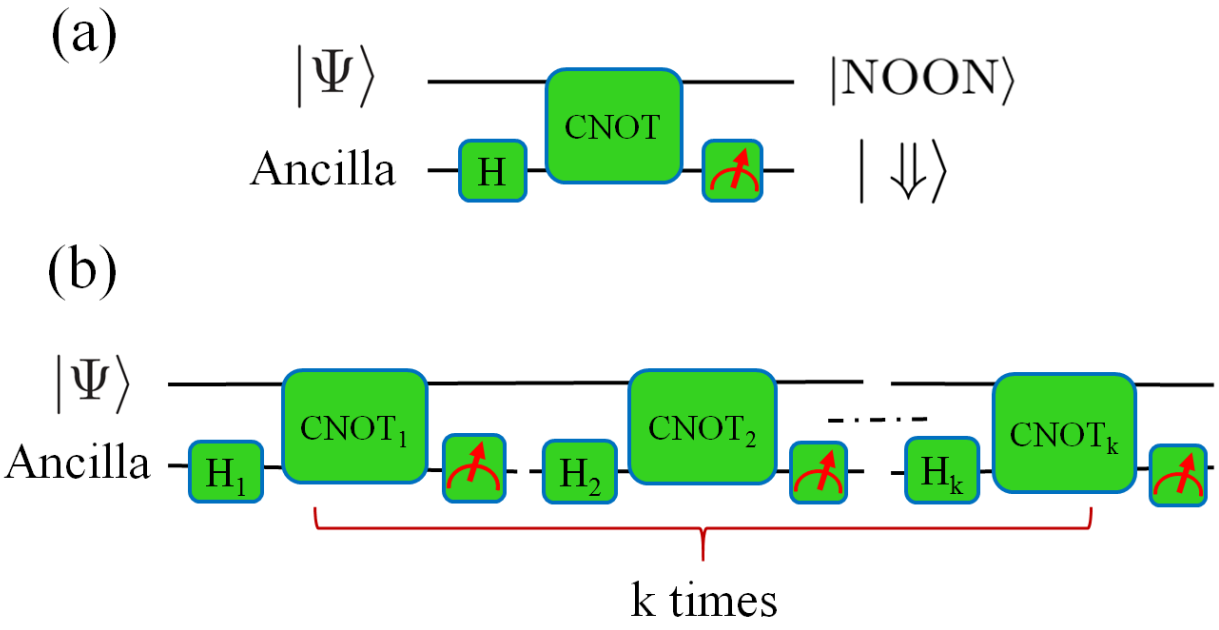

Figure 2.9: Reversal of a partial collapse of a N00N state induced by a weak measurement: (a) single-step and (b) k-step recovery procedures: H, generalized Hadamard gate; CNOT, CNOT gate. (Yusef Maleki and Aleksei M. Zheltikov,2018)

At the next step, the ancilla qubit is detected. When the outcome of this measurement is $|\Downarrow\rangle$, the N00N state is fully recovered [Fig.2.9(a)]. The success probability of this outcome is

$$p = \cos^2\theta = \frac{e^{-2N\gamma t}}{1+e^{-2N\gamma t}}. \tag{2.36}$$

If the outcome of ancilla-qubit detection is $|\Uparrow\rangle$, implying that

$$|\Psi\rangle = \frac{1}{\sqrt{1+e^{-4N\gamma t}}}(|N\rangle\otimes|0\rangle + e^{-2N\gamma t}|0\rangle\otimes|N\rangle), \tag{2.37}$$

the procedure should be repeated with the ancilla qubit set as $\tan\theta = e^{2N\gamma t}$. If the outcome of ancilla-qubit detection is now $|\Downarrow\rangle$, then the N00N state is recovered. Otherwise, we need to keep repeating this procedure setting the ancilla qubit as $\tan\theta = e^{kN\gamma t}$ at the kth step until ancilla-qubit detection yields the desired outcome [Fig.4.7(b)].

2.8 Quantum Metrology with Spin Cat States

A superposition of the spin coherent states can be expressed as

$$|\psi, j\rangle = \mathcal{N}(|\theta_1, \varphi_1, j\rangle + |\theta_2, \varphi_2, j\rangle). \tag{2.38}$$

The normalization factor of this cat state is given by

$$\mathcal{N} = \left[2 + \frac{(1+\bar{\delta}\gamma)^{2j} + (1+\bar{\gamma}\delta)^{2j}}{(1+|\delta|^2)^j(1+|\gamma|^2)^j}\right]^{-1/2} \tag{2.39}$$

A special class of this state could be given as

$$|\varphi, j\rangle = \mathcal{N}(|\theta, 0, j\rangle + |\pi - \theta, 0, j\rangle), \tag{2.40}$$

We are going to consider the performance of the spin cat state in Eq. (2.38) as a probe for the phase estimation. The parameter that we are interested in estimating is introduced as the phase shift ξ through $e^{i\xi J_z}$ to the state Eq. (2.38). Now, we are interested in determining the minimum error which can be obtained using such a cat state.

For the spin cat state in Eq. (2.38), the error of phase measurement $\Delta\xi$ is limited from below by the CRB, as mentioned above. To determine the CRB, one needs to obtain the quantum Fisher information $\mathcal{F}_Q$. Maximizing the quantum Fisher information results in minimum CRB. Therefore, states with larger quantum Fisher information are more desirable for phase estimation protocols.

For the cat state in Eq. (2.38), we find the Fisher information to be

$$\mathcal{F}_Q = 4(\mathcal{G}_2 + \mathcal{G}_1 - \mathcal{G}_1^2). \tag{2.41}$$

where,

$$\mathcal{G}_1 = 2j\mathcal{N}^2\left[\frac{|\gamma|^2}{1+|\gamma|^2} + \frac{|\delta|^2}{1+|\delta|^2} + \frac{(1+\bar{\delta}\gamma)^{2j-1}\bar{\delta}\gamma + (1+\bar{\gamma}\delta)^{2j-1}\bar{\gamma}\delta}{(1+|\delta|^2)^j(1+|\gamma|^2)^j}\right], \tag{2.42}$$

and

$$\mathcal{G}_2 = 2j(2j-1)\mathcal{N}^2\left[\frac{|\gamma|^4}{(1+|\gamma|^2)^2}+\frac{|\delta|^4}{(1+|\delta|^2)^2}+\frac{(1+\bar{\delta}\gamma)^{2j-2}(\bar{\delta}\gamma)^2+(1+\bar{\gamma}\delta)^{2j-2}(\bar{\gamma}\delta)^2}{(1+|\delta|^2)^j(1+|\gamma|^2)^j}\right]. \tag{2.43}$$

This provides an analytical solution for the spin cat state metrology in Eq. (2.38). From this expression, we immediately observe that the quantum Fisher information is a function of $\phi = \varphi_2 - \varphi_1$, thus CRB only depends on the phase differences rather than each of phases independently. Also, the quantum Fisher information is proportional to $2j$. Considering the photonic realization of the spin cat state, for instance, $2j$ is just the number of the photons N that is used to generate the spin cat states.

We note that $j = 1/2$ and $j = 1$ should be considered more carefully when $\bar{\gamma}\delta = -1$, due to the fact that some powers in the above expressions vanish. Thus, we will explicitly find the expressions for the Fisher information in these cases.

For $j = 1/2$, we simply have

$$\mathcal{F}_Q = 4\mathcal{N}^2\left[\frac{|\gamma|^2}{1+|\gamma|^2}+\frac{|\delta|^2}{1+|\delta|^2}+\frac{\bar{\delta}\gamma+\bar{\gamma}\delta}{(1+|\delta|^2)^{1/2}(1+|\gamma|^2)^{1/2}}\right] \tag{2.44}$$

Since $j = 1/2$ corresponds to $N = 1$, it does not provide quantum enhancement as shot-noise limit coincides with HL. Therefore, we investigate higher spin states. The cat states with $j = 1$, corresponds to two-photon states. For this case we have

$$\mathcal{G}_1 = 2\mathcal{N}^2\left[\frac{|\gamma|^2}{1+|\gamma|^2}+\frac{|\delta|^2}{1+|\delta|^2}+\frac{(1+\bar{\delta}\gamma)\bar{\delta}\gamma+(1+\bar{\gamma}\delta)\bar{\gamma}\delta}{(1+|\delta|^2)(1+|\gamma|^2)}\right], \tag{2.45}$$

and

$$\mathcal{G}_2 = 2\mathcal{N}^2\left[\frac{|\gamma|^4}{(1+|\gamma|^2)^2}+\frac{|\delta|^4}{(1+|\delta|^2)^2}+\frac{(\bar{\delta}\gamma)^2+(\bar{\gamma}\delta)^2}{(1+|\delta|^2)(1+|\gamma|^2)}\right]. \tag{2.46}$$

with

$$\mathcal{N} = \left[2 + \frac{(1+\bar{\delta}\gamma)^2 + (1+\bar{\gamma}\delta)^2}{(1+|\delta|^2)(1+|\gamma|^2)}\right]^{-1/2} \tag{2.47}$$

To analyse the performance of spin-1 probes, let us consider the states of the form

$$|\varphi, 1\rangle = \mathcal{N}(|\theta, \varphi, 1\rangle + |\pi - \theta, \varphi + \phi, 1\rangle), \tag{2.48}$$

Note that φ does not affect CRB and only the phase difference ϕ is important. For $\phi = \pi$ we have the superposition of two antipodal spin coherent states on the Bloch sphere, the so-called antipodal cat states. We plot phase estimation error bound for various ϕ in Fig. 2.10. Interestingly, the antipodal cat state reaches HL ($\Delta\xi = 1/2$) for any θ in this case. Thus, antipodal cat states are optimal in this case and provide a better sensitivity compared to the states of the type Eq.(2.40). The HL can also be directly obtain from the above analytical expression for the CRB. All of the states reach the HL for $\theta = 0, \pi$, as expected. This is due to the fact that, at these points, the cat states recast the superposition of the north and the south poles of the Bloch sphere, where the azimuthal phases become irrelevant. In other words, the cat states reduced to the conventional NOON states. The states with $\phi \neq \pi$ provide maximum error for $\theta = \pi/2$. In this case, both coherent states lay on the great circle at $z = 0$ on the Bloch sphere. The cat state with $\phi = 0$, reduces to the shot-noise limit at $\theta = \pi/2$.

To consider the effects of polar angles on the metrology, we present the CRB as a function of θ_1 and θ_2 in Fig. 2.11, for $\phi = 0$ and $\phi = \pi$. This Figure shows that minimum error for such cat states are those with $\theta_2 = \pi - \theta_1$. This also shows that the antipodal cat states reach HL for all cases.

Now, a natural question is whether all antipodal cat states provide HL precision, with any j. To figure this out, and to consider the cat states with larger j in more details, let us consider the states of the form

$$|\varphi, j\rangle = \mathcal{N}(|\theta, \varphi, j\rangle + |\pi - \theta, \varphi + \phi, j\rangle). \tag{2.49}$$

We plot the CRB as a function of θ for various cases in Fig. 2.12.

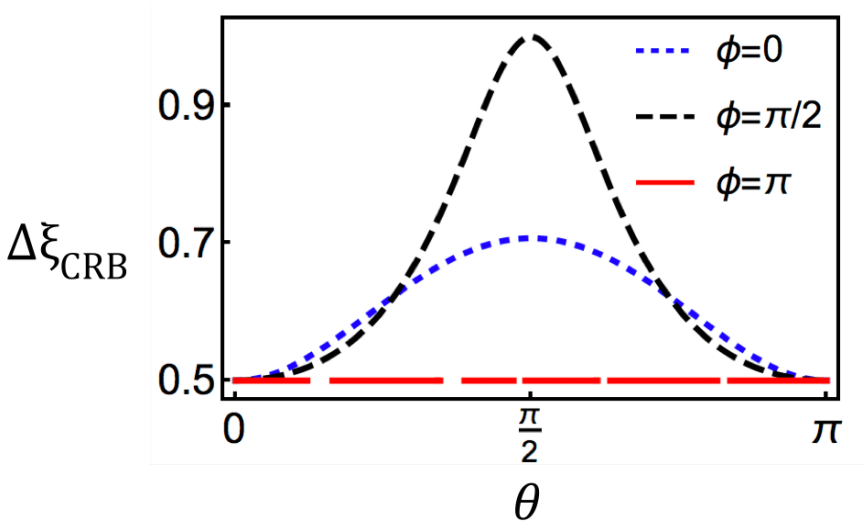

Figure 2.10: The CRB in terms of θ. $\phi = 0$ dotted. $\phi = \pi/2$ dashed. $\phi = \pi$ solid.

It is clear that, in these cases the antipodal cat states do not provide the HL anymore. However, in all cases the antipodal cat states provide better precision compared to the cases with $\phi = 0$ as in Eq. (2.40). First, let us see if there is any antipodal cat states which could provide HL metrology. Noting that, for the antipodal cat states we have $\bar{\gamma}\delta = -1$, the quantum Fisher information in Eq. (2.41) can be simplified to

$$\mathcal{F}_Q = 4\left[j(2j-1)\frac{1+|\gamma|^4}{(1+|\gamma|^2)^2} + j - j^2\right]. \tag{2.50}$$

This provides a closed-form expression of the Fisher information of any antipodal cat state with j larger than 1. Now, the HL precision could be achieved under the condition $\mathcal{F}_Q = N^2 = 4j^2$. Combining this with $\mathcal{F}_Q$ we immediately find that HL could be fulfilled only for $|\gamma| = 0$ or ∞. Or equivalently for $\theta = 0, \pi$. However, this means that the cat state reduces to the superposition of the north and south poles of the Bloch sphere, which is nothing but the conventional N00N state. Therefore, it is quite interesting that $j = 1$ antipodal cat state is the only state of this type which provides HL for any θ. Another interesting insight from the above relation can be achieved is that maximum error (minimum Fisher information) can be obtained for $|\gamma| = 1$ ($\theta = \pi/2$). This maximum error is given by the shot-noise limit as the Fisher information in this case reduces

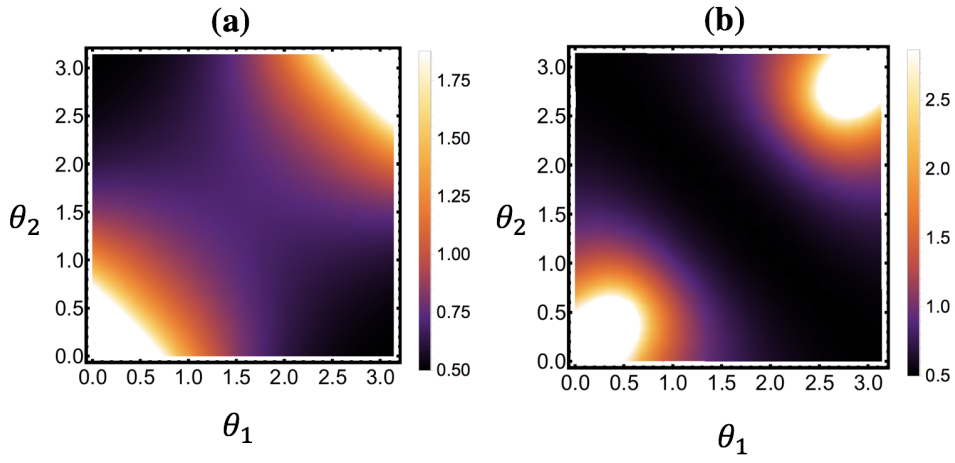

Figure 2.11: Density of the CRB in terms of θ_1 and θ_2. (a) $\phi = 0$. (b) $\phi = \pi$.

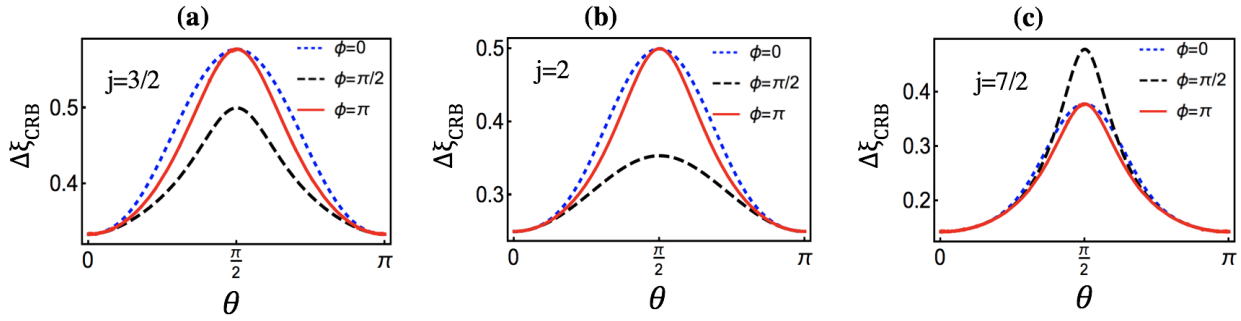

Figure 2.12: The CRB in terms of θ. $\phi = 0$ dotted. $\phi = \pi/2$ dashed. $\phi = \pi$ solid.

to $\mathcal{F}_Q = 2j$. Geometrically, this means that any antipodal cat state on the $z = 0$ circle of the Bloch sphere (on the equator) provides shot-noise limit sensitivity, while any other state away from this circle provides quantum enhancement, suppressing the shot-noise limit. In other words, the precision with antipodal cat states vary between shot-noise limit on the equator of the Bloch sphere to the HL on the poles. The further away from the equator we move, the more sensitivity could be attained. The other important feature that can be observed from Fig. 2.12 is that, for all spins, the cat states with $\phi = \pi$ provide better sensitivity compared to the ones with $\phi = 0$. To see if this could be the case for all spins, we find the Fisher information for the states with $\phi = 0$. For

these states $\bar{\gamma}\delta = 1$, and the Fisher information reduces to

$$\mathcal{F}_Q = 4\left[\frac{j(2j-1)}{1+\mathcal{A}^{2j}}\left(1-\frac{1}{2}\mathcal{A}^2+\frac{1}{2}\mathcal{A}^{2j}\right)+j-j^2\right], \tag{2.51}$$

where

$$\mathcal{A} = \frac{2|\gamma|}{1+|\gamma|^2}.$$

With this relation, it is straightforward to prove that the Fisher information of the antipodal cat states in Eq. (19) is always larger, providing a better error suppression in phase estimation. Both of these class of states provide shot-noise limit at $\theta = \pi/2$.

In [63], it was found that for the states in the class of Eq. (2.40), when $j \geqslant 20$, and $\theta \leqslant 7\pi/20$, the CRB could be approximately obtained as

$$\Delta\xi_{CRB} \simeq \left(\frac{1+\tan^2\theta/2}{1-\tan^2\theta/2}\right)N^{-1}, \tag{2.52}$$

where, $N = 2j$. Now, we would like to see how this result could be understood considering the more generic and exact result of Eq. (2.51). To understand this, we simply seek the condition such that $\mathcal{A}^{2j} \ll 1$. That means we take $\theta \neq \pi/2$, and take j large enough. With this approximation we attain

$$\mathcal{F}_Q \simeq 4\left[j^2 - j(2j-1)\frac{1}{2}\mathcal{A}^2\right]. \tag{2.53}$$

Since, j is large enough, $j(2j-1) \simeq 2j^2$, we attain

$$\mathcal{F}_Q \simeq 4j^2\left[1-\mathcal{A}^2\right] = N^2\left[\frac{1-|\gamma|^2}{1+|\gamma|^2}\right]. \tag{2.54}$$

Considering the fact that $|\gamma| = \tan^2\theta/2$, we immediately arrive at the result of [63]. As an interesting feature, the large spin limit of the antipodal cat state also provides the same result, as above. Our proof suggests that this approximated solution could be valid beyond the scope of approximation made in Ref. [63], and demonstrates the significance of the generic and exact

solution provided in this work.

The other class of states shown in Fig. 2.12, is the states with $\phi = \pi/2$. Such a cat state provides much better error sensitivity for $j = 3/2$ and 2, while it does not provide a better error suppression for $j = 7/2$, when compared to $\phi = 0, \pi$. Hence, these states are highly dependant on the spins of the system. In other words, by fixing all parameters except the spin, for some states we can suppress the shot noise limit, while for others we may not. Therefore, delicate engineering of the phases can be used to determines states that can be better than antipodal cat states for the phase estimation purposes. Comparing the subplots in Fig. 2.12, it is clear that by increasing spin the error is more suppressed for $\phi = 0\&\pi$. However, it may not be the case for $\phi = \pi/2$. Note that, it is usually believed that increasing number of photons can assist in attaining better resolution; however, our observations shows that it may not be the case in general. That means, feeding more photons to the scheme may even degrade the resolution of phase sensitivity. This feature, could not be captured in the limited class of sta] tes in Ref. [63], where the precision always increases as the spin enhances. This reveals the significant role of the azimuthal angles on phase estimation. To analytically find the CRB for $\phi = \pi/2$, we can obtain the Fisher information elements such that

$$\mathcal{G}_1 = \frac{j}{1 + \frac{2^j \cos(\frac{\pi}{2} j)|\gamma|^{2j}}{(1+|\gamma|^2)^{2j}}} \left[1 - \frac{2^{j+1/2} \sin(\frac{\pi}{4}[2j-1])|\gamma|^{2j}}{(1+|\gamma|^2)^{2j}}\right], \tag{2.55}$$

and

$$\mathcal{G}_2 = \frac{j(2j-1)}{1 + \frac{2^j \cos(\frac{\pi}{2} j)|\gamma|^{2j}}{(1+|\gamma|^2)^{2j}}} \left[\frac{1+|\gamma|^4}{(1+|\gamma|^2)^2} - \frac{2^j \sin(\frac{\pi}{2} j)|\gamma|^{2j}}{(1+|\gamma|^2)^{2j}}\right]. \tag{2.56}$$

From these expressions it is easy to verify the behavior of cat state which is presented in Fig. 2.12. For instance, at $\theta = \pi/2$, for $j = 3/2$ we obtain $\Delta\xi_{CRB} = 1/2$, for $j = 2$ we get $\Delta\xi_{CRB} = 1/\sqrt{8}$ and for $j = 7/2$ we obtain $\Delta\xi_{CRB} \approx 0.48$.

To illustrate the effect of variation in the polar angles, we plot the CRB of the antipodal spin cat states with $j = 3\&10$ in Fig. 2.13. In both cases, it could be concluded that the error could be large when $\theta_1 = \theta_1$, and when both coherent states are on the same poles the error diverges, as expected.

While, the error could be reduced as the coherent states move further towards the opposite poles on the Bloch sphere, providing HL at the opposite poles. Hence, a class of cat states of the form

$$|\psi, j\rangle = \mathcal{N}(|\theta, \varphi, j\rangle + |\theta, \varphi + \pi, j\rangle), \tag{2.57}$$

can never beat the shot noise limit, independent of the spins and coherence parameters. Thus, these states are not quantum metrologically useful. Similar observations could be achieved for $\phi = 0$.

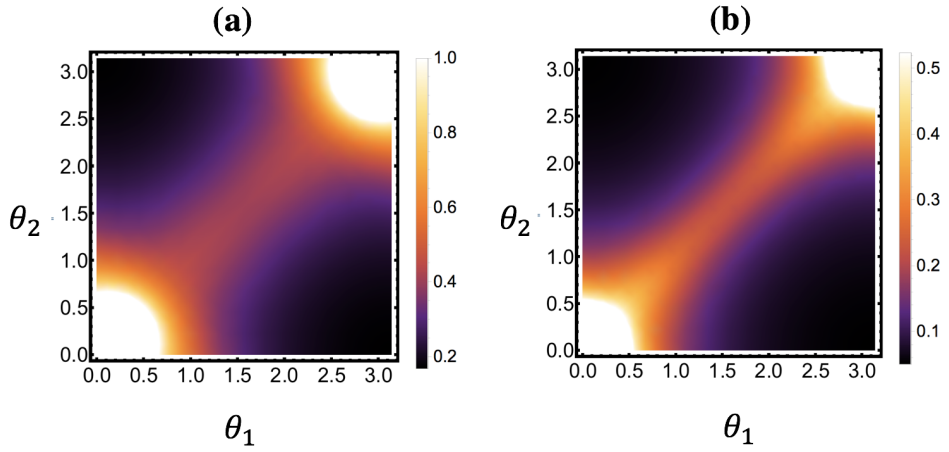

Figure 2.13: Density of the CRB in terms of θ_1 and θ_2 for $\phi = \pi$. (a) $j = 3$. (b) $j = 10$.

As a specific consequence of, our result, using a single spin coherent state as a probe, i.e., $|\psi, j\rangle = |\theta, \varphi, j\rangle$, the Fisher information can be obtained to be

$$\mathcal{F}_Q = 8j \frac{|\gamma|^2}{(1 + |\gamma|^2)^2} = 2j\mathcal{A}. \tag{2.58}$$

Therefore, a single spin coherent state, can never beat the shot-noise limit, and hence, spin cat states are crucial for attaining quantum advantages.

3. MACROSCOPIC TRIPARTITE ENTANGLEMENT OF NITROGEN-VACANCY CENTERS IN DIAMOND COUPLED TO A SUPERCONDUCTING RESONATOR [1]

3.1 Introduction

In this chapter, we consider a hybrid quantum device containing three separated NVEs coupled to a common coplanar waveguide resonator (CPWR) (see Fig. 3.1), where, the collective magnetic coupling between NVEs and CPWR is used to generate entanglement among the NVEs which are initially in their ground states following [64, 65]. This provides a practical architecture for realizing multipartite entangled states in NVEs, which is of paramount importance in the NVE-assisted quantum network and is a valuable physical resource in large-scale quantum information processing.

Detecting entanglement in a quantum system is of paramount importance in quantum information science [66–68]. The most general approach for detection of quantum entanglement in any given quantum system is based on the notion of entanglement witness [66–68], as a physical observable which can be engineered experimentally. Thus, we consider the detection of tripartite entanglement among NVEs by exploiting suitable entanglement witnesses. The dynamics of the expectation value of the entanglement witnesses provide a useful tool for quantifying and detecting entanglement. The generated state can have a large overlap with maximally entangled GHZ by controlling the relavant parameters in the system. The effects of decoherence on the expectation value of the entanglement witnesses can be destructive, and in some cases preventing the entanglement to be detected.

We are going to show that the entanglement generation is highly dependent on the initial state of the hybrid system, where a proper preparation of CPWR can be used for entangling NVEs.

[1] This chapter is partly based on the following journal publications with the permission: (i) Reprinted with permission from "Witnessing quantum entanglement in ensembles of nitrogen–vacancy centers coupled to a superconducting resonator" by Yusef Maleki, Aleksei Zheltikov, 2018 *Opt. Express* **26** 17849-17858, Copyright [2020] by The Optical Society (OSA). (ii) Reprinted with permission from "Macroscopic tripartite entanglement of nitrogen-vacancy centers in diamond coupled to a superconducting resonator" by Yusef Maleki, Aleksei Zheltikov, 2019 *J. Opt. Soc. Am. B* **36** 443-450, Copyright [2020] by The Optical Society (OSA).

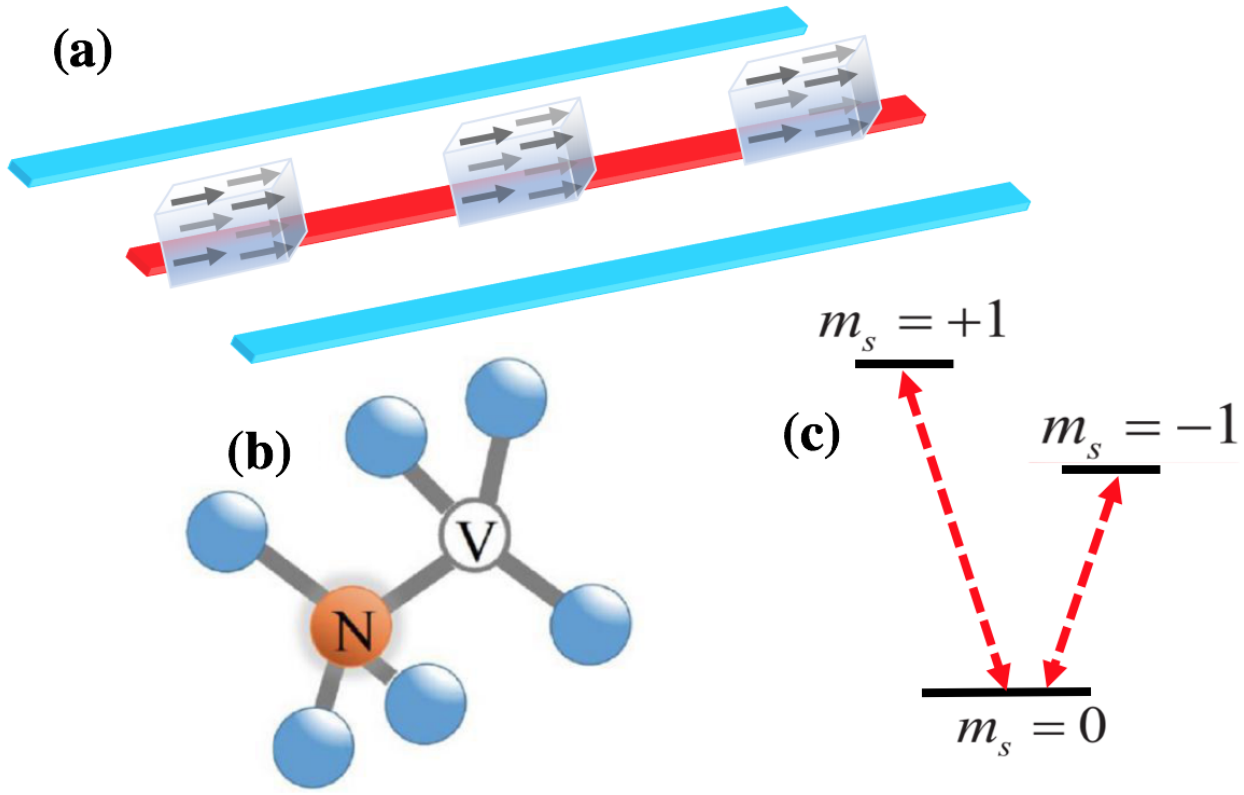

Figure 3.1: (a) Three ensembles of NV centers coupled to a superconducting coplanar waveguide resonator. (b, c) Crystal-lattice (b) and energy (c) diagrams of an NV center in diamond. (Yusef Maleki and Aleksei M. Zheltikov,2019)

When the CPWR is initially prepared as a cat state of coherent states, the entanglement of NVEs oscillates periodically, and the maximal entanglement always happens when the CPWR disentangles from the rest of the system. The entanglement degree between the NVEs strongly depends on the initial state of the CPWR, the collective coupling parameter and the interaction time. The maximal entanglement can be tuned by adjusting these parameters, enabling generation of highly entangled quasi-GHZ macroscopic entangled states as well as controlling the entanglement.

3.2 Entanglement generation

The superconducting coplanar waveguide resonator consisting of the length L, the capacitance C_c, and the inductance F_c contains two nearby lateral ground planes and a narrow center conductor, which can be described by the harmonic oscillator operators, and thus, its Hamiltonian can be

written as $H_C = \hbar\omega_c a^\dagger a$, where a ($a^\dagger$) is the annihilation (creation) operator of the microwave mode of the resonator, and its corresponding eigenfrequency is determined by [69, 70]

$$\omega_c = 2\pi/\sqrt{C_c F_c}.$$

The distributions of current and voltage inside the CPWR can be described as

$$I_{qpw} = i\sqrt{C_c/F_c}(a^\dagger - a)\sin(2\pi/Lx),$$

and

$$V_{qpw} = \sqrt{\omega_c/C_c}(a^\dagger + a)\cos(2\pi/Lx).$$

The ground state of an NV center, as was already discussed, is a spin triplet with zero-magnetic-field splitting $D_{gs}/2\pi$ = 2.87 GHz between the $m_s = 0$ sublevel and the degenerate $m_s = \pm 1$ sublevels (see Fig.3.1 (b)&(c)). An external magnetic field B_{ext} applied along the [111] direction of the diamond crystal lattice (parallel to the resonator plane) removes the degeneracy of $|m_s = \pm 1\rangle$ sublevels, by inducing Zeeman splitting and tunes the transition energies. Again, considering only the two $m_s = 0$ to $m_s = -1$ sublevels we can isolate our investigation into a two-level system. Thus, for an ansanble of spins in each NVE, the HP transformation is vaid [49].

With this description, the total Hamiltonian of the NVE–CPWR hybrid system considered here can now be written (in units of $\hbar = 1$) as

$$H = \omega_c a^\dagger a + \sum_{j=1}^{3} \omega_{NV} b_j^\dagger b_j + \sum_{j=1}^{3} g_j (b_j^\dagger a + a^\dagger b_j), \tag{3.1}$$

where g_i is the coupling strength for the ith NVE and the CPWR. We assume that the frequency of the NVEs are tuned to be at resonance with the CPWR $\omega_c = \omega = \omega_{NV}$.

We are going to show now that, starting from this Hamiltonian, we can create an entangled state shared among the the NVE memories. To this end, we prepare the CPWR (up to a normalization

factor) in the macroscopic cat even (odd) state

$$|\alpha\rangle_c \pm |-\alpha\rangle_c$$

where the plus (minus) sign is for the even (odd) cat state. Here, $|\alpha\rangle_c$ denotes the coherent state of the microwave mode. The cat state described here can be generated by first keeping all the NVEs off the resonance with the CPWR and coupling it to a qubit [71]. The dynamics of the resonator–qubit system can be used to generate the desire cat state. This method can generate a large cat state consisting of more than 100 photons in a superconducting resonator [71] . Thus, the resonator is prepared in cat state, and the i-th NVE in its ground state $|0\rangle$. The initial state of the entire system is thus given as

$$|\psi_{\pm}(0)\rangle = \frac{1}{\sqrt{2 \pm 2e^{-2|\alpha|^2}}}(|\alpha\rangle_c \pm |-\alpha\rangle_c)|0\rangle|0\rangle|0\rangle. \tag{3.2}$$

The time evolved wave function $|\psi_{\pm}(t)\rangle$ of the whole NVEs–CPWR system can be obtained by applying the time evolution operator $U(t) = e^{-iHt/\hbar}$ on $|\psi_{\pm}(0)\rangle$, and the dynamics of operator $O(t)$ can be given as $O(t) = U(t)O(0)U^{\dagger}(t)$, where $O(0) \equiv O$ is the operator at $t = 0$.

The time evolved wave function $|\psi(t)\rangle$ of the whole NVEs–CPWR system can be obtained by applying the time evolution operator $U(t) = e^{-iHt/\hbar}$ on $|\psi(0)\rangle$, and the dynamics of operator $O(t)$ can be given as $O(t) = U(t)O(0)U^{\dagger}(t)$, where $O(0) \equiv O$ is the operator at $t = 0$. Considering the dynamics of the operators of the subsystems using Hesenberg equation, i.e., $dO(t)/dt = -i/\hbar[H, O]$, we have

$$\begin{pmatrix} da(t)/dt \\ db_1(t)/dt \\ db_2(t)/dt \\ db_3(t)/dt \end{pmatrix} = \begin{pmatrix} -i\omega & -ig_1 & -ig_2 & -ig_3 \\ -ig_1 & -i\omega & 0 & 0 \\ -ig_2 & 0 & -i\omega & 0 \\ -ig_3 & 0 & 0 & -i\omega \end{pmatrix} \begin{pmatrix} a(t) \\ b_1(t) \\ b_2(t) \\ b_3(t) \end{pmatrix}.$$

Thus, the NVE–CPWR system initially prepared in the state given by Eq.(3.2) evolves in time

according to

$$|\psi_{\pm}(t)\rangle = |\alpha(t)\rangle_c \otimes |\beta_1(t)\rangle \otimes |\beta_2(t)\rangle \otimes |\beta_3(t)\rangle$$
$$\pm |-\alpha(t)\rangle_c \otimes |-\beta_1(t)\rangle \otimes |-\beta_2(t)\rangle \otimes |-\beta_3(t)\rangle, \tag{3.3}$$

where

$$\alpha(t) = e^{-i\omega t}\alpha\cos(Gt),$$

and

$$\beta_i(t) = -ie^{-i\omega t}\alpha\frac{g_i\sin(Gt)}{G}.$$

Also, the parameter G is given by

$$G = \sqrt{g_1^2 + g_2^2 + g_3^2}.$$

Generally, both the NVEs and the CPWR may become entangled as a result of this time evolution. However, we are concerned here with the entanglement that builds up in the three NVEs. To quantify this entanglement, we trace out the CPWR subspace to obtain the reduced density operator related to the NVEs,

$$\rho_{NV\pm}(t) = Tr_{CPWR}(|\psi_{\pm}(t)\rangle\langle\psi_{\pm}(t)|,$$

which gives

$$\rho_{NV\pm}(t) = N_{\pm}^2[|\beta_1(t)\rangle\langle\beta_1(t)| \otimes |\beta_2(t)\rangle\langle\beta_2(t)| \otimes |\beta_3(t)\rangle\langle\beta_3(t)|$$
$$+|-\beta_1(t)\rangle\langle-\beta_1(t)| \otimes |-\beta_2(t)\rangle\langle-\beta_2(t)| \otimes |-\beta_3(t)\rangle\langle-\beta_3(t)|$$
$$\pm q(t)||\beta_1(t)\rangle\langle-\beta_1(t)| \otimes |\beta_2(t)\rangle\langle-\beta_2(t)| \otimes |\beta_3(t)\rangle\langle-\beta_3(t)|$$
$$\pm q(t)|-\beta_1(t)\rangle\langle\beta_1(t)| \otimes |-\beta_2(t)\rangle\langle\beta_2(t)| \otimes |-\beta_3(t)\rangle\langle\beta_3(t)|]. \tag{3.4}$$

Here,

$$q(t) = e^{-2|\alpha|^2 \cos^2(Gt)}$$

and N is the normalization factor, which can be written as

$$N_{\pm} = [2 \pm 2e^{-2|\alpha|^2}]^{\frac{-1}{2}}$$

With an appropriate encoding of the logical bases, the above density matrix can be mapped onto a three-qubit state. With this goal in mind, we choose the following orthogonal basis:

$$|\mathbf{0}\rangle_i \equiv |\beta_i(t)\rangle, \quad |\mathbf{1}\rangle_i \equiv \frac{1}{\sqrt{1-p_i^2(t)}}(|-\beta_i(t)\rangle - p_i(t)|\beta_i(t)\rangle),$$

where

$$p_i(t) = e^{-2(g_i/G)^2|\alpha|^2 \sin^2(Gt)}.$$

The coherent states $|\pm\beta_i(t)\rangle$ can then be expressed as

$$|\beta_i(t)\rangle \equiv |\mathbf{0}\rangle_i, \qquad |-\beta_i(t)\rangle \equiv p_i(t)|\mathbf{0}\rangle_i + \sqrt{1-p_i^2(t)}|\mathbf{1}\rangle_i.$$

3.3 Witnessing entanglement in the system

In order for detecting entanglement in tripartite state one can use a relevant entanglement witness. Here, we use the entanglement witness of the GHZ state for both even and odd input cat states which can detect the states close to the GHZ state [72, 73]. The three-qubit GHZ state is defined as [72, 73]

$$|GHZ\rangle = \frac{1}{\sqrt{2}}(|000\rangle + |111\rangle).$$

First, we consider the detection of entanglement for the even coherent state input $N_+(|\alpha\rangle_c + |-\alpha\rangle_c)$ with the density matrix $\rho_{NV+}(t)$. The corresponding entanglement witness for the even coherent

state input can be given as [72, 73]

$$\hat{W}_{GHZ} = \frac{1}{2} I \otimes I \otimes I - |GHZ\rangle\langle GHZ|$$

This witness can detect genuine three-partite entanglement when

$$Tr(\hat{W}_{GHZ}\rho_{NV+}(t)) < 0.$$

The expectation value of the witness operator $\hat{W}_{GHZ}$ with respect to $\rho_{NV+}(t)$, after encoding to a three-qubit density matrix, can be calculated as

$$\begin{aligned} EW = Tr(\hat{W}_{GHZ}\rho_{NV\pm}(t)) = \frac{1}{4+4e^{-2|\alpha|^2}}[p_1^2(t) + p_2^2(t) \\ + p_3^2(t) - p_1^2(t)p_2^2(t) - p_1^2(t)p_3^2(t) - p_2^2(t)p_3^2(t) - 2[q(t) \\ + p_1(t)p_2(t)p_3(t)]\sqrt{1-p_1^2(t)}\sqrt{1-p_2^2(t)}\sqrt{1-p_3^2(t)}]. \end{aligned} \tag{3.5}$$

If one of NVEs does not couple to the rest of the system then one has a biseperable state where the entanglement may be generated between the two remaining NVEs. For instance, if the first NVE remains uncoupled to the rest of the system ($g_1 = 0$), then we have $p_1(t) = 0$. Hence, the expectation value of entanglement witness will reduce to

$$EW(p_1(t) = 0) = \frac{1}{4+4e^{-2|\alpha|^2}}[1 - p_2^2(t)p_3^2(t)].$$

Thus, the entanglement witness above can be negative only when the entanglement is distributed among all the three NVEs, otherwise the expectation value of the entanglement witness shall not be negative.

We plot the dynamics of the expectation values of the entanglement witness in Fig.3.2 for various coherence parameters. Fig.3.2(a) depicts EW when the coupling strength of the NVEs are

the same, i.e., $g_1 = g_2 = g_3$. In this case $p_1(t) = p_2(t) = p_3(t) = p(t)$ and EW simplifies to

$$EW(p(t)) = \frac{[1-p^2(t)]}{4+4e^{-2|\alpha|^2}}[3p^2(t) - 2[q(t)+p^3(t)]\sqrt{1-p^2(t)}].$$

Thus, detection of entanglement requires

$$3p^2(t) - 2[q(t)+p^3(t)]\sqrt{1-p^2(t)} < 0.$$

Accordingly, the entangled state can be detected when Gt is close enough to $(2k+1)\pi/2$, and EW presents a periodic behavior in terms of Gt. For large enough α, EW can be close to $-1/2$ indicating a large overlap between the density matrix and the three-qubit GHZ state. Fig.3.2(b) is plotted for $g_2 = 0.5g_1$ and $g_3 = 1.5g_1$. The variation in the coupling of each of the NVEs does not effect the periodic pattern of the EW, where only the overall coupling G effects the periodic behavior of the EW in time. In both cases the minimum of EW can be found at $Gt = (2k+1)\pi/2$, where the resonator is completely depleted from the photons and all the photons are shared as expectations of the NVEs. When the couplings are not identical the overlap of the density matrix and the GHZ state is smaller. As can be seen from Fig.3.2(b) when the coherence parameter α is very small, EW mostly becomes a positive number and detection of largely entangled state fails. As is clear from Fig.3.2 when α is very large, the range of Gt at the vicinity of $(2k+1)\pi/2$ where the entanglement can be detected shrinks. For $\alpha \to \infty$, $EW \to -1/2$ when $Gt = (2k+1)\pi/2$; otherwise, $EW \to 0$.

Now, we consider detection of entanglement when the input state is an odd cat state of the form $N_-(|\alpha\rangle_c - |-\alpha\rangle_c)$; here, the density matrix of the final state is given by $\rho_{NV-}(t)$. In this case we use an other form of the maximally entangled GHZ state which can be obtained from a local operation on the GHZ state as

$$(I \otimes I \otimes \sigma_z)|GHZ\rangle = \frac{1}{\sqrt{2}}(|000\rangle - |111\rangle).$$

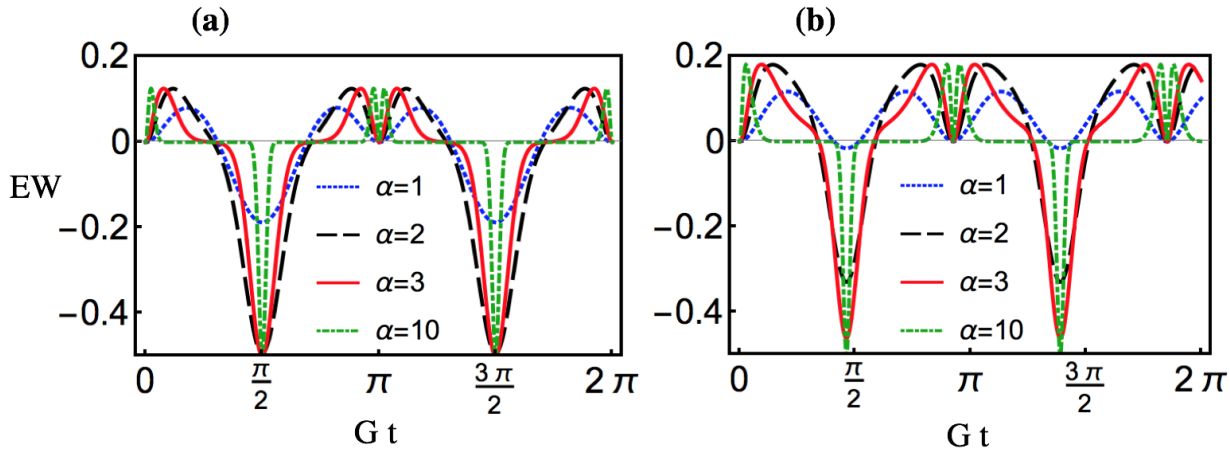

Figure 3.2: Time evolution of EW for entanglement of ensembles of NV centers with even cat state as the input state, for various coherence parameters α. (a) For $g_1 = g_2 = g_3$. (b) For $g_2 = 0.5g_1$ and $g_3 = 1.5g_1$. (Yusef Maleki and Aleksei M. Zheltikov,2018)

The corresponding entanglement witness for the odd cat input state can be given as [72, 73]

$$\hat{W'}_{GHZ} = \frac{1}{2} I \otimes I \otimes I - (I \otimes I \otimes \sigma_z)|GHZ\rangle\langle GHZ|(I \otimes I \otimes \sigma_z)$$

The expectation value of the witness operator $\hat{W'}_{GHZ}$ with respect to $\rho_{NV-}(t)$, after encoding to a three-qubit density matrix, can be calculated as

$$\begin{aligned} EW = Tr(\hat{W'}_{GHZ}\rho_{NV-}(t)) = \frac{1}{4 - 4e^{-2|\alpha|^2}}[p_1^2(t) + p_2^2(t) \\ + p_3^2(t) - p_1^2(t)p_2^2(t) - p_1^2(t)p_3^2(t) - p_2^2(t)p_3^2(t) - 2[q(t) \\ - p_1(t)p_2(t)p_3(t)]\sqrt{1 - p_1^2(t)}\sqrt{1 - p_2^2(t)}\sqrt{1 - p_3^2(t)}]. \end{aligned} \tag{3.6}$$

The expectation values of the entanglement witness are again periodic functions of Gt (Fig. 3.3). However, we see that EW have larger peak values. In this case when $p_1(t) = p_2(t) = p_3(t) = p(t)$, EW simplifies to

$$EW(p(t)) = \frac{[1 - p^2(t)]}{4 - 4e^{-2|\alpha|^2}}[3p^2(t) - 2[q(t) - p^3(t)]\sqrt{1 - p^2(t)}].$$

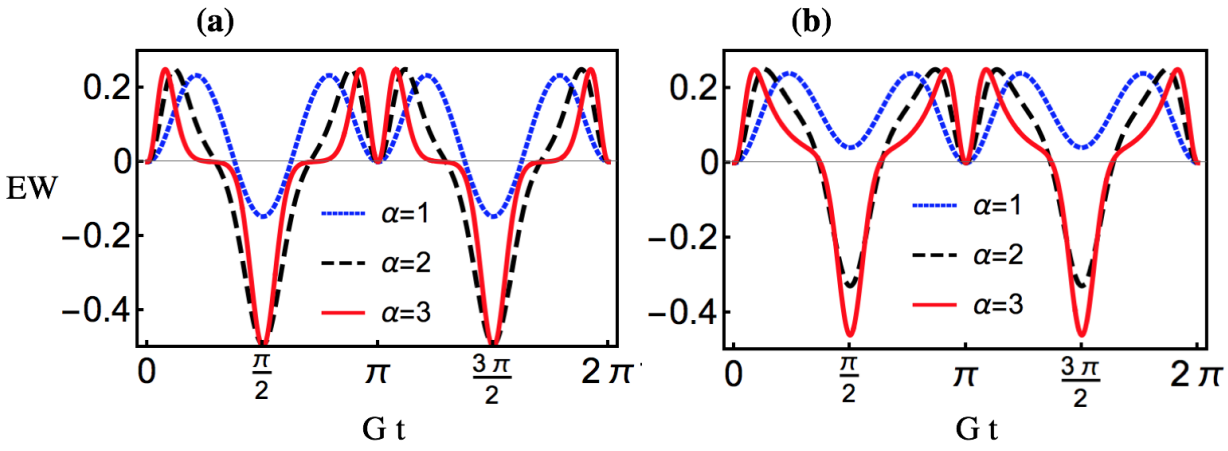

Figure 3.3: Time evolution of EW for entanglement of ensembles of NV centers with odd cat state as the input state, for various coherence parameters α. (a) For $g_1 = g_2 = g_3$. (b) For $g_2 = 0.5g_1$ and $g_3 = 1.5g_1$. (Yusef Maleki and Aleksei M. Zheltikov,2018)

Thus, entanglement can be detected when

$$3p^2(t) - 2[q(t) - p^3(t)]\sqrt{1 - p^2(t)} < 0.$$

Comparing this inequality with a similar condition obtained for even-cat input states, we see that, entanglement detection in the case of odd-cat input state imposes more stringent requirements on $p(t)$. When α is small, entanglement detection through the entanglement witness fails.

As is readily seen in Fig. 3.3, minimum EW values are achieved at $Gt = (2k+1)\pi/2$, when all the photons are shared between the NVEs, leaving the resonator completely depleted of photons. When the couplings between individual NVEs are not identical, the overlap of the NVE state and the GHZ state is smaller. As can be seen from Fig. 3.3(b) when the coherence parameter α is small, EW becomes positive, and entanglement detection fails. When α is very large, entanglement can be detected only within a very narrow range of Gt near $(2k + 1)\pi/2$. For $\alpha \to \infty$, we have $EW \to -1/2$ when $Gt = (2k + 1)\pi/2$; $EW \to 0$ otherwise.

To quantify the overlap between the considered class of entangled states and the maximally entangled GHZ state, we consider the fidelity of the considered entangled states with respect to the

ideal GHZ states. Applying a standard definition of the fidelity [2]

$$F(\rho,\sigma) = Tr(\sqrt{\sqrt{\rho}\sigma\sqrt{\rho}})^2$$

to the density matrices ρ and σ of the considered entangled states and the ideal GHZ states, we find

$$F_{\pm} = \frac{1}{4 \pm 4q(t)p_1(t)p_2(t)p_3(t)}[1 + p_1^2(t)p_2^2(t)p_3^2(t) \pm 2q(t)p_1(t)p_2(t)p_3(t) + (1 - p_1^2(t))(1 - p_2^2(t)) \times(1 - p_3^2(t)) + 2[q(t) \pm p_1(t)p_2(t)p_3(t)]\sqrt{1 - p_1^2(t)}\sqrt{1 - p_2^2(t)}\sqrt{1 - p_3^2(t)}],$$

where the fidelity F_+ and F_- measures the closeness of the state with the density matrix ρ_{NV+} to the maximally entangled GHZ state $|GHZ\rangle$ and F_- characterizes the closeness of the state with ρ_{NV-} to the GHZ state $(\sigma_z \otimes I \otimes I)|GHZ\rangle$.

In the special case of $p_1(t) = p_2(t) = p_3(t) = p(t)$, $F_{\pm}$ simplifies to

$$F_{\pm} = \frac{1}{4 \pm 4q(t)p_1(t)p_2(t)p_3(t)}[1+p^6(t)\pm 2q(t)p^3(t)+2(q(t)\pm p^3(t))(1-p^2(t))^{3/2}+(1-p^2(t))^3].$$

For both even- and odd-cat input states, the fidelity is a periodic function of dimensionless time Gt (Fig. 3.4), reaching its maximum value at $Gt = (2k + 1)\pi/2$. As the coherence parameter increases, the NVE state gets closer to the maximally entangled state, with the fidelity approaching 1 for moderate values of the coherence parameter. This indicates that NVEs are approaching maximally entangled GHZ states. At $t = 0$, the fidelity is exactly $1/2$, as expected, since all the NVEs are in their ground states.

3.3.1 Effect of decoherence on EW

In any realistic experimental implementation, entanglement detection is inevitably subject to decoherence. To examine decoherence effects, we consider an experimental scheme where the resonator is tuned to the zero-field splitting frequency of NV centers with a suitable choise of electric circuit parameters. Specifically, to tune the resonator frequency to $D_{gs}/2\pi$ = 2.87 GHz,

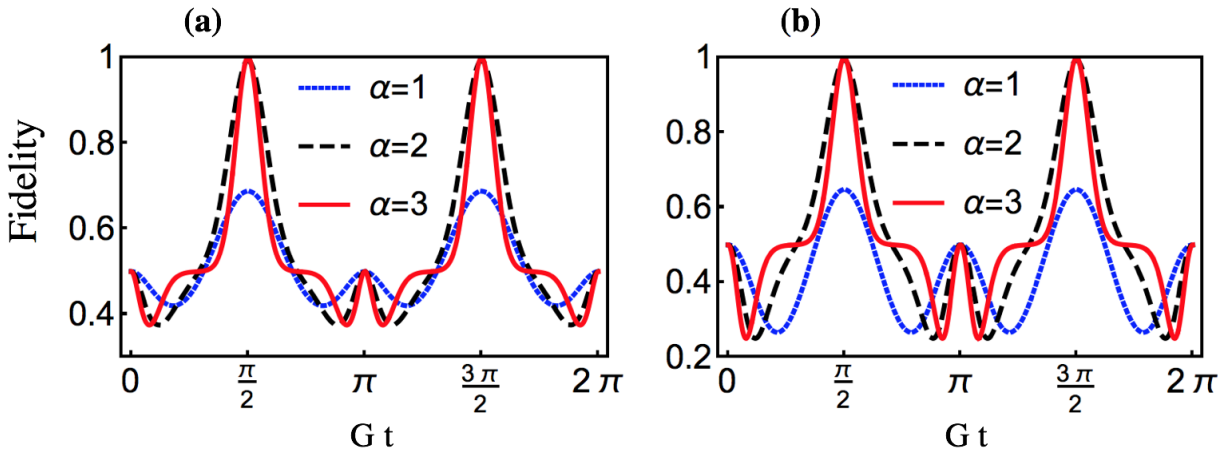

Figure 3.4: Time dependence of the fidelity (a) F_+ and (b) F_- with $g_1 = g_2 = g_3$. (Yusef Maleki and Aleksei M. Zheltikov,2018)

the CPWR should be designed to have an inductance F_c = 60.7 nH and a capacitance C_c = 2 pF [69].

For a single NV center placed 1 μm above the center, the coupling strength induced by the CPWR conductor is $g_0/2\pi \approx 12$ Hz. This is well below the decoherence rate of the resonator, $\kappa/2\pi \approx 1$ MHz. However, for $\approx 10^{12}$ NV centers coupled to a superconducting resonator, a collective coupling, $g/2\pi \approx 10$ MHz, exceeding the coherence rate of both the CPWR and diamonds can be achieved [30], enabling the desired strong coupling regime. With these experimental parameters, the first maxima of entanglement are observed at $t \approx 14$ ns, i.e., well within the lifetime of microwave photons in a superconducting resonator (≈ 1 ms). To let the NVE–CPWR coupling reach its maximum, the NVEs should be positioned symmetrically at the points where the magnetic field of the resonator reaches its maximum.

The coherence time of NV centers in diamond is extraordinarily long, especially at lower temperatures. Quantum control techniques based on dynamically decoupling pulse sequences enable a further suppression of NV spin decoherence. CPWRs are operated at temperatures of a few millikelvin. Decoherence due to NV centers can be efficiently suppressed at these temperatures, leaving decoherence related to the CPWR the dominant source of decoherence. We include these

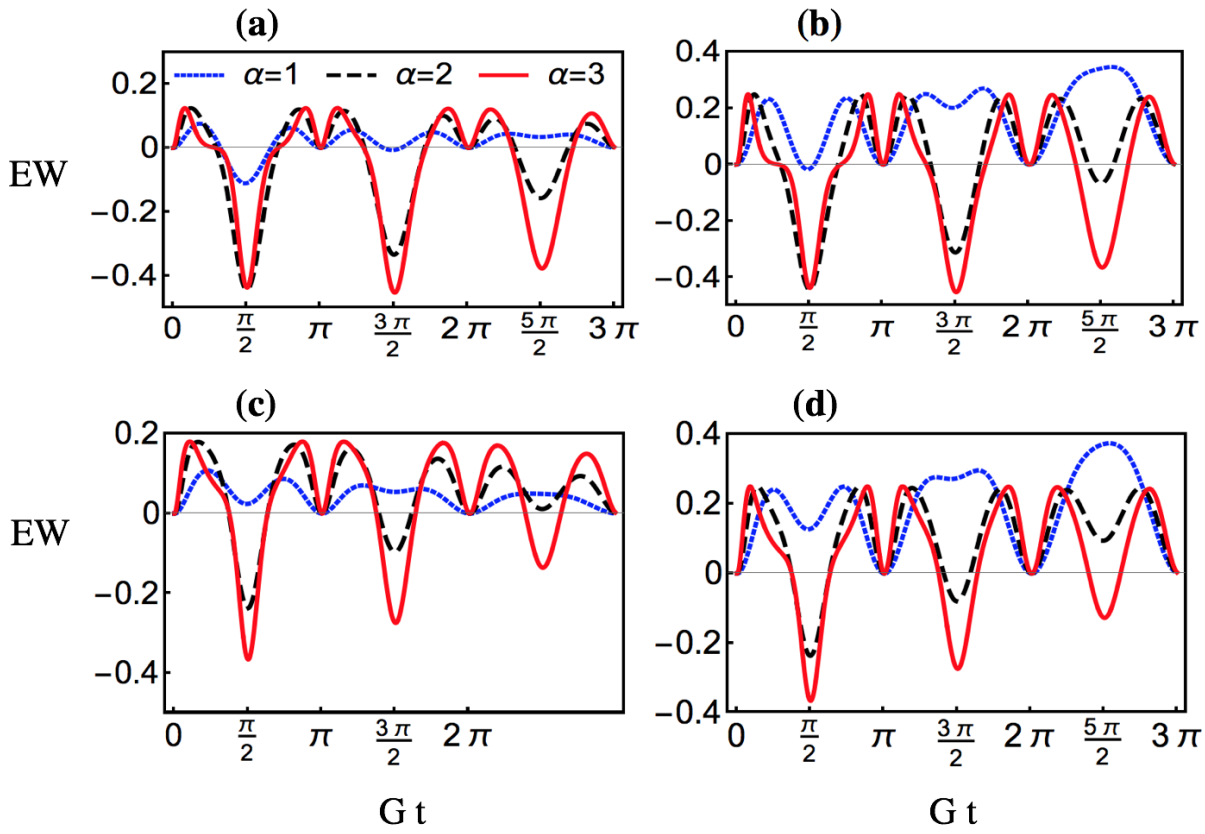

Figure 3.5: Time evolution of EW for an NVE with decoherence for (a, b) $g_1 = g_2 = g_3$ and (c, d) $g_1 = 1, g_2 = 0.5 g_3 = 1.5$: (a, c) even-cat input state and (b, d) odd-cat input state. (Yusef Maleki and Aleksei M. Zheltikov,2018)

effects in our model through the quantum jump approach, leading to a modified Hamiltonian

$$H_T = H - i\frac{\kappa}{2}a^\dagger a, \tag{3.7}$$

where H is the Hamiltonian as defined by Eq. (3.1).

The dynamics of the CPWR modes is now governed by

$$a(t) = e^{-i(\omega - i\kappa/4)t}[\cos(\sqrt{G^2 - (\kappa/4)^2}t)a(0) + i\frac{\kappa/4}{\sqrt{G^2 - (\kappa/4)^2}}\sin(\sqrt{G^2 - (\kappa/4)^2}t)a(0)$$
$$- i\frac{1}{\sqrt{G^2 - (\kappa/4)^2}} \times \sin(\sqrt{G^2 - (\kappa/4)^2}t)(g_1 b_1(0) + g_2 b_2(0) + g_3 b_3(0))], \tag{3.8}$$

The initial state defined by Eq. (3.2) evolves to the state

$$|\psi'_{\pm}(t)\rangle = |\alpha'(t)\rangle_c \otimes |\beta'_1(t)\rangle \otimes |\beta'_2(t)\rangle \otimes |\beta'_3(t)\rangle \\ \pm |-\alpha'(t)\rangle_c \otimes |-\beta'_1(t)\rangle \otimes |-\beta'_2(t)\rangle \otimes |-\beta'_3(t)\rangle. \tag{3.9}$$

Here,

$$\alpha'(t) = e^{-i(\omega - i\kappa/4)t}\alpha[\cos(G\zeta t) + i(\lambda/\zeta)\sin(G\zeta t)], \tag{3.10}$$

$$\beta'_i(t) = -ie^{-i(\omega - i\kappa/4)t}\alpha\frac{g_i}{G\zeta}\sin(G\zeta t) \tag{3.11}$$

are the time-dependent coherence parameters

$$\lambda = \kappa/4G, \qquad \text{and} \qquad \zeta = \sqrt{1-(\kappa/4G)^2}.$$

In Figs. 3.5(a) and 3.5(b), we plot the EW dynamics for even- and odd-cat input states in the case when the coupling strengths of all the NVEs are the same, $g_1 = g_2 = g_3$ and $\lambda = 0.1$. For both classes of input states, EW is seen to decrease as a function of time due to the dissipation of microwave photons from the resonator. For small coherence parameters, the damping can make entanglement detection completely impossible. This limitation is especially serious in the case of odd-cat input states. For large coherence parameters, however, entanglement can still be efficiently detected via the entanglement witnesses. Specifically, for the first peak in entanglement dynamics, observed at $Gt = \pi/2$, the effect of damping is still weak in the case of a high-quality resonator, allowing a robust generation of strongly entangled macroscopic quasi-GHZ states. At later moments of times, damping inevitably becomes a significant factor, leading to a loss of photons from the resonator. These photons can be detected with a suitable photon-counting scheme. No photon count in such a scheme would indicate that all the entanglement is shared among the NV memories.

Figures 3.5)(c) and 3.5)(d) display the EW dynamics in a system where the individual NVE–resonator coupling strengths g_i are not equal to each other (we set $g_1 = 1, g_2 = 0.5, g_3 = 1.5$). For

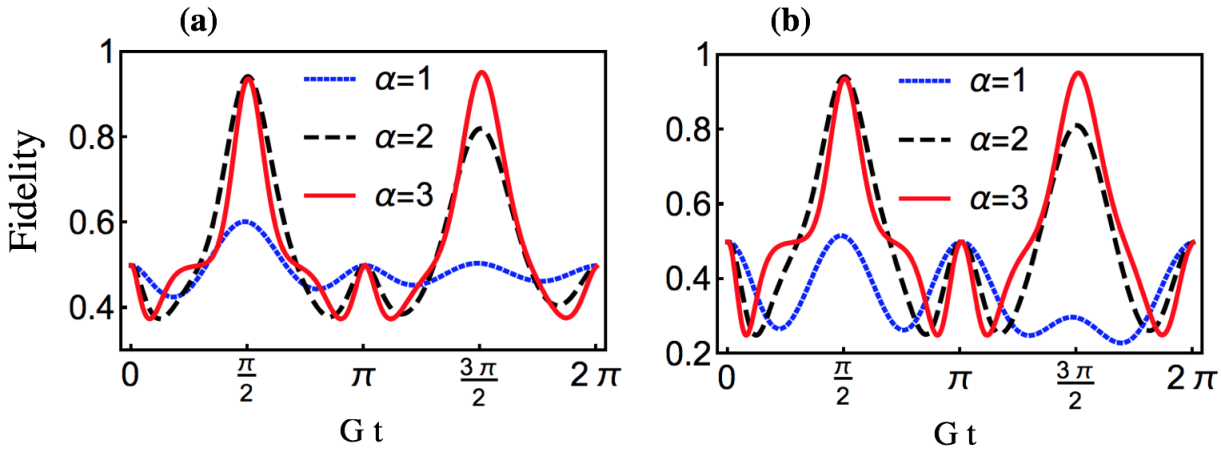

Figure 3.6: Effect of decoherence on the time evolution of the fidelity (a) F_+ and (b) F_- with $g_1 = g_2 = g_3$. (Yusef Maleki and Aleksei M. Zheltikov,2018)

large α, the behavior of EW is similar to the dynamics of EW in a system with equal g_i (Figs. 4(a), 4(b)). However, since a system with unequal g_i features a weaker NVE entanglement, the entanglement witnesses fail to detect the entanglement in such a system already for $\alpha \simeq 1$ (Figs. 3.5)(c), 3.5)(d)).

Figure 3.6) illustrates the influence of decoherence on the fidelity of the generated NVE state calculated with respect to the maximally entangled GHZ state. Similar to the case of no decoherence (Fig. 3.4), the fidelity reaches its maximum at $Gt = (2k+1)\pi/2$. However, unlike the case of no decoherence, the fidelity never reaches 1 at these points, decreasing from one maximum to another. The rate of this decoherence-induced fidelity decay depends on the coherence parameter. Specifically, for $\alpha = 2$, the fidelity is still larger than 0.94 at $Gt = \pi/2$ for both even- and odd-cat inputs, deceasing at later moments of time.

3.4 Quantifying entanglement among NVEs

Now that we have carefully analyzed the entanglement detection of the system, we would like to take an step further and quantify the entanglement among the NVEs. We are going to show that the entanglement generation is highly dependent on the initial state of the hybrid system, where a proper preparation of CPWR can be used for entangling NVEs. When the CPWR is initially

prepared as a cat state of coherent states, the entanglement of NVEs oscillates periodically, and the maximal entanglement always happens when the CPWR disentangles from the rest of the system. The entanglement degree between the NVEs strongly depends on the initial state of the CPWR, the collective coupling parameter and the interaction time. The maximal entanglement can be tuned by adjusting these parameters, enabling generation of highly entangled quasi-GHZ macroscopic entangled states as well as controlling the entanglement.

We are going to show now that, we can create an entangled state shared among the the NVE memories. To this end, we prepare the CPWR (up to a normalization factor) in the macroscopic cat state $|\alpha\rangle_c + e^{i\theta}|-\alpha\rangle_c$, and the i-th NVE in its ground state $|0\rangle$. Here, $|\alpha\rangle_c$ denotes the coherent state of the microwave mode. The initial state of the entire system is thus given as

$$|\psi(0)\rangle = \frac{1}{\sqrt{2+2\cos\theta e^{-|\alpha|^2/2}}}(|\alpha\rangle_c + e^{i\theta}|-\alpha\rangle_c)|0\rangle|0\rangle|0\rangle. \tag{3.12}$$

The dynamics of the operators of the subsystems using Hesenberg equation, read

$$\begin{pmatrix} da(t)/dt \\ db_1(t)/dt \\ db_2(t)/dt \\ db_3(t)/dt \end{pmatrix} = \begin{pmatrix} -i\omega & -ig & -ig & -ig \\ -ig & -i\omega & 0 & 0 \\ -ig & 0 & -i\omega & 0 \\ -ig & 0 & 0 & -i\omega \end{pmatrix} \begin{pmatrix} a(t) \\ b_1(t) \\ b_2(t) \\ b_3(t) \end{pmatrix}.$$

Where we have assumed that $g_1 = g_2 = g_3$ for the NVEs. Solving this for the operators of the system, the time dependent operator of the resonator reads

$$a(t) = e^{-i\omega t}[\cos(\sqrt{3}gt)a(0) - i\frac{\sin(\sqrt{3}gt)}{\sqrt{3}}(b_1(0)+b_2(0)+b_3(0))], \tag{3.13}$$

and the dynamics of the operator of the NV ensembles is governed by

$$b_1(t) = e^{-i\omega t}[-i\frac{\sin(\sqrt{3}gt)}{\sqrt{3}}a(0) + \frac{\cos(\sqrt{3}gt)}{3}\sum_{i=1}^{3} b_i(0) + (2b_1(0) - b_2(0) - b_3(0))/3.$$

$$b_2(t) = e^{-i\omega t}[-i\frac{\sin(\sqrt{3}gt)}{\sqrt{3}}a(0) + \frac{\cos(\sqrt{3}gt)}{3}\sum_{i=1}^{3} b_i(0) + (2b_2(0) - b_1(0) - b_3(0))/3.$$

$$b_3(t) = e^{-i\omega t}[-i\frac{\sin(\sqrt{3}gt)}{\sqrt{3}}a(0) + \frac{\cos(\sqrt{3}gt)}{3}\sum_{i=1}^{3} b_i(0) + (2b_3(0) - b_1(0) - b_2(0))/3.$$

Therefore, the initial state given in Eq.(3.12), at time t, evolves to

$$|\psi(t)\rangle = |\alpha(t)\rangle_c \otimes |\beta(t)\rangle \otimes |\beta(t)\rangle \otimes |\beta(t)\rangle + e^{i\theta}|-\alpha(t)\rangle_c \otimes |-\beta(t)\rangle \otimes |-\beta(t)\rangle \otimes |-\beta(t)\rangle. \quad (3.14)$$

Where the time dependent coherence parameters are

$$\alpha(t) = e^{-i\omega t}\alpha\cos(\sqrt{3}gt)$$

and

$$\beta(t) = -ie^{-i\omega t}\alpha\frac{\sin(\sqrt{3}gt)}{\sqrt{3}}.$$

In general, all of the subsystems including the NVEs and the CPWR may become entangled by the time evolution process; however, we only are interested in the entanglement between three NV ensembles. Therefore, we obtain the reduced density operator of the NVEs by tracing out the

CPWR subspace, i.e., $\rho_{NV}(t) = Tr_{CPWR}(|\psi(t)\rangle\langle\psi(t)|)$, which results in

$$\begin{aligned}\rho_{NV}(t) = N^2[&|\beta(t)\rangle\langle\beta(t)| \otimes |\beta(t)\rangle\langle\beta(t)| \otimes |\beta(t)\rangle\langle\beta(t)| \\ &+ |-\beta(t)\rangle\langle-\beta(t)| \otimes |-\beta(t)\rangle\langle-\beta(t)| \otimes |-\beta(t)\rangle\langle-\beta(t)| \\ &+ e^{-i\theta}q(t)|\beta(t)\rangle\langle-\beta(t)| \otimes |\beta(t)\rangle\langle-\beta(t)| \otimes |\beta(t)\rangle\langle-\beta(t)| \\ &+ e^{i\theta}q(t)|-\beta(t)\rangle\langle\beta(t)| \otimes |-\beta(t)\rangle\langle\beta(t)| \otimes |-\beta(t)\rangle\langle\beta(t)|] \end{aligned} \tag{3.15}$$

Where

$$q(t) = e^{-2|\alpha|^2\cos^2(\sqrt{3}gt)},$$

and the normalization factor N is given as

$$N = [2 + 2\cos\theta e^{-2|\alpha|^2}]^{\frac{-1}{2}}.$$

The above density matrix can be mapped to a three qubit state with an appropriate encoding of the logical bases. Therefore,we can choose the orthogonal basis for each subsystem as

$$|0\rangle \equiv |\beta(t)\rangle, \quad |1\rangle \equiv \frac{1}{\sqrt{1-p^2(t)}}(|-\beta(t)\rangle - p(t)|\beta(t)\rangle)$$

Where $p(t) = e^{-\frac{2}{3}|\alpha|^2\sin^2(\sqrt{3}gt)}$.

Thus, the coherent states $|\pm\beta(t)\rangle$ can be expressed in two orthogonal basis as

$$|\beta(t)\rangle \equiv |0\rangle, \qquad |-\beta(t)\rangle \equiv p(t)|0\rangle + \sqrt{1-p^2(t)}|1\rangle.$$

Replacing coherent states with these orthogonal bases in $\rho_{NV}(t)$, degenerates the density matrix to a three-qubit state.

To understand the entanglement characteristics of the density matrix in Eq.(3.15), we need to quantify the entanglement. For a general mixed three-qubit state of ρ_{ABC}, the entanglement can be

quantified by the three tangle which is defined as [74]

$$\tau_{ABC} = \min[C^2_{A(BC)}] - C^2_{AB} - C^2_{AC}. \tag{3.16}$$

Where $C^2_{A(BC)}$ must be minimized for all possible decomposition of the density matrix ρ_{ABC}. Also, $C_{\mu\nu}$ is the concurrence of a two-qubit density operator $\rho_{\mu\nu}$. In this sense, ρ^* is the complex conjugate of ρ and σ_y is the spin flip operator. Therefore, $C_{A(BC)}$ represent the bipartite entanglement of the system in which A is on of the partitions and BC together form the other partition of the system.

Using the three tangle τ_{ABC}, the entanglement of the system can analytically be quantified as

$$\tau_{123} = \frac{e^{-4|\alpha|^2\cos^2(\sqrt{3}gt)}[1 - e^{-\frac{4}{3}|\alpha|^2\sin^2(\sqrt{3}gt)}]^3}{[1 + \cos\theta e^{-2|\alpha|^2}]^2}, \tag{3.17}$$

Where, the index (123) of the three tangle represent that the entanglement is among the first, the second and the third spin memories. The tripartite entanglement among NVE ensembles is a function of the coherence parameter α, the local phase θ, the collective coupling strength between the NVE ensembles of the resonator g, and the interaction time t. These parameters can be used for controlling the entanglement among the diamonds. We present the entanglement dynamics of the NVE centers versus the dimensionless parameter $\sqrt{3}gt$ in Fig.3.7(a). Accordingly, entanglement of the system demonstrates a periodic behavior in terms of gt, where the maximum of the entanglement occurs at $\sqrt{3}gt = \pi(n + 1/2)$ with an integer n. The periodic behavior of the entanglement as well as the position of its maximums are independent of the coherence parameter and the local phase θ.

Furthermore, the entanglement improves as the coherence parameter $|\alpha|$ increases. For $|\alpha| \gtrsim 3$ maximum entanglement among the spin memories can be generated.

In Fig. 3.7(b) entanglement of the spin ensembles versus $\sqrt{3}gt$ for various local phase θ is presented. Accordingly, the entanglement of the system improves as the local phase increases from 0 to π. This immediately suggests that the even cat state $|\alpha\rangle_e = |\alpha\rangle_c + |-\alpha\rangle_c$ input of the

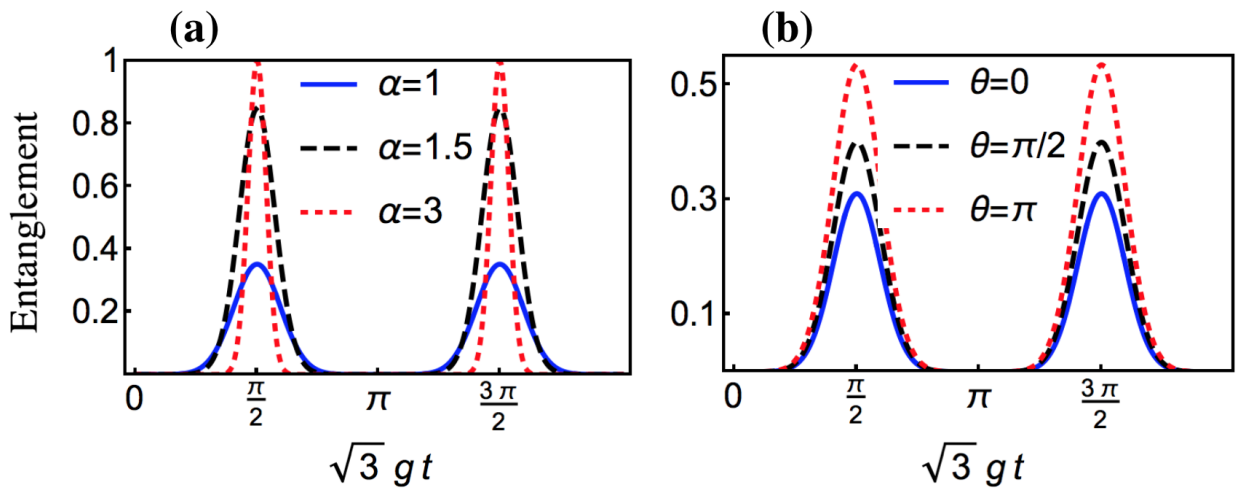

Figure 3.7: Entanglement dynamics of three ensembles of NV centers with even coherent states as the initial state of the waveguide resonator for various coherence parameter (a). Entanglement dynamics of three-tangle among three ensembles of NV centers with cat states as the initial state of the waveguide resonator for various phase parameter θ, with $|\alpha| = 1$ (b). (Yusef Maleki and Aleksei M. Zheltikov,2019)

initial state generates minimum entanglement, while the odd cat state $|\alpha\rangle_o = |\alpha\rangle_c - |-\alpha\rangle_c$ can generate the maximum of the entanglement in this scenario. The effect of θ can be significantly remarkable when the coherence parameter is relatively small; while, it becomes negligible for large enough $|\alpha|$. With this description, we can set an upper bound for the entanglement of the system as $\tau_{123} \leq \frac{(1+e^{-\frac{2}{3}|\alpha|^2})^3}{(1-e^{-2|\alpha|^2})^2}$. Thus, $\tau_{123} = 0$ ($\tau_{123} = 1$) in the limit $|\alpha| \to 0$ ($|\alpha| \to \infty$).

To understand the relation between the degree of entanglement with the input energy of the system we calculate the dynamics of average photon number of the CPWR $\langle a^\dagger(t)a(t)\rangle$ as

$$\langle a^\dagger(t)a(t)\rangle = |\alpha|^2 \cos^2(\sqrt{3}gt)\frac{1+\cos\theta e^{-2|\alpha|^2}}{1-\cos\theta e^{-2|\alpha|^2}}$$

Thus, the excitation of the resonator periodically oscillate by the factor $\cos^2(\sqrt{3}gt)$ as presented in Fig.3.8, where the degree of entanglement the average number of photons dynamics are depicted. Accordingly, both entanglement and the photon number average present a periodic evolution. The entanglement reaches its maximum when the photons of resonator is completely de-

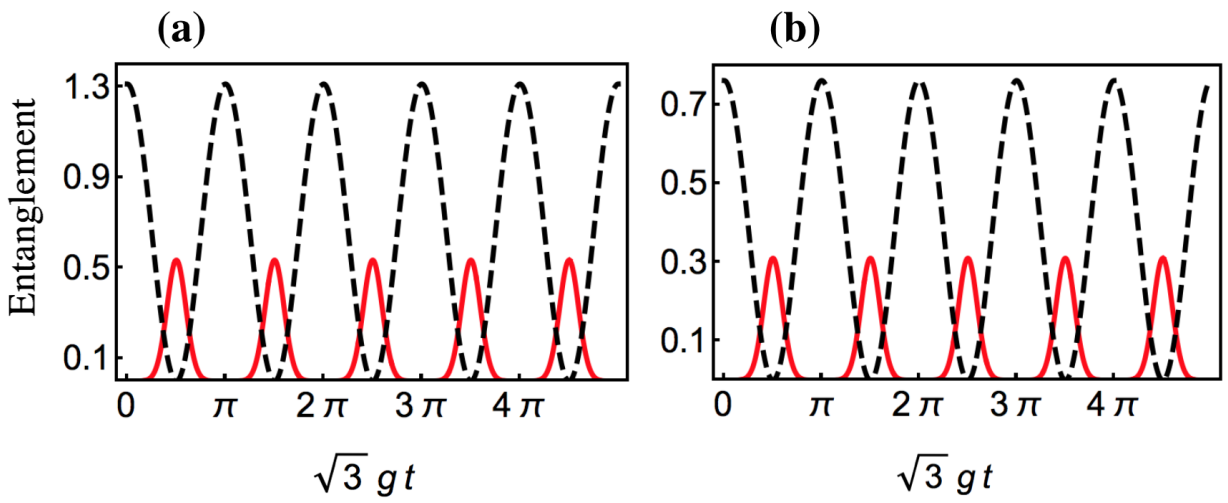

Figure 3.8: Dynamics of the entanglement (solid curve) and average photon number (dashed curve) of three ensembles of NV centers as a function of $\sqrt{3}gt$ for resonator initially prepared in odd coherent state (a), and even coherent state (b) with with $|\alpha| = 1$. (Yusef Maleki and Aleksei M. Zheltikov,2019)

pleted ($\langle a^{\dagger}(t)a(t)\rangle = 0$), which suggests that the resonator becomes disentangled from the rest of the system at these picks, and the state of the NV ensembles (up to a normalization factor) can be described by a pure quasi-GHZ state as

$$|\Psi\rangle = |\frac{\alpha}{\sqrt{3}}\rangle|\frac{\alpha}{\sqrt{3}}\rangle|\frac{\alpha}{\sqrt{3}}\rangle + e^{i\theta}|-\frac{\alpha}{\sqrt{3}}\rangle|-\frac{\alpha}{\sqrt{3}}\rangle|-\frac{\alpha}{\sqrt{3}}\rangle. \tag{3.18}$$

Where the unimportant phase factor for $-ie^{-i\omega\pi/2\sqrt{3}g}$ is dropped in coherence parameter, which can be saturated in α.

For large enough $|\alpha|$, the two coherent states $|\frac{\alpha}{\sqrt{3}}\rangle$ and $|-\frac{\alpha}{\sqrt{3}}\rangle$ become orthogonal and the overall state reduces to maximally entangled GHZ state. According to Fig.3.8 when the resonator field is initially prepared in an odd coherent state both entanglement and mean photon number is larger compared to that of even coherent state when α is fixed, indicating that the average photon number is also increasing as the local phase increases from 0 to π. Specifically, for $|\alpha| = 1$ as depicted in Fig.3, the entanglement, and average photon number are, respectively, about 0.53 and

1.31 for the odd cat state; while for the even coherent state, the entanglement and average photon number are, respectively, about 0.31 and 0.76.

To get a better insight into dynamics of the entanglement of the system we investigate the entanglement between any pair of the diamond NV ensembles, where by using concurrence it can be calculated as

$$C = \frac{e^{-2/3(1+2\cos^2(\sqrt{3}gt))|\alpha|^2} - e^{-2|\alpha|^2}}{1 + \cos\theta e^{-2|\alpha|^2}} \tag{3.19}$$

Entanglement dynamics of concurrence between any pair of ensembles of NV centers among three with even coherent states ($\theta = 0$) as the initial state of the waveguide resonator for various coherence parameter is presented in Fig.3.9(a). In this case, the entanglement starts from 0 and increases as the coherence parameter increases beyond 0 and it gets its maximum (≈ 0.34) at coherence parameter of $|\alpha| \approx 1.02$; then it decreases as the coherence increases further and the bipartite entanglement approaches 0 for sufficiently large $|\alpha|$. The maximum of the entanglement occurs at $\sqrt{3}gt = \pi(n + 1/2)$.

Similar dynamical characteristic can be seen for various parameters of θ except $\theta = \pi(2n + 1)$ (odd coherent cat state), where the entanglement asymptotically approaches 2/3 for $|\alpha| \to 0$ (see Fig.3.9(b)). In the case of odd coherent state input, the entanglement immediately increases to 2/3 from zero, indicating that such entanglement can be generated with sufficiently small energy stored in the CPWR.

Next, we analyze the effects of decoherence on the entanglement evolution of the system.

Adopting these experimental values discussed earlier, the first maxima of the entanglement in τ_{123} occur at about $t \approx 14$ ns, far below the lifetime of microwave photons in superconducting cavities of about 1 ms [34]. To make the coupling between an NVE and the CPWR reach its maximal values, the NVEs should be located symmetrically in the position where the magnetic field of the resonator is maximum.

The dynamics of the operator of the resonator which takes into account effect of the dissipation

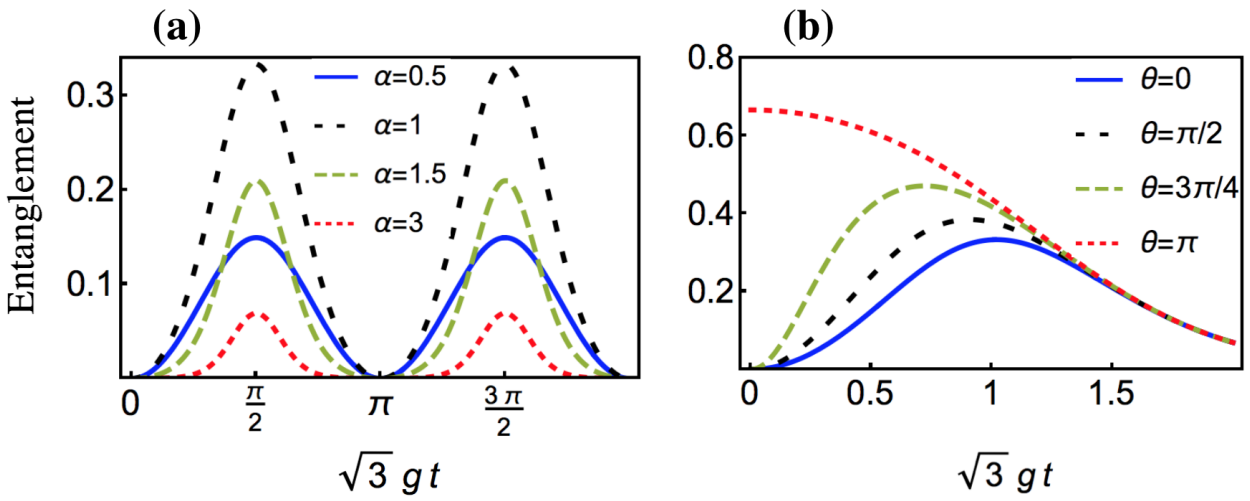

Figure 3.9: Dynamics of the entanglement between any pair of ensembles of NV centers as a function of $\sqrt{3}gt$ for various α with $\theta = 0$ (a), and for various θ with $|\alpha| = 1$ (b). (Yusef Maleki and Aleksei M. Zheltikov,2019)

can be obtained as

$$a(t) = e^{-i(\omega - i\kappa/4)t}[\cos(\sqrt{3g^2 - (\kappa/4)^2}t)a(0) \\ -i\frac{g}{\sqrt{3g^2-(\kappa/4)^2}}\sin(\sqrt{3g^2 - (\kappa/4)^2}t)(b_1(0) + b_2(0) + b_3(0))], \quad (3.20)$$

Therefore, the initial state given in Eq.(3.2), at time t, evolves to

$$|\psi(t)\rangle = |\alpha'(t)\rangle_c \otimes |\beta'(t)\rangle \otimes |\beta'(t)\rangle \otimes |\beta'(t)\rangle \\ +e^{i\theta}|-\alpha'(t)\rangle_c \otimes |-\beta'(t)\rangle \otimes |-\beta'(t)\rangle \otimes |-\beta'(t)\rangle. \quad (3.21)$$

Where the time dependent coherence parameters are

$$\alpha'(t) = e^{-i(\omega - i\lambda/4)gt}\alpha[\cos(\sqrt{3}gt\zeta) - i\frac{\lambda}{\sqrt{3}\zeta}\sin(\sqrt{3}gt\zeta)], \\ \beta'(t) = -ie^{-i(\omega - i\lambda/4)gt}\alpha\frac{1}{\sqrt{3}\zeta}\sin(\sqrt{3}gt\zeta). \quad (3.22)$$

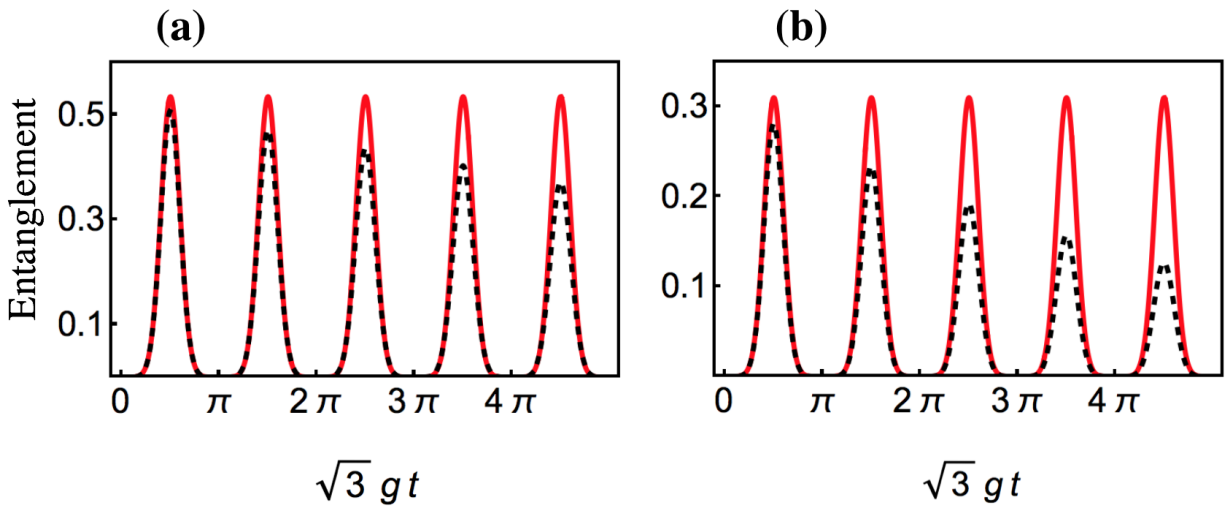

Figure 3.10: Dynamics of the entanglement of three ensembles of NV centers as a function of $\sqrt{3}gt$, for $\lambda = 0$ (solid curve) and $\lambda = 0.1$ (dashed curve), for resonator initially prepared in odd coherent state (a) and even coherent state (b) with with $|\alpha| = 1$. (Yusef Maleki and Aleksei M. Zheltikov,2019)

Where $\lambda = \kappa/g$, and $\zeta = \sqrt{1 - (\lambda/4\sqrt{3})^2}$.

To understand the effects of the damping of the resonator on the entanglement among the NVE memories, we plot the dynamics of the entanglement for even and odd coherent state when $\lambda = 0.1$, and compare it to the case with no damping in Fig.3.10. It is found that the amount of entanglement among three memories degrades, due to the dissipation of microwave photons in the resonators to the surrounding environment with the evolution of the time. The effect of damping on the entanglement can be negligible at first pick of the entanglement dynamics ($\sqrt{3}gt = \pi/2$), for high-quality resonators, that can ensure robust generation of highly entangled macroscopic quasi-GHZ state in the solid state memories; however, it may become significant at later times as the system dissipates to the environment. The loss from the resonator to the environment can be monitored by photon counting detectors, where no photo-detection implies that the entanglement is perfectly shared among the NV memories.

4. QUANTUM ENTANGLEMENT IN NONORTHOGONAL STATES [1]

4.1 Introduction

Entangled nonorthogonal states have occupied a distinguished position due to their vast applications in various quantum optics and information physics. Entangled coherent and squeezed states, entangled SU(2) and SU(1,1) coherent states as well as nonlinear coherent states are some typical examples of entangled nonorthogonal states [75–78]. In this chapter, entanglement of multi-qubit nonorthogonal coherent states (CSs), where each qubit is described in the framework of superposition of linearly independent nonorthogonal states such as $\{|\alpha_1\rangle, |\alpha_2\rangle\}$, will be investigated [79–85].As a part of this study the required criteria for maximal entanglement of bipartite nonorthogonal will be addressed. In fact, we are going to show that by encoding logical qubits in terms of nonorthogonal CSs states in a multi-dimensional Hilbert space demonstrates a promising strategy in performing various quantum tasks [76, 84–86]. In particular, the generalization of such states to the three dimensional structure (or qutrits), where each mode is described based on three linearly independent nonorthogonal CSs states such as $\{|\alpha_1\rangle, |\alpha_2\rangle, |\alpha_3\rangle\}$, is important from both practical and fundamental perspectives. It is notable that three-dimensional entanglement provides significant advantages in quantum communication over the conventional qubit entanglement. It provides enhanced channel capacity [87], and higher security in some quantum protocols [88–90], and also is more robust against environmental noise [91, 92]. This enhancement is due to the access to larger Hilbert spaces in qutrit states which provide a richer yet more intricate and somewhat complicated structure.

Therefore, the importance from fundamental perspective as well as many practical advantages of entangled nonorthogonal states in three dimension, motivate us to introduce a generic multipartite superposition of such nonorthogonal states and to explore its entanglement in detail. These states which, via an appropriate encoding of qutrit logical basis, recast entangled qutrit states, can

[1] This capter is partly based on Ref. [96]. Reprinted with permission from " Linear entropy of multiqutrit nonorthogonal states" by Yusef Maleki, Aleksei Zheltikov, 2019 *Opt. Express* **27** 8291-8307, Copyright [2020] by The Optical Society (OSA).

provide a richer physical structure as they provide remarkable advantages over the qubit-based operations in various information processing tasks such as enhancing the channel capacity in quantum communication and providing higher security in some protocols [87, 89].

In this chapter, we demonstrate that such three dimensional cat states of coherent states can be manipulated Optomechanical cavities and beam splitters [52, 93–95]. We find explicit expressions for the linear entropy of the nonorthogonal states, for both two- and multi-mode scenarios, which can fully capture the entanglement of the states and characterize its entropy. Even though we study coherent and squeezed states in particular; however, this expression may be applied to any given nonorthogonal qutrit state such as multi-mode SU(2) and SU(1,1) coherent states, deformed, nonlinear and also pair coherent states. By comparing the results to the entanglement of two dimensional nonorthogonal coherent states, we observe that this result is a further generalization of the entanglement of the two dimensional nonorthogonal states, and it exposes some of the characteristics of two and three dimensional states. Subsequently, we present a detailed investigation of the linear entropy of generic multi-qutrit coherent states and examine the role of parameters that control the entanglement of the states and expose some important features of the states. Furthermore, we study the three dimensional multi-mode superposition of squeezed states and explore their entanglement characteristics. It is found that coherent states of three dimensional superpositions are more entangled than their squeezed vacuum counterparts, when the number of modes and the controlling parameters are the same. We follow [96] in this chapter.

4.2 Generation of the generalized entangled cat states

Manipulating quantum information processing with three dimensional quantum states or qutrits, provides the opportunity of getting access to larger Hilbert spaces, which can result in significant improvements over qubits in various tasks such as enhanced channel capacity in quantum communication and higher security [87, 89]. Therefore, it would be important to study multi-qutrit entangled nonorthogonal states, and examine their properties. The Glauber coherent state which is a typical example of nonothogonal states and is defined as the eigenstate of the annihilation

operator of the bosonic Harmonic oscillator. In the Fock basis, it can be given as [75].

$$|\alpha\rangle = e^{-\frac{|\alpha|^2}{2}} \sum_{n=0}^{\infty} \frac{\alpha^n}{\sqrt{n!}} |n\rangle,$$

where α is an arbitrary complex number. The overlap between two coherent states $|\alpha\rangle$ and $|\gamma\rangle$ is [79]

$$\langle\alpha|\gamma\rangle = \exp[-1/2(|\alpha|^2 + |\gamma|^2 - 2\alpha^*\gamma)].$$

To study the entropy of three dimensional nonorthogonal states we suppose that $|\alpha_1\rangle$, $|\alpha_2\rangle$ and $|\alpha_3\rangle$ are linearly independent normalized states that span the space of the first subsystem, and $|\beta_1\rangle$, $|\beta_2\rangle$ and $|\beta_3\rangle$ are linearly independent normalized states that span the space of the second subsystem. These states may not be orthogonal mutually, in general, for both subsystems. Therefore, a general form of a superposition of a pure two-qutrit nonorthogonal state may be given as

$$|\Psi\rangle = \mu|\alpha_1\rangle|\beta_1\rangle + \lambda|\alpha_2\rangle|\beta_2\rangle + \nu|\alpha_3\rangle|\beta_3\rangle. \tag{4.1}$$

Such generalized states can be prepared using optomechanical Fabry-Perot cavities [94] as shown in Fig.4.1. In the optical cavity the moving mirror generates the mechanical mode.

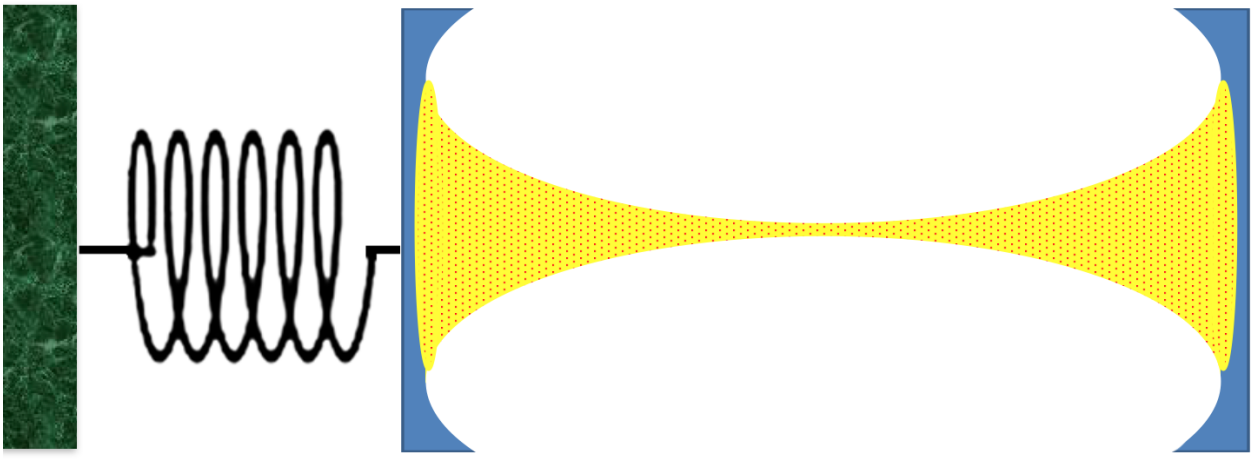

Figure 4.1: Schematics of an optomechanical Fabry-perot cavity.

Let us assume the cavity resonance frequency to be ω_0 and the mechanical mode as a harmonic oscillator with the frequency ω_m, then the Hamiltonian of the system can be written as

$$H = \hbar\omega_0 a^\dagger a + \hbar\omega_m b^\dagger b - \hbar g a^\dagger a(b + b^\dagger). \tag{4.2}$$

Where a ($a^\dagger$) and b ($b^\dagger$) stand for the annihilation (creation) operators of the cavity mode and the mechanical modes, respectively. The time evolution operator for this Hamiltonian is given by [93]

$$U(t) = e^{-i\zeta a^\dagger a t} e^{i\kappa^2 (a^\dagger a)^2 (t - \sin t)} e^{\kappa a^\dagger a(\eta b^\dagger - \eta^* b)t} e^{-ib^\dagger b t}. \tag{4.3}$$

Where $\zeta = \omega_0/\omega_m$, $\eta = (1 - e^{-it})$, and t represent the dimension-less time, which is the actual time T multiplied by ω_m. Also, the scaled coupling constant is denoted by $\kappa = g/\omega_m$. It is notable that the magnitude of the coupling parameter κ can be manipulated even to reach the order of unity with experimentally feasible parameters. For example, consider a Fabry-perot cavity with length $l \sim 1$ m, $\omega_0 \sim 10^{16} s^{-1}$, $\omega_m \sim 1$ KHz and the mass of the moving mirror $m \sim 10$ mg [93].

We suppose that at $t = 0$ both the mechanical and the cavity modes are in coherent state. Thus, the initial state is

$$|\Psi\rangle = |\alpha_1\rangle_c |\beta\rangle_m, \tag{4.4}$$

where $|\alpha_1\rangle_c$ and $|\beta\rangle_m$ are the initial coherent states of the field and the mechanical mirror, respectively. The time evolution of the system using Eq.4.3 is

$$|\Psi(t)\rangle = e^{-\frac{|\alpha_1|^2}{2}} \sum_{n=0}^{\infty} \frac{[\alpha_1 e^{-i\zeta t} e^{i\kappa Im[\beta\eta e^{-it}]}]^n}{\sqrt{n!}} e^{i\kappa^2 n^2 (t - \sin t)} |n\rangle_c \otimes |\beta e^{-it} + \kappa n\eta\rangle_m. \tag{4.5}$$

At $t = 2\pi$ the mechanical mode returns to its initial state and decouples from the cavity mode, and

the cavity mode degenerates to

$$|\Psi\rangle_c = e^{-\frac{|\alpha|^2}{2}} \sum_{n=0}^{\infty} \frac{\alpha^n}{\sqrt{n!}} e^{i2\pi\kappa^2 n^2} |n\rangle_c, \tag{4.6}$$

with $\alpha = e^{-i\zeta 2\pi}\alpha_1$. Now, for $\kappa = 0.5$ we get the cat state

$$|\psi\rangle_c = \frac{1}{\sqrt{2}}[e^{i\frac{\pi}{4}}|\alpha\rangle_c + e^{-i\frac{\pi}{4}}|-\alpha\rangle_c], \tag{4.7}$$

and for $\kappa = \frac{1}{\sqrt{6}}$ we get

$$|\psi\rangle_c = \mu|-\alpha\rangle_c + \lambda|\alpha e^{i\frac{\pi}{3}}\rangle_c + \nu|\alpha e^{-i\frac{\pi}{3}}\rangle_c, \tag{4.8}$$

with $\mu = 1$ and $\lambda = -\nu = (1 + e^{i\frac{\pi}{3}})/i\sqrt{3}$. To generate an entangled state we send the generated state through a 50/50 beam splitter. For two modes given with annihilation operators a_0 and a_1, the 50/50 beam splitter can described by the operator [52]

$$U = \exp[\frac{\pi}{4}(a_0^\dagger a_1 - a_1^\dagger a_0)].$$

Now, under the action of this beam splitter, the cat state in Eq. 4.8 results in an two-mode entangled state

$$|\psi\rangle = \mu|\frac{-\alpha}{\sqrt{2}}\rangle|\frac{-\alpha}{\sqrt{2}}\rangle + \lambda|\frac{\alpha e^{i\frac{\pi}{3}}}{\sqrt{2}}\rangle|\frac{\alpha e^{i\frac{\pi}{3}}}{\sqrt{2}}\rangle + \nu|\frac{\alpha e^{-i\frac{\pi}{3}}}{\sqrt{2}}\rangle|\frac{\alpha e^{-i\frac{\pi}{3}}}{\sqrt{2}}\rangle$$

To produce more generalized state and have more control on the parameters, we next apply displacement operators then applying displacement operators $\hat{D}(\gamma, \delta) = \hat{D}(\gamma)_1 \otimes \hat{D}(\delta)_2$ on both modes, and by redefining the parameters the state reduces to the form of Eq.(4.1). If the optical mode , up to normalization factor, was prepared in

$$|\psi\rangle_c = a|0\rangle_c + b|\alpha\rangle_c, \tag{4.9}$$

at $t = 2\pi$ the cavity state will reduce to

$$|\psi\rangle_c = a|0\rangle_c + \frac{b}{\sqrt{2}}[e^{i\frac{\pi}{4}}|\alpha\rangle_c + e^{-i\frac{\pi}{4}}|-\alpha\rangle_c], \tag{4.10}$$

Once again we apply the displacement operator $\hat{D}(\beta)$ on the state and get

$$|\psi\rangle = a|\beta\rangle + \frac{be^{i(\frac{\pi}{4}+Im(\beta\alpha^*))}}{\sqrt{2}}|\beta+\alpha\rangle + \frac{be^{-i(\frac{\pi}{4}+Im(\beta\alpha^*))}}{\sqrt{2}}|\beta-\alpha\rangle. \tag{4.11}$$

Now, redefining

$$\mu = be^{-i(\frac{\pi}{4}+Im(\beta\alpha^*))}/\sqrt{2}$$
$$\lambda = a$$
$$\nu = be^{i(\frac{\pi}{4}+Im(\beta\alpha^*))}/\sqrt{2}$$

and sending the state through a beam splitter results in

$$|\psi\rangle = \mu|\frac{\beta-\alpha}{\sqrt{2}}\rangle|\frac{\beta-\alpha}{\sqrt{2}}\rangle + \lambda|\frac{\beta}{\sqrt{2}}\rangle|\frac{\beta}{\sqrt{2}}\rangle + \nu|\frac{\beta+\alpha}{\sqrt{2}}\rangle|\frac{\beta+\alpha}{\sqrt{2}}\rangle. \tag{4.12}$$

For generating more general state one can displace each mode to get a superposition of various coherent state. If we assume $\beta = 2\alpha$, $a = 1$, and $b = \sqrt{2}e^{i\frac{\pi}{4}}$ in the above generated state, then the state reduces to

$$|\psi\rangle = |\frac{\alpha}{\sqrt{2}}\rangle|\frac{\alpha}{\sqrt{2}}\rangle + |\frac{2\alpha}{\sqrt{2}}\rangle|\frac{2\alpha}{\sqrt{2}}\rangle + i|\frac{3\alpha}{\sqrt{2}}\rangle|\frac{3\alpha}{\sqrt{2}}\rangle, \tag{4.13}$$

We can redefine $\frac{\alpha}{\sqrt{2}} \to \alpha$ which gives

$$|\psi\rangle = |\alpha\rangle|\alpha\rangle + |2\alpha\rangle|2\alpha\rangle + i|3\alpha\rangle|3\alpha\rangle. \tag{4.14}$$

Which is an example of the more general case discussed earlier.

4.3 Linear entropy of two-qutrit states

In quantum computing with qutrits we use three mutually orthogonal basis $\{|0\rangle, |1\rangle, |2\rangle\}$ as the logical states. We can introduce an encoding of these logical states in terms of nonorthogonal states of the first subsystem in the state given by

$$|0\rangle \equiv |\alpha_1\rangle, \quad |1\rangle \equiv \frac{|\alpha_2\rangle - p_1|\alpha_1\rangle}{N_1},$$

$$|2\rangle \equiv \frac{(p_1 p_3 - p_2)|\alpha_1\rangle + (\bar{p}_1 p_2 - p_3)|\alpha_2\rangle + N_1^2|\alpha_3\rangle}{N N_1},$$

in which we have

$$p_1 = \langle\alpha_1|\alpha_2\rangle,\ p_2 = \langle\alpha_1|\alpha_3\rangle,\ p_3 = \langle\alpha_2|\alpha_3\rangle,\ N_i = \sqrt{1 - |p_i|^2},$$

$$N = [1 - |p_1|^2 - |p_2|^2 - |p_3|^2 + p_1\bar{p}_2 p_3 + \bar{p}_1 p_2 \bar{p}_3]^{\frac{1}{2}}.$$

Where $\bar{p}_i$ is the complex conjugate of p_i. This specific encoding of the qutrit computational basis allows one to express the nonorthogonal states $|\alpha_1\rangle$, $|\alpha_2\rangle$ and $|\alpha_3\rangle$ in terms of orthogonal logical basis $\{|0\rangle, |1\rangle, |2\rangle\}$ such that

$$|\alpha_1\rangle \equiv |0\rangle, \quad |\alpha_2\rangle \equiv N_1|1\rangle + p_1|0\rangle,$$

$$|\alpha_3\rangle \equiv \frac{N|2\rangle + p_2 N_1|0\rangle - (\bar{p}_1 p_2 - p_3)|1\rangle}{N_1},$$

Similarly, the standard qutrit basis of the second subsystem $\{|\tilde{0}\rangle, |\tilde{1}\rangle, |\tilde{2}\rangle\}$ can be encoded in its nonorthogonal basis

$$|\tilde{0}\rangle \equiv |\beta_1\rangle, \quad |\tilde{1}\rangle \equiv \frac{|\beta_2\rangle - q_1|\beta_1\rangle}{M_1},$$

$$|\tilde{2}\rangle \equiv \frac{(q_1 q_3 - q_2)|\beta_1\rangle + (\bar{q}_1 q_2 - q_3)|\beta_2\rangle + M_1^2|\beta_3\rangle}{M M_1},$$

in which we have

$$q_1 = \langle\beta_1|\beta_2\rangle,\ q_2 = \langle\beta_1|\beta_3\rangle,\ q_3 = \langle\beta_2|\beta_3\rangle,\ M_i = \sqrt{1-|q_i|^2},$$

$$M = [1 - |q_1|^2 - |q_2|^2 - |q_3|^2 + q_1\bar{q}_2 q_3 + \bar{q}_1 q_2 \bar{q}_3]^{\frac{1}{2}}.$$

We note that the encoding is essential in utilizing these nonorthogonal states in various quantum information tasks. The transformation of nonorthogonal basis to the orthogonal standard qutrit basis illustrates that the (unnormalized) state (4.1) can be converted to a qutrit state

$$|\Psi\rangle = (\mu + \lambda q_1 p_1 + \nu p_2 q_2)|0\tilde{0}\rangle + (\nu p_2 \frac{q_3 - \bar{q}_1 q_2}{M_1} + \lambda M_1 p_1)|0\tilde{1}\rangle$$

$$+(\nu q_2 \frac{p_3 - \bar{p}_1 p_2}{N_1} + \lambda N_1 q_1)|1\tilde{0}\rangle + (\nu \frac{(p_3 - \bar{p}_1 p_2)}{N_1} \frac{(q_3 - \bar{q}_1 q_2)}{M_1}$$

$$+\lambda N_1 M_1)|1\tilde{1}\rangle + \nu p_2 \frac{M}{M_1}|0\tilde{2}\rangle + \nu q_2 \frac{N}{N_1}|2\tilde{0}\rangle + (\nu \frac{p_3 - \bar{p}_1 p_2}{N_1} \frac{M}{M_1})$$

$$|1\tilde{2}\rangle + \nu \frac{q_3 - \bar{q}_1 q_2}{M_1} \frac{N}{N_1}|2\tilde{1}\rangle + \nu \frac{N}{N_1} \frac{M}{M_1}|2\tilde{2}\rangle. \tag{4.15}$$

By an appropriate encoding, we observe that $|\Psi\rangle$ recasts a two-qutrit state, which can be entangled or seperable in general. Therefore, it would be interesting to investigate entanglement of such system state and analyze its properties. To this aim, we use linear entropy as a measure of entanglement that can be utilized for quantifying entanglement of a qudit system states [14]

$$I_{lin} = \frac{d}{d-1}(1 - Tr{\rho_1}^2). \tag{4.16}$$

In this expression d is the dimension of the state vector, and hence, for a qutrit state $d = 3$. Also, ρ_1 is the density operator of the first subsystem that is obtained after tracing over the second subsystem $\rho_1 = Tr_2(|\Psi\rangle\langle\Psi|)$. Hence, one may work out the entropy of the state (4.1) using the linear entropy and examine its entanglement properties. Therefore, we present the entropy of the two-qutrit state

as

$$I_{lin} = \frac{2d}{d-1}\frac{\Delta_1 + 2(\Delta_2 + \Delta_3 + \Delta_4)}{\mathcal{N}^2}, \tag{4.17}$$

where

$$\Delta_1 = |\mu\lambda|^2 {M_1}^2 {N_1}^2 + |\mu\nu|^2 {M_2}^2 {N_2}^2 + |\lambda\nu|^2 {M_3}^2 {N_3}^2$$

$$\Delta_2 = |\mu|^2 \mathrm{Re}[\bar{\lambda}\nu(\bar{q}_1 q_2 - q_3)(\bar{p}_1 p_2 - p_3)]$$

$$\Delta_3 = |\lambda|^2 \mathrm{Re}[\bar{\mu}\nu(q_1 q_3 - q_2)(p_1 p_3 - p_2)]$$

$$\Delta_4 = |\nu|^2 \mathrm{Re}[\bar{\mu}\lambda(\bar{q}_3 q_2 - q_1)(\bar{p}_3 p_2 - p_1)]$$

$$\mathcal{N} = |\mu|^2 + |\lambda|^2 + |\nu|^2 + 2Re(\bar{\mu}\lambda q_1 p_1 + \bar{\mu}\nu q_2 p_2 + \bar{\lambda}\nu q_3 p_3).$$

Proof:

One may work out the density operator of the first subsystem by tracing over the second subsystem as $\rho_1 = Tr_2(|\Psi\rangle\langle\Psi|)$. In the standard qutrit basis it reads

$$\rho_1 = (I \otimes \langle 0|)|\Psi\rangle\langle\Psi|(I \otimes |0\rangle) + (I \otimes \langle 1|)|\Psi\rangle\langle\Psi|(I \otimes |1\rangle)$$

$$+(I \otimes \langle 2|)|\Psi\rangle\langle\Psi|(I \otimes |2\rangle).$$

With this regard, we find the density matrix of the first subsystem that is given as a 3×3 matrix of qutrit form. Here, we use $\widetilde{\rho}_1$ for unnormalized density matrix (since the qutrit state $|\Psi\rangle$ in (4.1) is not normalized, in general), and ρ_1 for the normalized density matrix. Therefore, the (unnormalized) density matrix of the first subsystem can be derived as

$$\widetilde{\rho}_1 = [|\mu|^2 + |\lambda|^2|p_1|^2 + |\nu|^2|p_2|^2 + \mu\bar{\lambda}\bar{q}_1\bar{p}_1 + \mu\bar{\nu}\bar{q}_2\bar{p}_2 + \lambda\bar{\nu}\bar{q}_3 p_1\bar{p}_2$$

$$+\mu\bar{\lambda}\bar{q}_1\bar{p}_1 + \bar{\mu}\nu q_2 p_2 + \bar{\lambda}\nu q_3\bar{p}_1 p_2]|0\rangle\langle 0| + [|\lambda|^2 p_1 N_1 + \mu\bar{\lambda}\bar{q}_1 N_1$$

$$|\nu|^2 p_2\frac{\bar{p}_3 - \bar{p}_2 p_1}{N_1} + \mu\bar{\nu}\bar{q}_2\frac{(\bar{p}_3 - \bar{p}_2 p_1)}{N_1} + \lambda\bar{\nu}\bar{q}_3 p_1\frac{(\bar{p}_3 - \bar{p}_2 p_1)}{N_1} + \bar{\lambda}\nu$$

$$q_3 N_1 p_2]|0\rangle\langle 1| + [|\lambda|^2 \bar{p}_1 N_1 + |\nu|^2 \bar{p}_2 \frac{p_3 - p_2\bar{p}_1}{N_1} \bar{\mu}\lambda q_1 N_1 + \bar{\mu}\nu q_2$$

$$\frac{(p_3 - p_2\bar{p}_1)}{N_1} + \bar{\lambda}\nu q_3 \bar{p}_1 (p_3 - p_2\bar{p}_1) + \lambda\bar{\nu}\bar{q}_3 N_1 \bar{p}_2]|1\rangle\langle 0| + [|\lambda|^2 N_1^2$$

$$+|\nu|^2 \frac{|p_3 - p_2\bar{p}_1|^2}{{N_1}^2} + \lambda\bar{\nu}\bar{q}_3(\bar{p}_3 - \bar{p}_2 p_1) + \bar{\lambda}\nu q_3(p_3 - p_2\bar{p}_1)]|1\rangle\langle 1|$$

$$+[(|\nu|^2 p_2 \frac{N}{N_1} + (\mu\bar{\nu}\bar{q}_2 + \lambda\bar{\nu}\bar{q}_3 p_1)\frac{N}{N_1}]|0\rangle\langle 2| + [\bar{\mu}\nu q_2 + \bar{\lambda}\nu q_3 \bar{p}_1)\frac{N}{N_1}$$

$$+|\nu|^2 \bar{p}_2 \frac{N}{N_1}]|2\rangle\langle 0| + [|\nu|^2 \frac{(p_3 - p_2\bar{p}_1)}{N_1}\frac{N}{N_1}]|1\rangle\langle 2| + [|\nu|^2 \frac{(\bar{p}_3 - \bar{p}_2 p_1)}{N_1}$$

$$\frac{N}{N_1}]|2\rangle\langle 1| + [|\nu|^2 \frac{N^2}{{N_1}^2}]|2\rangle\langle 2|.$$

This density matrix is rather complicate to evaluate the linear entropy of the state and get a simplified form; therefore, we may discompose the density operator in terms of matrices A and B as

$$\widetilde{\rho}_1 = A + B + B^\dagger,$$

where the matrix A is given by

$$A = (|\mu|^2 + |\lambda|^2|p_1|^2 + |\nu|^2|p_2|^2)|0\rangle\langle 0| + (|\lambda|^2 p_1 N_1 + |\nu|^2 p_2$$

$$\frac{\bar{p}_3 - \bar{p}_2 p_1}{N_1})|0\rangle\langle 1| + (|\lambda|^2 N_1 \bar{p}_1 + |\nu|^2 \bar{p}_2 (\frac{p_3 - p_2\bar{p}_1}{N_1}))|1\rangle\langle 0| +$$

$$[|\lambda|^2 N_1^2 + |\nu|^2 \frac{|p_3 - p_2\bar{p}_1|^2}{{N_1}^2}[|1\rangle\langle 1| + |\nu|^2 p_2 \frac{N}{N_1}|0\rangle\langle 2| + |\nu|^2 \bar{p}_2 \frac{N}{N_1}$$

$$|2\rangle\langle 0| + |\nu|^2 \frac{(p_3 - p_2\bar{p}_1)}{N_1}\frac{N}{N_1}|1\rangle\langle 2| + |\nu|^2 \frac{(\bar{p}_3 - \bar{p}_2 p_1)}{N_1}\frac{N}{N_1}|2\rangle\langle 1|$$

$$+|\nu|^2 \frac{N^2}{{N_1}^2}|2\rangle\langle 2|,$$

and the matrix B is given by

$$B = (\mu\bar{\lambda}\bar{q}_1\bar{p}_1 + \mu\bar{\nu}\bar{q}_2\bar{p}_2 + \lambda\bar{\nu}\bar{q}_3 p_1\bar{p}_2)|0\rangle\langle 0| + (\lambda\bar{\nu}\bar{q}_3 N_1\bar{p}_2)|1\rangle\langle 0|$$

$$+(\mu\bar{\lambda}\bar{q}_1 N_1 + \mu\bar{\nu}\bar{q}_2\frac{(\bar{p}_3 - \bar{p}_2 p_1)}{N_1} + \lambda\bar{\nu}\bar{q}_3 p_1\frac{(\bar{p}_3 - \bar{p}_2 p_1)}{N_1}|0\rangle\langle 1|$$

$$+(\lambda\bar{\nu}\bar{q}_3(\bar{p}_3 - \bar{p}_2 p_1))|1\rangle\langle 1| + ((\mu\bar{\nu}\bar{q}_2 + \lambda\bar{\nu}\bar{q}_3 p_1)\frac{N}{N_1})|0\rangle\langle 2|.$$

We note that $A^\dagger = A$, but $B^\dagger \neq B$. Furthermore, the normalized density matrix is given as

$$\rho_1 = \frac{\widetilde{\rho}_1}{Tr\widetilde{\rho}_1}.$$

Thus, the linear entropy can be expressed as

$$I_{lin} = \frac{d}{d-1}(1 - \frac{Tr\widetilde{\rho}_1^2}{Tr^2\widetilde{\rho}_1}) = \frac{d}{d-1}\frac{Tr^2\widetilde{\rho}_1 - Tr\widetilde{\rho}_1^2}{Tr^2\widetilde{\rho}_1}.$$

We can expresses the terms $Tr^2\widetilde{\rho}_1$ and $Tr\widetilde{\rho}_1^2$, in as the matrix traces of combinations of A and B

$$Tr^2\widetilde{\rho}_1 = Tr^2 A + Tr^2 B + Tr^2 B^\dagger + 2TrATrB + 2TrATrB^\dagger + 2TrBTrB^\dagger,$$

also

$$Tr\widetilde{\rho}_1^2 = TrA^2 + TrB^2 + TrB^{\dagger 2} + 2Tr(AB) + 2Tr(AB^\dagger) + 2Tr(BB^\dagger).$$

Thus, the linear entropy may be rewritten as

$$I_{lin} = \frac{d}{(d-1)Tr^2\widetilde{\rho}_1}[(Tr^2 A - TrA^2)+$$

$$(Tr^2 B - TrB^2) + (Tr^2 B^\dagger - TrB^{\dagger 2})$$

$$+2(TrATrB - Tr(AB)) + 2(TrATrB^\dagger - TrAB^\dagger)$$

$$+2(TrBTrB^\dagger - TrBB^\dagger)].$$

We leave it to the reader to verify that

$$Tr^2 A - TrA^2 = 2[|\mu|^2|\lambda|^2 N_1^2 + |\mu|^2||\nu|^2 N_2^2 + |\lambda|^2|\nu|^2 N_3^2]$$

$$Tr^2B - TrB^2 = 2|\lambda|^2\mu\bar{\nu}\bar{q}_1\bar{q}_3(\bar{p}_1\bar{p}_3 - \bar{p}_2)$$

$$Tr^2B^\dagger - TrB^{\dagger 2} = 2|\lambda|^2\bar{\mu}\nu q_1 q_3(p_1 p_3 - p_2)$$

$$TrATrB - Tr(AB) = -|\mu|^2|\lambda\bar{\nu}\bar{q}_3(p_1\bar{p}_2 - \bar{p}_3) - |\lambda|^2\mu\bar{\nu}\bar{q}_2$$

$$(\bar{p}_1\bar{p}_3 - \bar{p}_2) - |\nu|^2\mu\bar{\lambda}\bar{q}_2(\bar{p}_2 p_3 - \bar{p}_1)$$

$$TrATrB^\dagger - Tr(AB^\dagger) = -|\mu|^2\bar{\lambda}\nu q_3(\bar{p}_1 p_2 - p_3) - |\lambda|^2\bar{\mu}\nu q_2$$

$$(p_1 p_3 - p_2) - |\nu|^2\bar{\mu}\lambda q_2(p_2\bar{p}_3 - p_1)$$

$$TrBTrB^\dagger - Tr(BB^\dagger) = -|\mu|^2|\lambda|^2|q_1|^2N_1^2 - |\mu|^2|\nu|^2|q_2|^2N_2^2$$

$$-|\lambda|^2|\nu|^2|q_3|^2N_3^2 + |\mu|^2\bar{\lambda}\nu\bar{q}_1 q_2(\bar{p}_1 p_2 - p_3) + |\mu|^2\lambda\bar{\nu}q_1\bar{q}_2$$

$$(\bar{p}_2 p_1 - \bar{p}_3) + |\nu|^2\mu\bar{\lambda}\bar{q}_2 q_3(\bar{p}_2 p_3 - \bar{p}_1) + |\nu|^2\bar{\mu}\lambda q_2\bar{q}_3(\bar{p}_3 p_2 - p_1)$$

Now, putting everything together it is straightforward to verify the linear entropy of the qutrit system in Eq.(4.17).

As was expected I_{lin} is symmetric in terms of the parameters of the first and the second subsystem. This expression fully captures the entanglement of qutrit nonorthogonal state and gives the unentangled and maximally entangled states. It can be observed that when at least two of the coefficients (μ, λ, ν) is zero or in the case that $p_i = q_i = \pm 1$ the entropy becomes zero. Now, if we take $\lambda = 0$ in the state (4.1), then the three dimensional state will reduce to a two dimensional system state

$$|\Psi\rangle = \mu|\alpha_1\rangle|\beta_1\rangle + \nu|\alpha_3\rangle|\beta_3\rangle. \tag{4.18}$$

In this case $\Delta_2 = \Delta_3 = \Delta_4 = 0$, and $\Delta_1 = |\mu\nu|^2{M_2}^2{N_2}^2$. Taking into account the fact that we are dealing with a two-dimensional state ($d = 2$), the linear entropy then will reduce to

$$I_{lin} = 4\frac{|\mu\nu|^2(1 - |p_2|^2)(1 - |q_2|^2)}{(|\mu|^2 + |\nu|^2 + 2Re(\bar{\mu}\nu q_2 p_2))^2}. \tag{4.19}$$

This is just the square of the concurrence [13] of nonorthogonal two-qubit coherent states which is studied widely in the literature. Therefore, the linear entropy in (4.17), captures the entanglement of both qubit (when one of the coefficient is zero) and qutrit nonorthogonal states, and hence, we can take $d = 3, 2$ in (4.17) for the qutrit and qubit system states respectively. To investigate the two-dimensional case in more detail, we define $|p_2| = \cos\theta_1$, and $|q_2| = \cos\theta_2$, with $0 \leq \theta_1, \theta_2 \leq \frac{\pi}{2}$. This change of variable results in

$$I_{lin} \leq \frac{4|\mu\nu|^2 \sin^2\theta_1 \sin^2\theta_2}{(|\mu|^2 + |\nu|^2 - 2|\mu\nu|\cos\theta_1\cos\theta_2)^2}.$$

By maximizing the right hand side in terms of the real parameters $|\mu|$ and $|\nu|$ we see that the maximum of the linear entropy occurs when $|\mu| = |\nu|$, and consequently

$$I_{lin} \leq \frac{\sin^2\theta_1 \sin^2\theta_2}{(1 - \cos\theta_1\cos\theta_2)^2}.$$

The right hand side of the inequality is equal or less than one, and hence, the maximality requires that $\theta_1 = \theta_2$, or equivalently, $|p_2| = |q_2|$. On the other hand, with this description, the inequality in above relations must reduce to equality for maximal entanglement, and as a result, one can verify that the two-qubit nonorthogonal CS is maximally entangled iff $\mu = \nu e^{i\theta}$ and $p_2 = -\bar{q}_2 e^{-i\theta}$. Thus, we just recovered the main result of the Ref. [76]. We note that the qutrit type entangled coherent states studied in the framework of the linear entropy in this work generalizes the qubit type entangled coherent states that are widely investigated in the literature [62]. We also note that in the orthogonality limit ($q_i = p_i = 0$), taking $\mu = \nu = 1$ and $\lambda = \pm 1$ we get the maximally entangled qutrit states

$$|\psi_\pm\rangle = \frac{1}{\sqrt{3}}(|00\rangle \pm |11\rangle + |22\rangle).$$

We note that, strictly within the framework of coherent states, the overlap of two coherent states is not zero ($|\langle\alpha|\gamma\rangle| = \exp[-1/2(|\alpha| - |\gamma|)^2]$). Thus, the orthogonality limit requires that the difference between coherence parameters in the modes to be relatively large. We note that, due to

the exponential behavior of the coherent state overlap parameters, even for relatively small values of the parameters α and γ this limit can be fulfilled, such that one may consider $\langle\alpha|\gamma\rangle \simeq 0$. Noting that for the coherence parameter α the average number of photons $\bar{n}$ can be expressed in terms of the coherence parameter as $\bar{n} = |\alpha|^2$, one observes that to approach the orthogonality limit, for generating the above maximally entangled state, we must be able to prepare coherent states with large enough average photon number. It is remarkable that such coherent states can be prepared using superconductor cavities and quantum circuits [97]. The generation of coherent state superposition of 100 photons has been realized [71]. Which makes the experimental possibility of such limit more feasible. The other interesting situation would be to consider the case where one of the subsystems is given in orthonormal basis and the other one in mutually nonorthogonal basis. Therefore, by taking the second subsystem in orthogonal basis the state (4.1) reduces to

$$|\Psi\rangle = \mu|\alpha_1\rangle|0\rangle + \lambda|\alpha_2\rangle|1\rangle + \nu|\alpha_3\rangle|2\rangle. \tag{4.20}$$

For this system state the entropy reads

$$I_{lin} = \frac{2d}{d-1}\frac{|\mu\lambda|^2 {N_1}^2 + |\mu\nu|^2 {N_2}^2 + |\lambda\nu|^2 {N_3}^2}{(|\mu|^2 + |\lambda|^2 + |\nu|^2)^2}. \tag{4.21}$$

It immediately follows that

$$I_{lin} < \frac{2d}{d-1}\frac{|\mu\lambda|^2 + |\mu\nu|^2 + |\lambda\nu|^2}{(|\mu|^2 + |\lambda|^2 + |\nu|^2)^2}.$$

We note that this condition may reduce to the equality only if $p_i = 0$, or equivalently the first subsystem happens to be in orthogonal basis as well; however, we have supposed that the first subsystem in nonorhogonal basis. Therefore, taking into account the fact that the right hand side of the inequality is equal or less than one (for both qubit and qutrit states), and hence, $I_{lin} < 1$. Thus, we conclude that there is no maximally entangled two or three dimensional state in which one of the subsystems is given in mutually orthogonal basis and the other subsystem in nonorthogonal

basis.

It is notable that by factoring out the coefficient $\mu \neq 0$ and saturating it in normalization factor and then redefining the coefficients, we can always rewrite the state unnormalized $|\Psi\rangle$ as

$$|\Psi\rangle = |\alpha_1\rangle|\beta_1\rangle + \lambda|\alpha_2\rangle|\beta_2\rangle + \nu|\alpha_3\rangle|\beta_3\rangle.$$

This is equivalent to taking $\mu = 1$. To illustrate the effects of different parameters that control the entanglement, let us take $q_i = p_i$ in Eq.(4.17) and investigate the entanglement of the system in different situations. First, we fix the overlap parameters ($p_i s$) and study the entropy of the state as a function of ν and λ. We report in the Fig.4.2 the entanglement of the system versus ν and λ. The entanglement for the case $p_1 = 0.1$, $p_2 = 0.1$ and $p_3 = 0.4$ is given in the plot A, and also for the $p_1 = 0.1$, $p_2 = 0.5$ and $p_3 = 0.3$ in the plot B. The density of entanglement corresponding to the figure A is presented in plot C, and the one corresponding to the plot B is presented in plot D. Clearly, when $\nu = \lambda = 0$, the state become a product state, and the entanglement is zero. We note that, according to the Fig.4.2, the entropy at the vicinity of the line $\nu = -\lambda$ can be larger than the other regions. It is also interesting to note that for nonzero $p_i s$, entanglement along the direction $\nu = \lambda$ can be less than the states with $\nu = -\lambda$. With this observations, we consider two different sets of the states (satisfying $q_i = p_i$) in more details

$$|\Psi\rangle^{\pm} = |\alpha_1\rangle|\beta_1\rangle \pm |\alpha_2\rangle|\beta_2\rangle + |\alpha_3\rangle|\beta_3\rangle. \tag{4.22}$$

It is remarkable that, as was observed in Fig.4.2, for given $p_i s$, $|\Psi\rangle^{-}$ tends to be more entangled than $|\Psi\rangle^{+}$. The linear entropy of $|\Psi\rangle^{\pm}$ reads

$$I_{lin} = 3\frac{(p_1^2-1)^2 + (p_2^2-1)^2 + (p_3^2-1)^2}{(3 \pm 2p_1^2 + 2p_2^2 \pm 2p_3^2)^2}$$

$$+ 6\frac{(p_2 - p_1p_3)^2 \pm (p_1 - p_2p_3)^2 \pm (p_3 - p_1p_2)^2}{(3 \pm 2p_1^2 + 2p_2^2 \pm 2p_3^2)^2}. \tag{4.23}$$

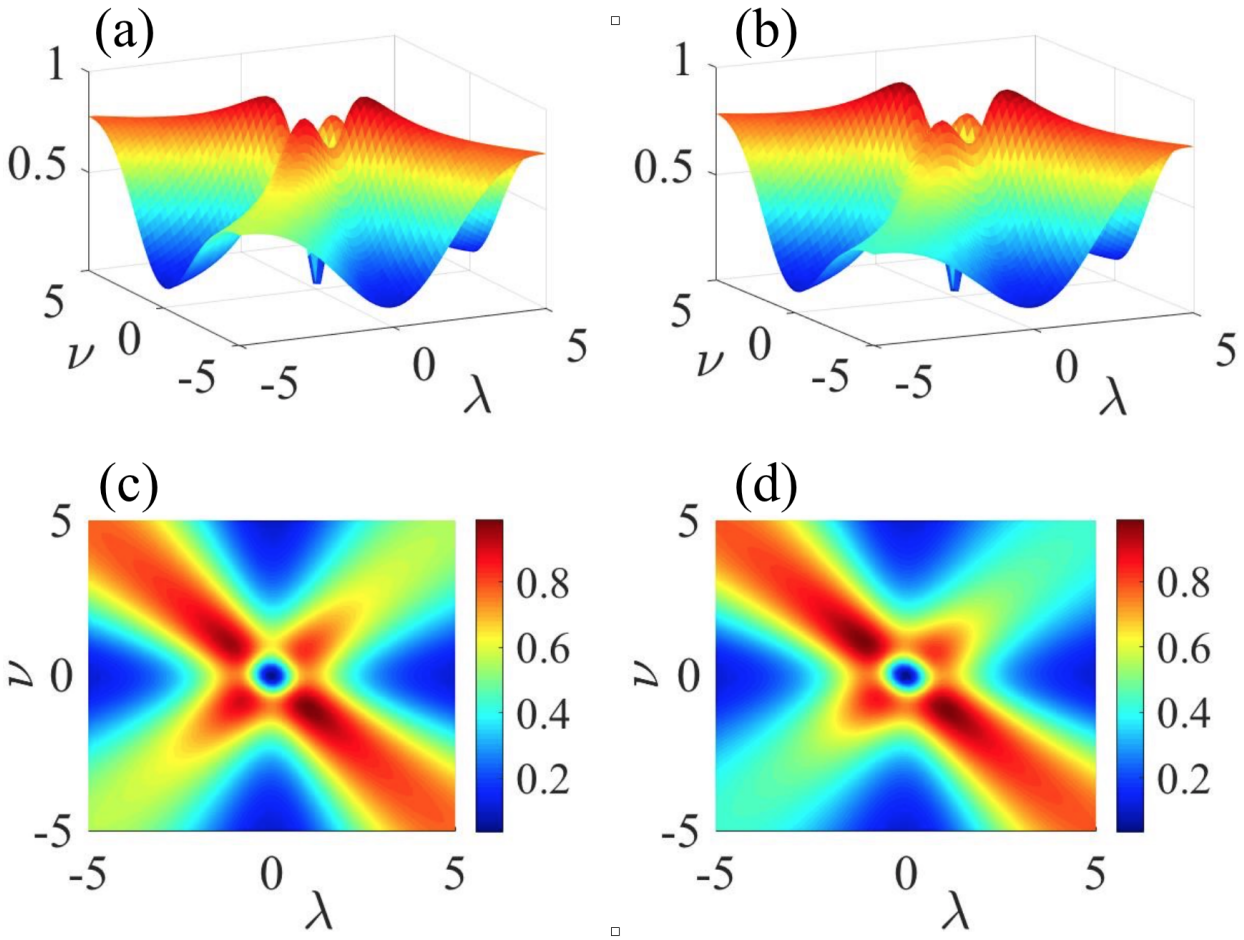

Figure 4.2: A: Entanglement of the state with $p_1 = 0.1$, $p_2 = 0.1$ and $p_3 = 0.4$. B: Entanglement of the state with $p_1 = 0.1$, $p_2 = 0.5$ and $p_3 = 0.3$. C: The density of entanglement corresponding to the A. D: The density of entanglement corresponding to the B.

Let us first consider the entropy of $|\Psi\rangle^-$ as a function of p_1 and p_3 for different values of p_2. Thus, the density of the entanglement of $|\Psi\rangle^-$ as a function of overlap parameters p_1 and p_3 is depicted in Fig.4.3. One can observe that $|\Psi\rangle^-$ is highly entangled for different values of overlap parameters, and the maximally entangled states in this set of states can be detected. According to Fig.4.3, the state becomes highly entangled at the vicinity of $p_1 = p_3$. And, we should stress that the entanglement increases as p_2 decreases. Now, we consider the entropy of $|\Psi\rangle^+$ as a function of

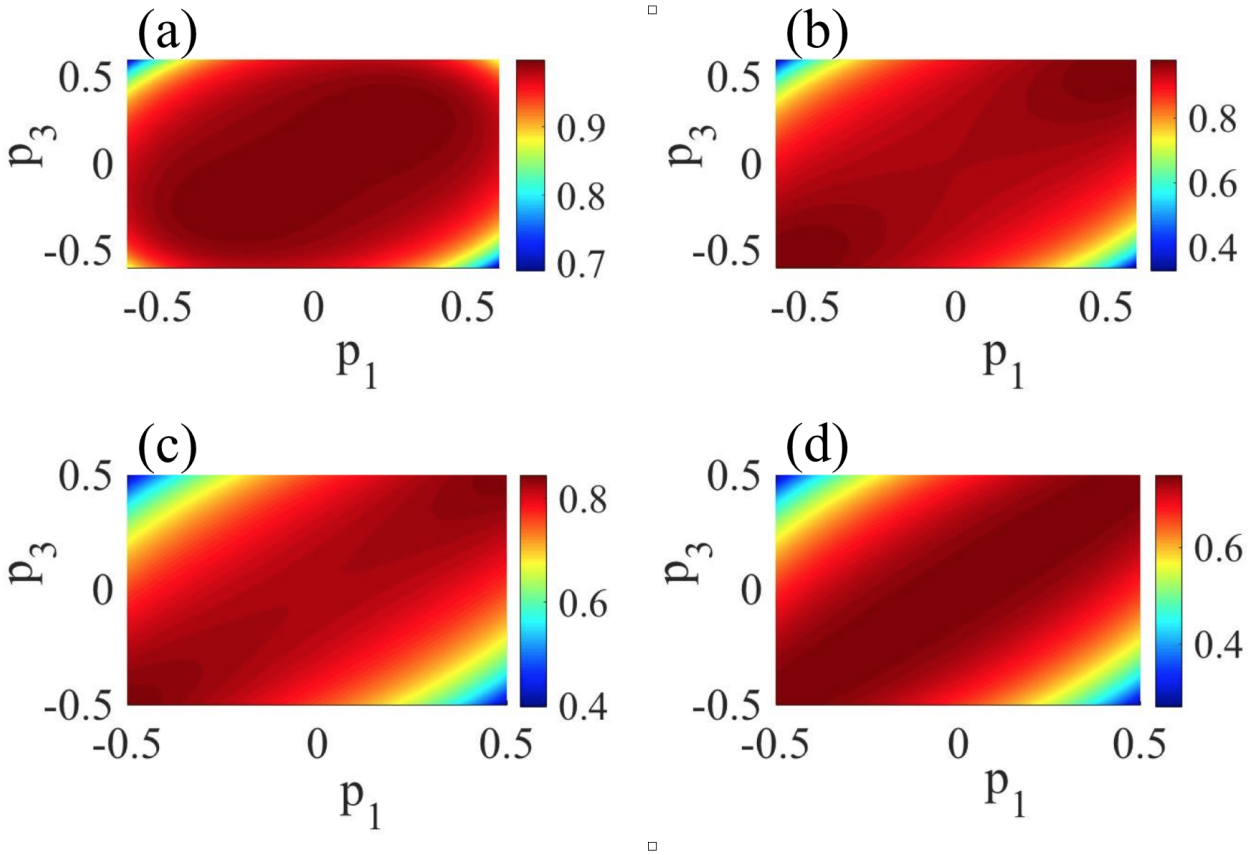

Figure 4.3: Density of Linear entropy of $|\Psi\rangle^-$ as a function of overlap parameters p_1 and p_3. (a) corresponds to $p_2 = 0.05$. (b) to $p_2 = 0.2$. (c) to $p_2 = 0.4$. And (d) to $p_2 = 0.5$. (Yusef Maleki and Aleksei M. Zheltikov,2019)

p_1 and p_3 for different values of p_2. We attribute the same values as in $|\Psi\rangle^-$ for p_2 in this case and study the entanglement properties of the system state. In Fig.4.4, the density of the entanglement of

$|\Psi\rangle^+$ as a function of overlap parameters p_1 and p_3 is given. One can observe that, the entanglement

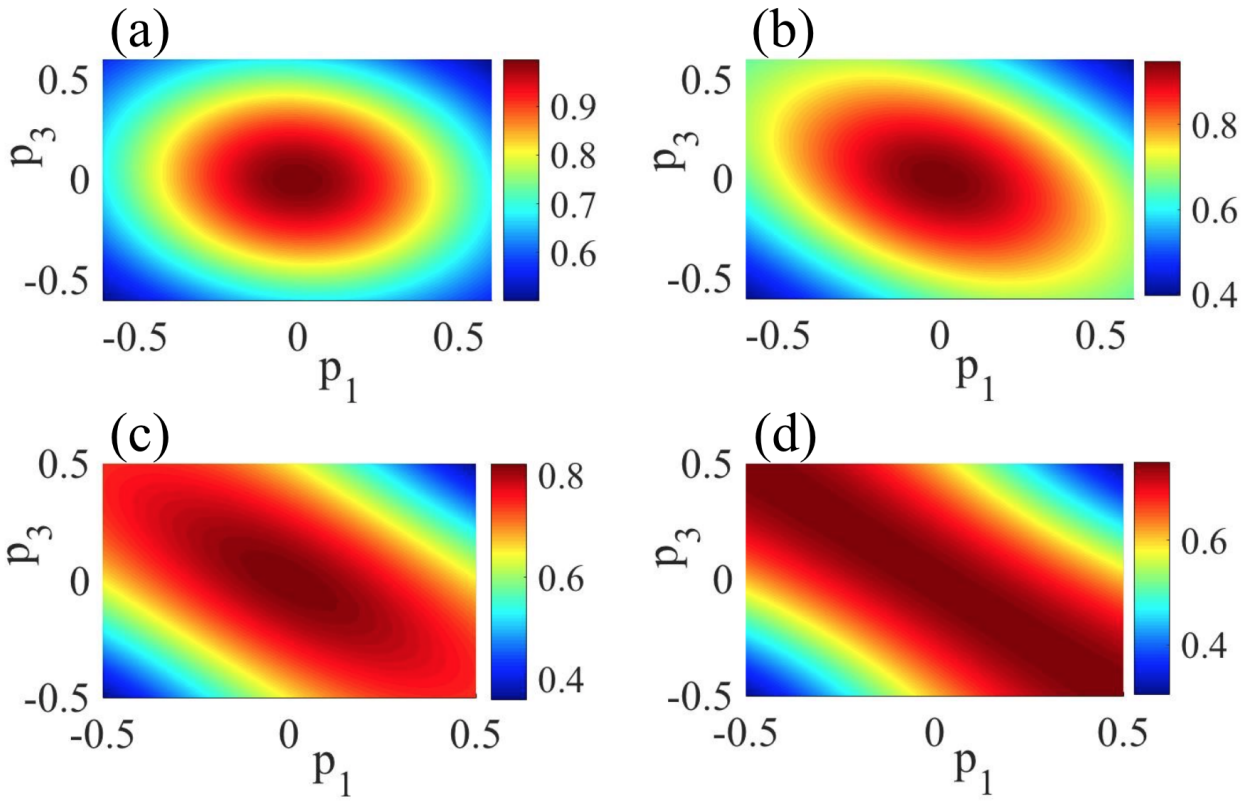

Figure 4.4: Density of Linear entropy of $|\Psi\rangle^+$ as a function of overlap parameters p_1 and p_3. The plot (a) corresponds to $p_2 = 0.05$. (b) to $p_2 = 0.2$. (c) to $p_2 = 0.4$. And (d) to $p_2 = 0.5$. (Yusef Maleki and Aleksei M. Zheltikov,2019)

increases as the overlap parameter p_2 decreases. Moreover, unlike the state $|\Psi\rangle^-$, in this case when $p_2 \neq 0$, the states at the vicinity of $p_1 = -p_3$ line attain more entanglement entropy than the other regions. Furthermore, by comparing entanglement in $|\Psi\rangle^-$ and $|\Psi\rangle^+$ we can see that the states in $|\Psi\rangle^-$ may be more entangled when both of the states take the same values of positive overlap parameters. It is also worth to compare this with two-qubit coherent states given as

$$|\Phi\rangle^{\pm} = |\alpha_1\rangle|\beta_1\rangle \pm |\alpha_2\rangle|\beta_2\rangle. \tag{4.24}$$

Taking the parameters to be real (without loss of generality), the concurrence of the states reads [36, 76]

$$C^{\pm} = \frac{\sqrt{(1-\langle\alpha_2|\alpha_1\rangle^2)(1-\langle\beta_2|\beta_1\rangle^2)}}{1 \pm \langle\alpha_2|\alpha_1\rangle\langle\beta_2|\beta_1\rangle}.$$

Where $\langle\alpha_2|\alpha_1\rangle = \exp[\frac{-1}{2}(\alpha_2 - \alpha_1)^2]$. It is evident that $|\Phi\rangle^-$ is more entangled than $|\Phi\rangle^+$ in the above scenario. Therefore, the states with all coefficients having positive or negative values, are less entangled than the ones that coefficients take the same values but not all have the same signs.

To get a better insight into entanglement behavior of these states let us consider typical examples of entangled coherent state as

$$|\psi\rangle = |\alpha\rangle|\alpha\rangle + e^{i\theta}|2\alpha\rangle|2\alpha\rangle + |3\alpha\rangle|3\alpha\rangle, \tag{4.25}$$

$$|\phi\rangle = |\alpha\rangle|\alpha\rangle + e^{i\theta}|2\alpha\rangle|2\alpha\rangle + e^{i\theta}|3\alpha\rangle|3\alpha\rangle, \tag{4.26}$$

Since $|\alpha\rangle$, $|2\alpha\rangle$, and $|3\alpha\rangle$ are linearly independent for all nonzero αs, these are two-qutrit coherent states. The linear entropy of the states as a function of α and θ is given in Fig.4.5, where Fig.4.5(a) corresponds to the state $|\psi\rangle$ and Fig.4.5(b) corresponds to the state $|\phi\rangle$.

In both states, entanglement is small for small enough coherence parameter α, but it enhances as the parameter $|\alpha|$ increases. For large enough $|\alpha|s$ ($|\alpha| > 2$), the states become maximally entangled and their entanglement is independent of local phase θ. Note that in the large coherence limit the coherent states tend to orthogonality and the orthogonal basis can be encoded such that $|0\rangle \equiv |\alpha\rangle$, $|1\rangle \equiv |2\alpha\rangle$ and $|2\rangle \equiv |3\alpha\rangle$. Therefore, in the strong regime ($|\alpha| \to \infty$) the three dimensional coherent state becomes maximally entangled. For example the state $|\psi\rangle$ shall read

$$|\psi\rangle = \frac{1}{\sqrt{3}}(|00\rangle + e^{i\theta}|11\rangle + |22\rangle).$$

However, for the weaker regime with smaller values of $|\alpha|$, the entanglement highly depends on the phase θ; it is minimum for $\theta = 0$, and increases as $|\theta|$ increases from 0 to π. For the very weak regime with $|\alpha| \to 0$, one has $I_{lin} = 0$. Furthermore, the entanglement of the state $|\psi\rangle$ is more

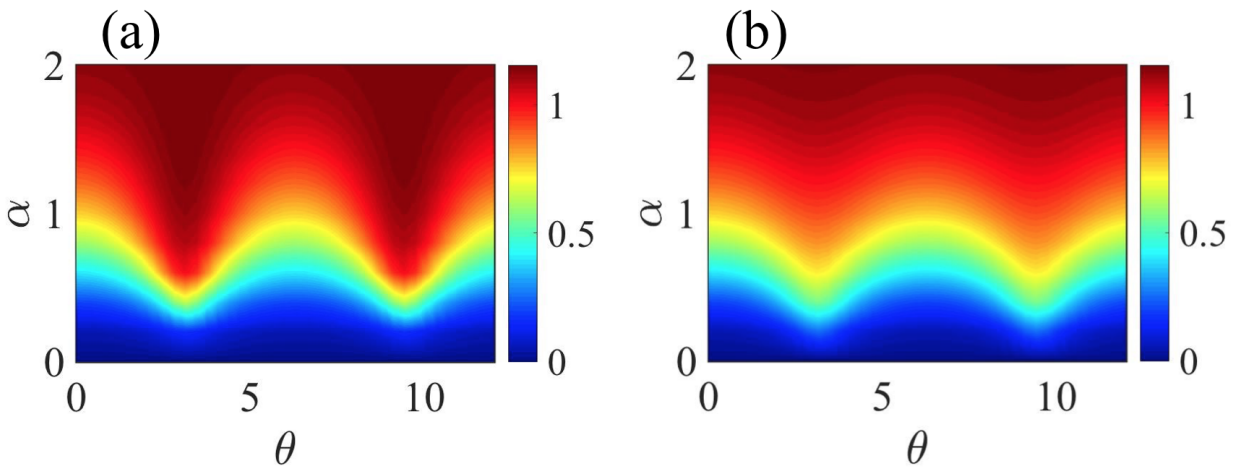

Figure 4.5: Linear entropy versus α and θ for two-qutrit coherent state state. (Yusef Maleki and Aleksei M. Zheltikov,2019)

dependant on the phase compared to the state $|\phi\rangle$, also its entanglement at $\theta = \pi$ is larger. As the last example of the two-mode entangled coherent states, we examine the entanglement of the state generated is previous section in Eq.(4.14). The linear entropy of the state reduces to

$$I_{lin} = 3\frac{(p_1^2-1)^2 + (p_2^2-1)^2 + (p_3^2-1)^2 + (p_1 - p_2p_3)^2}{(3+2p_1^2)^2}$$

with $p_1 = p_3 = e^{-\frac{1}{2}|\alpha|^2}$, and $p_2 = e^{-2|\alpha|^2}$. The state tends to maximal entanglement for $|\alpha| \gg 1 (p_i \to 1)$, and the entanglement becomes vanishingly small for the very small coherence parameter $|\alpha|$.

Thus, our analysis of linear entropy for multipartite nonorthogonal states paves the way for understanding the quantum correlations of higher dimensional systems and it provides an insight in controlling entanglement degree of such states in practice via manipulating the involved parameters in the system as well as highly entangled states generations.

4.4 Linear entropy of multi-qutrit states

In this section, we generalize the study of the two-qutrit scenario to the multi-qutrit states. To this aim, we suppose that in a multi-mode system state each subsystem contains k modes

$$|\Psi\rangle = \mu \underbrace{|\alpha_1\rangle...|\alpha_1\rangle}_{k} \underbrace{|\beta_1\rangle...|\beta_1\rangle}_{k} + \lambda|\alpha_2\rangle...|\alpha_2\rangle|\beta_2\rangle...|\beta_2\rangle$$

$$+ \nu|\alpha_3\rangle...|\alpha_3\rangle|\beta_3\rangle...|\beta_3\rangle. \tag{4.27}$$

For generating such entangled state, we can start with a single mode qutrit-like superposed coherent state $\mu|\alpha\rangle + \lambda|\beta\rangle + \nu|\gamma\rangle$, which, for example, can be produced by the method considered in second section. We can send this state though a network of beam splitters, shown in Fig.4.6, where each beam splitter is governed by $u_{i-1,i} = \exp[\theta_{i,j}(a_{i-1}^{\dagger}a_i - a_{i-1}^{\dagger}a_i)]$, with a_i and $a_i^{\dagger}$, being the annihilation and the creation operators of the ith mode, and acts on the modes $i-1$ and i. One can generate multi-mode entangled state of various coherence amplitude types by controlling the reflectivity of the beam splitter through θ. As an illustration, if we set the reflectivity of the beam splitters such that $B_{1,2}$, $B_{2,3}$,..., $B_{n-1,n}$ have the reflectivity of $\frac{1}{\sqrt{n}}$, $\frac{1}{\sqrt{n-1}}$,..., $\frac{1}{\sqrt{2}}$, respectively, then the generated state shall read

$$|\Psi\rangle = \mu|\alpha'\rangle|\alpha'\rangle...|\alpha'\rangle + \lambda|\beta'\rangle|\beta'\rangle...|\beta'\rangle + \nu|\gamma'\rangle|\gamma'\rangle...|\gamma'\rangle \tag{4.28}$$

where α', β' and γ', represent $\frac{\alpha}{\sqrt{n}}$, $\frac{\beta}{\sqrt{n}}$ and $\frac{\gamma}{\sqrt{n}}$, respectively.

One may define three mutually orthogonal standard qutrit basis as $\{|\mathbf{0}\rangle, |\mathbf{1}\rangle, |\mathbf{2}\rangle\}$. Thus, in analogy to the two-qutrit case, we introduce encoding of these logical basis in terms of nonorthogonal states such that

$$|\mathbf{0}\rangle = |\alpha_1\rangle...|\alpha_1\rangle,$$

$$|\mathbf{1}\rangle = \frac{|\alpha_2\rangle...|\alpha_2\rangle - p_1^k|\alpha_1\rangle...|\alpha_1\rangle}{N_1},$$

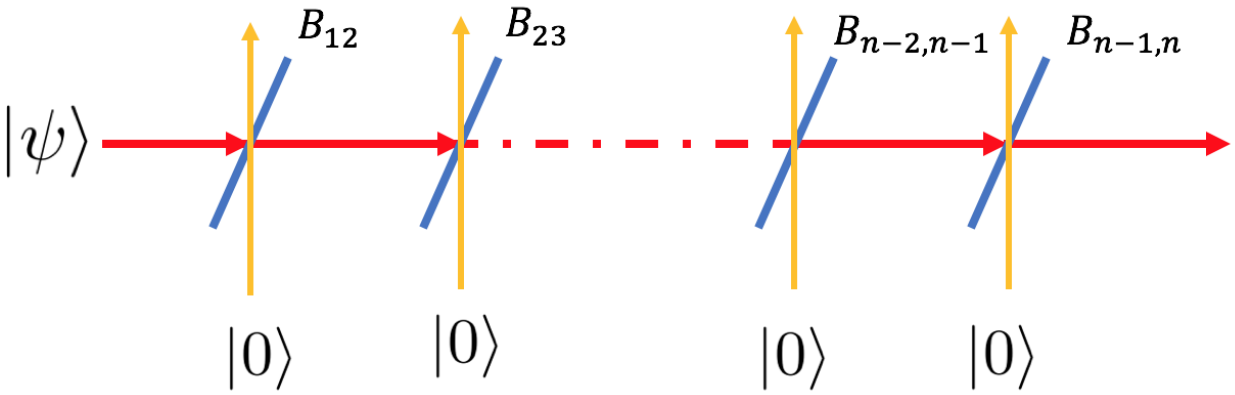

Figure 4.6: The beam splitter network for generation of multimode entangled state. $B_{i,j}$ represents the beam splitter action on the modes i and j.

$$|\mathbf{2}\rangle = \frac{(p_1^k p_3^k - p_2^k)|\alpha_1\rangle...|\alpha_1\rangle + (\bar{p}_1^k p_2^k - p_3^k)|\alpha_2\rangle...|\alpha_2\rangle}{NN_1}$$
$$+\frac{N_1^2|\alpha_3\rangle...|\alpha_3\rangle}{NN_1},$$

where the overlap parameters and the normalization factors are given as

$$p_1 = \langle\alpha_1|\alpha_2\rangle,\ p_2 = \langle\alpha_1|\alpha_3\rangle,\ p_3 = \langle\alpha_2|\alpha_3\rangle,\ N_i = \sqrt{1-|p_i|^{2k}},$$

$$N = [1 - |p_1|^{2k} - |p_2|^{2k} - |p_3|^{2k} + p_1^k \bar{p}_2^k p_3^k + \bar{p}_1^k p_2^k \bar{p}_3^k]^{\frac{1}{2}}.$$

In a similar manner, the nonorthogonal basis of the second subsystem can be used to encode the qutrit logical basis$\{|\tilde{\mathbf{0}}\rangle, |\tilde{\mathbf{1}}\rangle, |\tilde{\mathbf{2}}\rangle\}$ as

$$|\tilde{\mathbf{0}}\rangle \equiv |\beta_1\rangle...|\beta_1\rangle,$$
$$|\tilde{\mathbf{1}}\rangle \equiv \frac{|\beta_2\rangle...|\beta_2\rangle - p_1^k|\beta_1\rangle...|\beta_1\rangle}{M_1},$$
$$|\tilde{\mathbf{2}}\rangle \equiv \frac{(q_1^k q_3^k - q_2^k)|\beta_1\rangle...|\beta_1\rangle + (\bar{q}_1^k q_2^k - q_3^k)|\beta_2\rangle...|\beta_2\rangle}{MM_1}$$
$$+\frac{M_1^2|\beta_3\rangle...|\beta_3\rangle}{MM_1},$$

in which the overlap parameters and the normalization factors are

$$q_1 = \langle\alpha_1|\alpha_2\rangle,\ q_2 = \langle\alpha_1|\alpha_3\rangle,\ q_3 = \langle\alpha_2|\alpha_3\rangle,\ M_i = \sqrt{1-|q_i|^{2k}},$$

$$M = [1 - |q_1|^{2k} - |q_2|^{2k} - |q_3|^{2k} + q_1^k \bar{q}_2^k q_3^k + \bar{q}_1^k q_2^k \bar{q} p_3^k]^{\frac{1}{2}}.$$

Therefore, one may observe that the entropy of the system can be given by transforming $p_i \to p_i^k$, and $q_i \to q_i^k$ in the two-qutrit state. Thus the linear entropy of the multi-qutrit state reads

$$I_{lin} = \frac{2d}{d-1}\frac{\Delta_1^k + 2(\Delta_2^k + \Delta_3^k + \Delta_4^k)}{\mathcal{N}_k^2}, \tag{4.29}$$

where

$$\Delta_1^k \equiv |\mu\lambda|^2 {M_1}^2 {N_1}^2 + |\mu\nu|^2 {M_2}^2 {N_2}^2 + |\lambda\nu|^2 {M_3}^2 {N_3}^2$$

$$\Delta_2^k \equiv |\mu|^2 \mathrm{Re}[\bar{\lambda}\nu(\bar{q}_1^k q_2^k - q_3^k)(\bar{p}_1^k p_2^k - p_3^k)]$$

$$\Delta_3^k \equiv |\lambda|^2 \mathrm{Re}[\bar{\mu}\nu(q_1^k q_3^k - q_2^k)(p_1^k p_3^k - p_2^k)]$$

$$\Delta_4^k \equiv |\nu|^2 \mathrm{Re}[\bar{\mu}\lambda(\bar{q}_3^k q_2^k - q_1^k)(\bar{p}_3^k p_2^k - p_1^k)]$$

$$\mathcal{N}_k \equiv |\mu|^2 + |\lambda|^2 + |\nu|^2 + 2Re(\bar{\mu}\lambda q_1^k p_1^k + \bar{\mu}\nu q_2^k p_2^k + \bar{\lambda}\nu q_3^k p_3^k)$$

To illustrate the entanglement behavior of these states let us assume $p_i = q_i$, and $\mu = \nu = \pm\lambda = 1$. The entropy shall reduce to Eq.(4.23), but p_i replaced by p_i^k. Let us take $p_1 = p_3 = 0$, and study entanglement of the system as a function of p_2. This situation can be visualize by assuming $|\alpha_2\rangle$ in z direction of three-dimensional coordinate and $|\alpha_1\rangle$, and $|\alpha_3\rangle$ in x-y plane with arbitrary directions. In this framework, the linear entropy (for both $\lambda = \pm 1$) reduces to

$$I_{lin} = 3\frac{p_2^{4k} + 3}{(2p_2^{2k} + 3)^2}.$$

The entropy of the state as a function of p_2, for different mode number k, is presented in Fig.4.7.

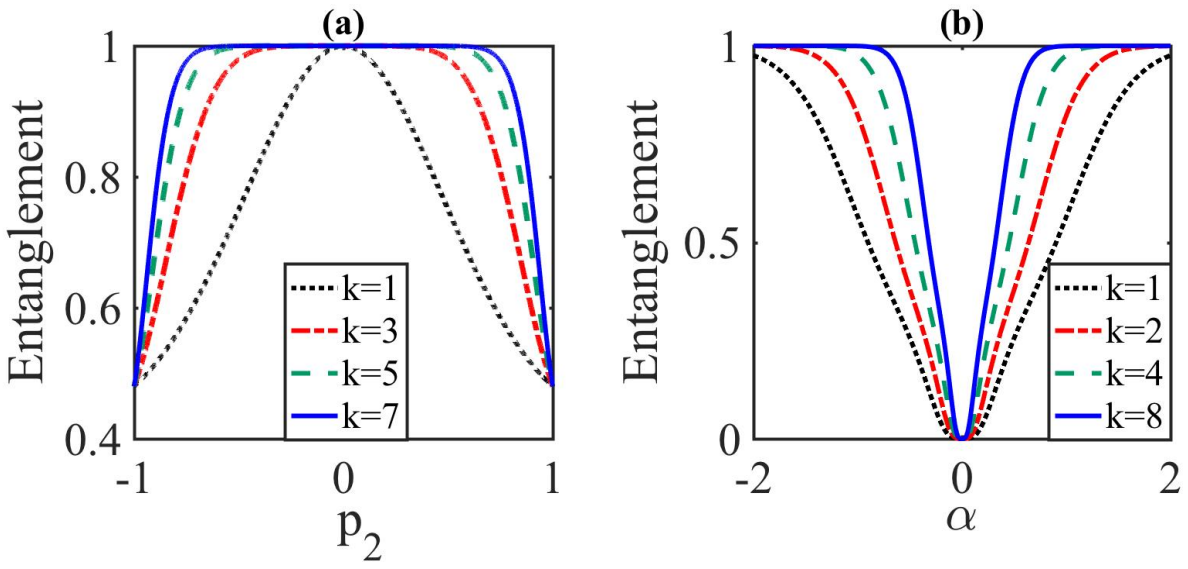

Figure 4.7: Entanglement of multi-qutrit state as a function of p_2, when $p_1 = p_3 = 0$ (a): The black, red, green and blue curves represent entropy for $k = 1, k = 3, k = 5$ and $k = 7$, respectively .Entanglement of multi-qutrit coherent state as a function of α (b): The black, red, green, and blue curves represent entropy for $k = 1, k = 2, k = 4, k = 8$, respectively. (Yusef Maleki and Aleksei M. Zheltikov,2019)

The state becomes maximally entangled when $|\alpha_1\rangle$ and $|\alpha_3\rangle$ are orthogonal, and the entanglement becomes independent of the mode number k. However, the entanglement reduces as $|p_2|$ increases, and when $p_2 = \pm 1$, one gets, from the equation above, $I_{lin} = 0.48$. We also observe that the entanglement increases by increasing the number of the modes in each subsystem (see Fig. 4.7), and the two-mode nonorthogonal states get the minimum entanglement in these set of states.

Finally, we consider the entropy of multi-mode coherent states, as an specific state of the form Eq. 4.28, in which each party contains k modes and is given as

$$|\Psi\rangle = \underbrace{|\alpha\rangle...|\alpha\rangle}_{k}\underbrace{|\alpha\rangle...|\alpha\rangle}_{k} - |2\alpha\rangle...|2\alpha\rangle|2\alpha\rangle...|2\alpha\rangle + |3\alpha\rangle...|3\alpha\rangle|3\alpha\rangle...|3\alpha\rangle. \tag{4.30}$$

This state can be deduced from Eq. 4.28 by setting $\alpha' \equiv \alpha$, $\beta' \equiv 2\alpha$, $\gamma' \equiv 3\alpha$, and specifying the coefficients.

The entropy of this state is depicted in the Fig.4.7.

Accordingly, The entanglement increases as the coherence parameter gets larger (stronger

regime), and it also enhances as the number of modes in the subsystems increases. For $k = 8$, the entropy is maximum even for relatively small coherence parameters ($|\alpha| \geq 1$), and for $k = 2$, the maximum can be obtained for $|\alpha| \geq 2$. Since, in the coherent state, the average of photons is given by $\bar{n} = |\alpha|^2$, the maximum entanglement is achievable for even rather small values of mean photon numbers ($\bar{n} = 4$), when k is large enough. For very large coherence parameter (strong regime), the nonorthogonal states will tend to orthogonality and the entangled coherent states shall be encoded as

$$|\Psi\rangle = \underbrace{|0\rangle...|0\rangle}_{k}\underbrace{|0\rangle...|0\rangle}_{k} - |1\rangle...|1\rangle|1\rangle...|1\rangle + |2\rangle...|2\rangle|2\rangle...|2\rangle.$$

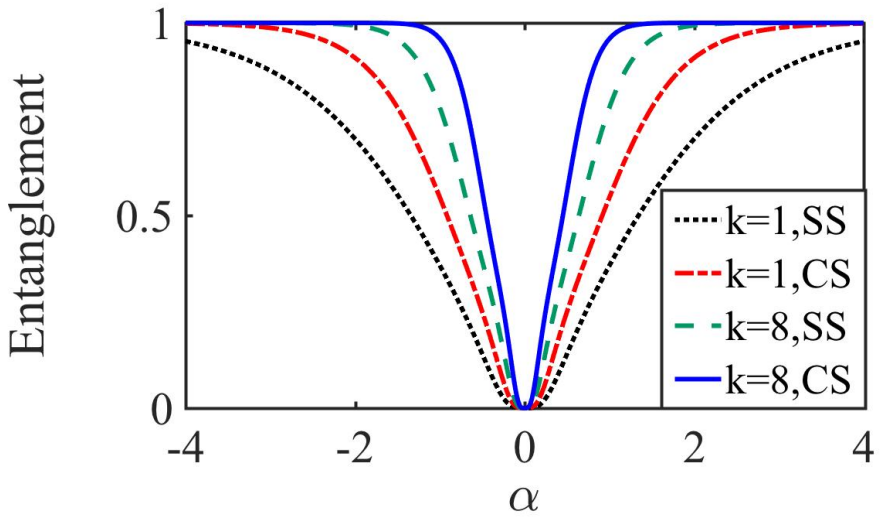

Figure 4.8: Entanglement of multi-qutrit coherent and squeezed state as a function of α. The black and the red curves represent the entanglement of superposed squeezed state (SS) and coherent state (CS), respectively, for $k = 1$. The green and the blue curves depict the entanglement of SS and CS, respectively, for $k = 8$. For both cases, coherent states represent more entanglement than squeezed states. (Yusef Maleki and Aleksei M. Zheltikov,2019)

One may also consider the entanglement of multi-mode squeezed vacuum states of the light in

the context of the state 4.30; that means the coherent states are replaced by squeezed states. We compare the entanglement of three-dimensional coherent and squeezed states in Fig.4.10, for $k = 1$, and $k = 8$. Accordingly, the three dimensional coherent states demonstrate more entanglement than squeezed states when the number of modes and other parameters are the same for both states. Furthermore, the more squeezed the states are (larger squeezing parameters), the more entangled the resultant state becomes.

4.5 Effects of decoherence

Manipulating a quantum system and performing quantum information processing is always subjected to various decoherence effects. A realistic quantum system is not completely closed and interacts with its environment. Thus, it is worthwhile to characterize the entanglement when the system interacts with the environment. Here, we explore entanglement of multimode entangled states when the system loses its coherence due to interactions with the environment [86]. As a practically significant example of a multiqutrit state subjected to decoherence, we consider a $2k$-mode superposition state

$$|\Psi\rangle = \mu_0|\alpha\rangle_A^{\otimes k}|\alpha\rangle_B^{\otimes k} + \mu_1|2\alpha\rangle_A^{\otimes k}|2\alpha\rangle_B^{\otimes k} + \mu_2|3\alpha\rangle_A^{\otimes k}|3\alpha\rangle_B^{\otimes k}. \tag{4.31}$$

In which $|\psi\rangle^{\otimes k} = |\psi\rangle \otimes ... \otimes |\psi\rangle$, k times, and the indexes A and B denote the first and the second partitions. Suppose we encode the information on multimode entangled coherent state $|\Psi\rangle$ and send each mode through a noisy channel, or equivalently each mode undergoes amplitude damping decoherence in a cavity. The information in this process is subjected to decoherence. In particular, a mode that travels through a noisy channel is characterized by [86]

$$|\alpha\rangle|0\rangle_E \rightarrow |\sqrt{\eta}\alpha\rangle|\sqrt{1-\eta}\alpha\rangle_E. \tag{4.32}$$

Where η is the channel lose due to decoherence. Considering the decay of the system inside a cavity, the decay parameter can be given as $\eta = e^{-\gamma t}$, γ being the decay rate of the cavity and t is

the storage time of the state inside the cavity.

If we take the state (4.31) and send each mode through a noisy channel, after tracing out the environment we get the mixed density matrix of multiqutrit system. Then one can introduce qutrit orthogonal basis similar to what we already introduced in this work and find the mixed density matrix of the system in orthogonal bases. To this end, to keep the consideration simple, yet to have an insight into the damping effect, we consider take $\mu_0 = 1$, $\mu_1 = 0$, and $\mu_2 = e^{i\theta}$, reducing the state to $|\Psi\rangle = |\alpha\rangle^{\otimes k}|\alpha\rangle^{\otimes k} + e^{i\theta}|3\alpha\rangle^{\otimes k}|3\alpha\rangle^{\otimes k}$. This stats, due to the damping effects degenerate to

$$\begin{aligned}|\Psi\rangle = (|\sqrt{\eta}\alpha\rangle_A^{\otimes k}|\sqrt{1-\eta}\alpha\rangle_E^{\otimes k}|)(\sqrt{\eta}\alpha\rangle_B^{\otimes k}|\sqrt{1-\eta}\alpha\rangle_E^{\otimes k}) \\ + e^{i\theta}(|\sqrt{\eta}3\alpha\rangle_A^{\otimes k}|\sqrt{1-\eta}3\alpha\rangle_E^{\otimes k})(|\sqrt{\eta}3\alpha\rangle_B^{\otimes k}|\sqrt{1-\eta}3\alpha\rangle_E^{\otimes k}).\end{aligned} \tag{4.33}$$

We trace over the modes belonging to the environment and encode the information in orthonormal computational qubit basis as

$$|\mathbf{0}\rangle \equiv |\sqrt{\eta}\alpha\rangle_A^{\otimes k}, \qquad |\mathbf{1}\rangle \equiv \frac{|\sqrt{\eta}3\alpha\rangle_A^{\otimes k} - e^{-2\eta|\alpha|^2}|\sqrt{\eta}\alpha\rangle_A^{\otimes k}}{\sqrt{1-e^{-4\eta|\alpha|^2}}}. \tag{4.34}$$

This reduced the states of the system to a mixed bipartite entangled state of a two–qubit form which can be represented by a 4×4 matrix. Thus, mapping to the orthogonal bases allows one to work out the concurrence as

$$C = \frac{1-e^{-4k\eta|\alpha|^2}}{1+\cos(\theta)e^{-4k|\alpha|^2}} e^{-4k(1-\eta)|\alpha|^2}. \tag{4.35}$$

We present the entanglement of the states subjected to decoherence in Fig. (4.9), for the different number of modes in each partition. We take $\theta = 0$ in Figs. 4.9(a) & (b). Accordingly, Fig. 4.9(a) presents entanglement of the system when there is no damping introduced to the system. This is comparable to Figs. 4.7(b) for the qutrit states, where the entanglement increases by increasing number of the modes, which agrees with the previous studies of the multimode nonorthogonal states. The concurrence in this case reduces to $C = (1-e^{-4k\alpha^2})/(1+e^{-4k\alpha^2})$,

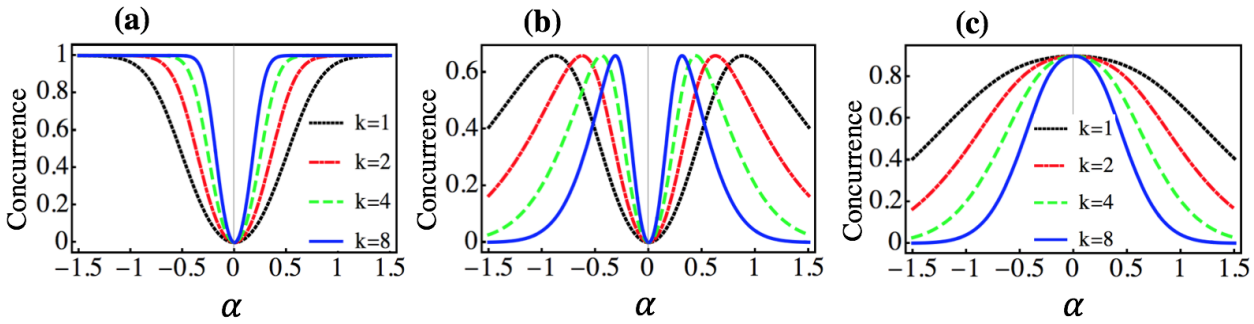

Figure 4.9: The effects of the damping on the concurrence of the multimode states versus the coherence parameter α. We have considered $\theta = 0$ in (a) and (b). $\eta = 1$ (a), $\eta = 0.9$ (b). Similarly, we have considered $\theta = \pi$ and $\eta = 0.9$ in (c). The black, red, green and blue curve corresponds to $k = 1, 2, 4$ and 8, respectively. (Yusef Maleki and Aleksei M. Zheltikov,2019)

which gives $C = 0$ for $\alpha = 0$ and $C \to 1$ for $|\alpha| \to \infty$. Fig. 4.9(b) presents the same situation except with damping effect introduced into the state. We have taken $\theta = 0.9$ in this plot, which can be translated to a cavity with the damping rate characterized by $\gamma \simeq 1MHz$, and the time interval of $t \simeq 0.1\mu s$. As is demonstrated in Fig. 4.9(b), decoherence affects the entanglement drastically in this case. For small coherence parameter α it is quite similar to the situation where there is no damping presented in Fig. 4.9(a). However, for each number of the modes, the entanglement reaches its maxima at a certain α, and decreases beyond that point, approaching zero for a very large α limit. Also, for large enough α, increasing the number of modes not only does not improve the entanglement but it also has an inverse impact on the entanglement. The maximum of the entanglement is independent of the number of the modes and can be determined by the nonlinear equation $(\eta - 1)e^{4k|\alpha|^2\eta} + \eta e^{4k|\alpha|^2(\eta-1)} + 1 = 0$, which numerically can determine the α that gives the maximum value. For instance, for $\eta = 0.9$, the maximum is given at about $4k|\alpha|^2 \simeq 3.12$. Thus, $\alpha \simeq \pm 0.88$ for $k = 1$, and $\alpha \simeq \pm 0.31$ for $k = 8$. The peak of the concurrence only depends on the channel lose which for $\eta = 0.9$ is about $C \simeq 0.66$ as shown in Fig. 4.9(b).

The other interesting situation is to consider the case $\theta = \pi/2$. For this case, the maximum of the entanglement occurs when $4k|\alpha|^2 = \frac{-1}{\eta}\log(1-\eta)$. The maximum of the concurrence reduces, thus, to $C = \eta(1-\eta)^{\frac{1-\eta}{\eta}}$.

We have only considered $\theta = 0$ in Figs. 4.9(a) & (b); however, similar characteristic can be

observed for other nonzero values of θ. The characteristics are drastically different when the phase θ is exactly equal π. This is shown in θ Fig. 4.9(c), where we have considered the same parameters as in Fig. 4.9(b) except for $\theta = \pi$. From the concurrence in Eq.(4.35), it is obvious that when there is no decoherence involved, the states with $\theta = \pi$ become maximally entangled independent of the coherence parameter α. This different characteristic is depicted in Fig. 4.10(a). Where, for any given $\theta \neq \pi$, the entanglement approaches zero for very small α, while it approaches 1 for such small α. According to Fig. 4.9(c), the entanglement decreases when we increase the number of the modes in the presence of decoherence. The maximum of the entanglement occurs when α is nonzero but very small. At such limit, the concurrence is less than 1 and is given by $C \to \eta$.

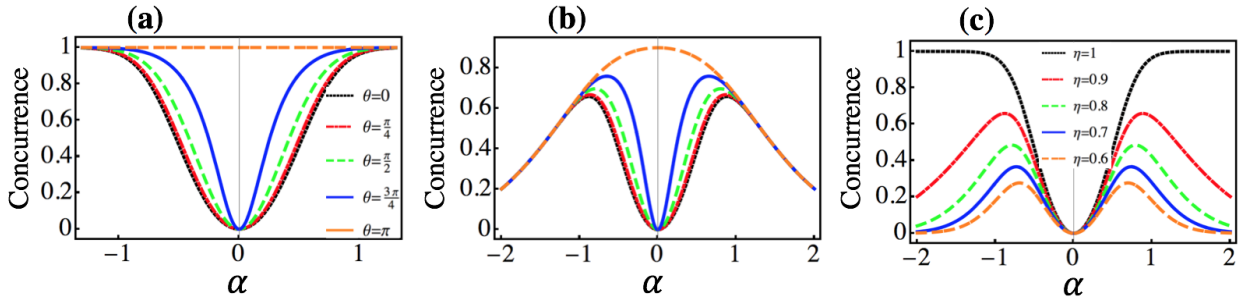

Figure 4.10: The effects of the damping on the concurrence of the multimode states versus the coherence parameter α. We have considered various θ in (a) and (b). $\eta = 1$ (a), $\eta = 0.9$ (b). Similarly, we have considered various η in (c).

In Figs. 4.10(a) & (b) we present the entanglement of the states subjected for various θ for the lose less and lossy channels. According to Fig. 4.10(a) the entanglement enhances when the phase α increases from 0 to π, which agrees with the previous results [82]. Fig. 4.10(b) represents the same situation except $\eta = 0.9$. As we can see, the decoherence affects the system remarkably, reducing the entanglement, specially when α is large enough. Accordingly, the maximum of the entanglement is $C \simeq 0.70$ for $\alpha = \pi/2$ and $C \simeq 0.76$ for $\alpha = 3\pi/4$.

Finally, we present the entanglement for various channel lose factor η in Fig. 4.10(c). As is expected, decreasing η translates into the larger lose in the system resulting in reduction in the

entanglement of the state. Also, the entanglement versus the coherence parameter α, represents some maxima which agrees with the previous figures.

4.6 Extention to higher dimensions

The discussion of the multiqutrit coherent state entanglement made so far can be extended to higher dimensions ($d \geq 4$) by carefully encoding the information in orthogonal bases. A generalized multimode superposition of CSs spanning d–level Hilbert space may be given in the following form

$$|\Psi_d^n\rangle = \mu_0|\alpha_1\rangle...|\alpha_n\rangle + \mu_1|\beta_1\rangle...|\beta_n\rangle + ... + \mu_{d-1}|\gamma_1\rangle...|\gamma_n\rangle. \tag{4.36}$$

We can consider that normalization factors be saturated in $\mu_i s$, and take the state normalized. To investigate bipartite entanglement in such a superposition, one can divide such multimode states into two partitions A and B, and consider it as a bipartite d–level state by defining $|\alpha_0^A\rangle \equiv |\alpha_1\rangle...|\alpha_m\rangle$, $|\beta_0^B\rangle \equiv |\alpha_{m+1}\rangle...|\alpha_n\rangle$, $|\alpha_1^A\rangle \equiv |\beta_1\rangle...|\beta_m\rangle$, $|\beta_1^B\rangle \equiv |\beta_{m+1}\rangle...|\alpha_n\rangle$,... $|\alpha_{d-1}^A\rangle \equiv |\gamma_1\rangle...|\gamma_m\rangle$, $|\beta_{d-1}^B\rangle \equiv |\gamma_{m+1}\rangle...|\gamma_n\rangle$. With this description general form of multi-qudit CS can rewritten as

$$|\Psi_d^n\rangle = \sum_{i=0}^{d-1} \mu_i|\alpha_i^A\rangle|\beta_i^B\rangle. \tag{4.37}$$

Similar to previous cases, we would like to represent this state in orthogonal qudit state basis $\{|e_0\rangle, |e_2\rangle, ...|e_{d-1}\rangle\}$, for first and $\{|f_0\rangle, |f_2\rangle, ...|f_{d-1}\rangle\}$, for second partition, respectively. Thus we write both subsystems in orthogonal bases. To this end, we have a set of nonorthogonal basis $\{|\alpha_0^A\rangle, |\alpha_1^A\rangle, ..., |\alpha_{d-1}^A\rangle\}$ describing subsystem A, and $\{|\beta_0^B\rangle, |\beta_1^B\rangle, ..., |\beta_{d-1}^B\rangle\}$ describing subsystem B. We introduce the following change of basis to the subspace A

$$|e_k\rangle \equiv \frac{|\alpha_k^A\rangle - \sum_{i=0}^{k-1}\langle e_i|\alpha_k^A\rangle|e_i\rangle}{||\ |\alpha_k^A\rangle - \sum_{i=0}^{k-1}\langle e_i|\alpha_k^A\rangle|e_i\rangle\ ||} = \frac{|\alpha_k^A\rangle - \sum_{i=0}^{k-1}\langle e_i|\alpha_k^A\rangle|e_i\rangle}{N_k}. \tag{4.38}$$

Where, $|e_0\rangle \equiv |\alpha_0^A\rangle$, and $||.||$ gives the norm of a vector. One may check that these basis make complete orthonormal basis; e.i. $\langle e_i|e_j\rangle = \delta_{ij}$. With this definition we can expand coherent states

in orthogonal basis

$$|\alpha_k^A\rangle = N_k|e_k\rangle + \sum_{i=0}^{k-1}\langle e_i|\alpha_k^A\rangle|e_i\rangle.$$

Similarly, for the subspace B we have

$$|f_k\rangle = \frac{|\beta_k^B\rangle - \sum_{i=0}^{k-1}\langle f_i|\beta_k^B\rangle|f_i\rangle}{||\ |\beta_k^B\rangle - \sum_{i=0}^{k-1}\langle f_i|\beta_k^B\rangle|f_i\rangle\ ||} = \frac{|\beta_k^B\rangle - \sum_{i=0}^{k-1}\langle f_i|\beta_k^B\rangle|f_i\rangle}{M_k}. \tag{4.39}$$

Where, $|f_0\rangle \equiv |\beta_0^B\rangle$.

With this extension, we can map the generalized multiqudit nonrthogonal states to orthogonal superposition via proper encoding of the information in orthonormal bases. This provides a platform for the extension of the study of this work to a generalized setting in higher dimensions.

4.7 The general case of multiqutrit states

Here, we extend our analysis to n-mode qutrit states with arbitrary n. To this end, we consider the first k modes of a state $|\Psi\rangle$ as the first partition and the remaining $n-k$ modes as the second partition:

$$|\Psi\rangle = \mu \underbrace{|\alpha_1\rangle...|\alpha_k\rangle}_{k}\underbrace{|\beta_1\rangle...|\beta_{n-k}\rangle}_{n-k} + \lambda|\alpha_{k+1}\rangle...|\alpha_{2k}\rangle|\beta_{n-k+1}\rangle...|\beta_{2(n-k)}\rangle$$
$$+\nu|\alpha_{2k+1}\rangle...|\alpha_{3k}\rangle|\beta_{2(n-k)+1}\rangle...|\beta_{3(n-k)}\rangle.$$

We introduce a standard orthogonal qutrit basis $\{|\mathbf{0}\rangle, |\mathbf{1}\rangle, |\mathbf{2}\rangle\}$, encoded through the first partition of $|\Psi\rangle$ as

$$|\mathbf{0}\rangle = |\alpha_1\rangle...|\alpha_k\rangle, \quad |\mathbf{1}\rangle = \frac{|\alpha_{k+1}\rangle...|\alpha_{2k}\rangle - \prod_{i=1}^{k} p_{i,k+i}|\alpha_1\rangle...|\alpha_k\rangle}{N_1},$$

$$|\mathbf{2}\rangle = \frac{(\prod_{i=1}^{k} p_{i,k+i}\prod_{i=1}^{k} p_{k+i,2k+i} - \prod_{i=1}^{k} p_{i,2k+i})|\alpha_1\rangle...|\alpha_k\rangle}{NN_1},$$

$$+(\prod_{i=1}^{k}\bar{p}_{i,k+i}\prod_{i=1}^{k} p_{i,2k+i} - p_{k+i,2k+i})|\alpha_{k+1}\rangle...|\alpha_{2k}\rangle + N_1^2|\alpha_{2k+1}\rangle...|\alpha_{3k}\rangle$$

where

$$p_{i,j} = \langle \alpha_i | \alpha_j \rangle, \quad N_1 = \sqrt{1 - |\prod_{i=1}^{k} p_{i,k+i}|^2},$$

$$N_2 = \sqrt{1 - |\prod_{i=1}^{k} p_{i,2k+i}|^2}, \quad N_3 = \sqrt{1 - |\prod_{i=1}^{k} p_{k+i,2k+i}|^2}$$

$$N = [1 - |\prod_{i=1}^{k} p_{i,k+i}|^2 - |\prod_{i=1}^{k} p_{i,2k+i}|^2 - |\prod_{i=1}^{k} p_{k+i,2k+i}|^2 + \prod_{i=1}^{k} p_{i,k+i} \prod_{i=1}^{k} \bar{p}_{i,2k+i} \prod_{i=1}^{k} p_{k+i,2k+i} + \prod_{i=1}^{k} \bar{p}_{i,k+i} \prod_{i=1}^{k} p_{i,2k+i} \prod_{i=1}^{k} \bar{p}_{k+i,2k+i}]^{\frac{1}{2}}.$$

A qutrit logic basis $\{|\tilde{\mathbf{0}}\rangle, |\tilde{\mathbf{1}}\rangle, |\tilde{\mathbf{2}}\rangle\}$ is encoded through the second partition of $|\Psi\rangle$ as

$$\{|\tilde{\mathbf{0}}\rangle = |\beta_1\rangle ... |\beta_{n-k}\rangle,$$

$$|\tilde{\mathbf{1}}\rangle = \frac{|\beta_{n-k+1}\rangle ... |\beta_{2(n-k)}\rangle - \prod_{i=1}^{(n-k)} q_{i,(n-k)+i} |\beta_1\rangle ... |\beta_k\rangle}{M_1},$$

$$|\tilde{\mathbf{2}}\rangle = \frac{(\prod_{i=1}^{(n-k)} q_{i,n-k+i} \prod_{i=1}^{(n-k)} q_{n-k+i,2(n-k)+i} - \prod_{i=1}^{(n-k)} q_{i,2(n-k)+i}) |\beta_1\rangle ... |\beta_k\rangle}{M M_1}$$

$$+ \frac{(\prod_{i=1}^{(n-k)} \bar{q}_{i,n-k+i} \prod_{i=1}^{k} q_{i,2n-k+i} - \prod_{i=1}^{(n-k)} q_{n-k+i,2k+i}) |\beta_{n-k+1}\rangle ... |\beta_{2(n-k)}\rangle}{M M_1},$$

$$+ \frac{N_1^2 |\beta_{2(n-k)+1}\rangle ... |\beta_{3(n-k)}\rangle}{M M_1}$$

where $q_{i,j} = \langle \beta_i | \beta_j \rangle$, and

$$M_1 = \sqrt{1 - |\prod_{i=1}^{(n-k)} q_{i,n-k+i}|^2},$$

$$M_2 = \sqrt{1 - |\prod_{i=1}^{(n-k)} q_{i,2(n-k)+i}|^2},$$

$$M_3 = \sqrt{1 - |\prod_{i=1}^{(n-k)} q_{n-k+i,2(n-k)+i}|^2},$$

$$M = [1 - |\prod_{i=1}^{(n-k)} q_{i,n-k+i}|^2 - |\prod_{i=1}^{(n-k)} q_{i,2(n-k)+i}|^2 - |\prod_{i=1}^{(n-k)} q_{k+i,2(n-k)+i}|^2$$

$$+ \prod_{i=1}^{(n-k)} q_{i,n-k+i} \prod_{i=1}^{(n-k)} \bar{q}_{i,2(n-k)+i} \prod_{i=1}^{k} q_{n-k+i,2(n-k)+i}$$

$$+ \prod_{i=1}^{(n-k)} \bar{q}_{i,(n-k)+i} \prod_{i=1}^{(n-k)} q_{i,2(n-k)+i} \prod_{i=1}^{(} n-k) \bar{q}_{n-k+i,2(n-k)+i}]^{\frac{1}{2}}.$$

The state $|\Psi\rangle$ can thus be represented as

$$|\Psi\rangle = (\mu + \lambda \prod_{i=1}^{(n-k)} q_{i,n-k+i} \prod_{i=1}^{k} p_{i,k+i} + \nu \prod_{i=1}^{(n-k)} q_{i,2(n-k)+i} \prod_{i=1}^{k} p_{i,2k+i})|0\tilde{0}\rangle$$

$$+(\frac{\nu}{M_1} \prod_{i=1}^{k} p_{i,2k+i}(\prod_{i=1}^{(n-k)} q_{n-k+i,2(n-k)+i} - \prod_{i=1}^{(n-k)} \bar{q}_{i,n-k+i} \prod_{i=1}^{(n-k)} q_{i,2(n-k)+i}) + \lambda M_1 \prod_{i=1}^{k} p_{i,k+i})|0\tilde{1}\rangle$$

$$+(\frac{\nu}{N_1} \prod_{i=1}^{(n-k)} q_{i,2(n-k)+i}(\prod_{i=1}^{k} p_{k+i,2k+i} - \prod_{i=1}^{k} \bar{p}_{i,k+i} \prod_{i=1}^{k} p_{i,2k+i}) + \lambda N_1 \prod_{i=1}^{(n-k)} q_{i,n-k+i})|1\tilde{0}\rangle$$

$$+(\nu \frac{(\prod_{i=1}^{k} p_{k+i,2k+i} - \prod_{i=1}^{k} \bar{p}_{i,k+i} \prod_{i=1}^{k} p_{i,2k+i})}{N_1}$$

$$\times \frac{(\prod_{i=1}^{(n-k)} q_{n-k+i,2(n-k)+i} - \prod_{i=1}^{(n-k)} \bar{q}_{i,n-k+i} \prod_{i=1}^{(n-k)} q_{i,2(n-k)+i})}{M_1}$$

$$+\lambda N_1 M_1)|1\tilde{1}\rangle + \nu \prod_{i=1}^{k} p_{i,2k+i} \frac{M}{M_1}|0\tilde{2}\rangle + \nu \prod_{i=1}^{(n-k)} q_{i,2(n-k)+i} \frac{N}{N_1}|2\tilde{0}\rangle$$

$$+(\nu \frac{\prod_{i=1}^{k} p_{k+i,2k+i} - \prod_{i=1}^{k} \bar{p}_{i,k+i} \prod_{i=1}^{k} p_{i,2k+i}}{N_1} \frac{M}{M_1})|1\tilde{2}\rangle$$

$$+ \nu \frac{\prod_{i=1}^{(n-k)} q_{n-k+i,2(n-k)+i} - \prod_{i=1}^{(n-k)} \bar{q}_{i,n-k+i} \prod_{i=1}^{(n-k)} q_{i,2(n-k)+i}}{M_1} \frac{N}{N_1}|2\tilde{1}\rangle + \nu \frac{N}{N_1} \frac{M}{M_1}|2\tilde{2}\rangle. \quad (4.40)$$

With the same algebra as in the case of a two-qutrit nonorthogonal state considered above, we find

that the linear entropy of the generalized multiqutrit state is given by

$$I_{lin} = \frac{2d}{d-1}\frac{\Delta_1^n + 2(\Delta_2^n + \Delta_3^n + \Delta_4^n)}{\mathcal{N}_n^2},$$

where

$$\Delta_1^n \equiv |\mu\lambda|^2 {M_1}^2 {N_1}^2 + |\mu\nu|^2 {M_2}^2 {N_2}^2 + |\lambda\nu|^2 {M_3}^2 {N_3}^2$$

$$\Delta_2^n \equiv |\mu|^2 \mathrm{Re}[\bar{\lambda}\nu(\prod_{i=1}^{(n-k)} \bar{q}_{i,n-k+i} \prod_{i=1}^{(n-k)} q_{i,2(n-k)+i} - \prod_{i=1}^{(n-k)} q_{n-k+i,2(n-k)+i})(\prod_{i=1}^{k} \bar{p}_{i,k+i} \prod_{i=1}^{k} p_{i,2k+i} - \prod_{i=1}^{k} p_{k+i,2k+i})]$$

$$\Delta_3^n \equiv |\lambda|^2 \mathrm{Re}[\bar{\mu}\nu(\prod_{i=1}^{(n-k)} \bar{q}_{i,n-k+i} \prod_{i=1}^{(n-k)} q_{n-k+i,2(n-k)+i} - \prod_{i=1}^{(n-k)} q_{i,2(n-k)+i})(\prod_{i=1}^{k} \bar{p}_{i,k+i} \prod_{i=1}^{k} p_{k+i,2k+i} - \prod_{i=1}^{k} p_{i,2k+i})]$$

$$\Delta_4^n \equiv |\nu|^2 \mathrm{Re}[\bar{\mu}\lambda(\prod_{i=1}^{(n-k)} \bar{q}_{n-k+i,2(n-k)+i} \prod_{i=1}^{(n-k)} q_{i,2(n-k)+i} - \prod_{i=1}^{(n-k)} q_{i,n-k+i})(\prod_{i=1}^{k} \bar{p}_{k+i,2k+i} \prod_{i=1}^{k} p_{i,2k+i} - \prod_{i=1}^{k} p_{i,k+i})]$$

$$\mathcal{N}_n \equiv |\mu|^2 + |\lambda|^2 + |\nu|^2 + 2Re[\bar{\mu}\lambda \prod_{i=1}^{(n-k)} q_{i,n-k+i} \prod_{i=1}^{k} p_{i,k+i} + \bar{\mu}\nu \prod_{i=1}^{(n-k)} q_{i,2(n-k)+i} \prod_{i=1}^{k} p_{i,2k+i} + \bar{\lambda}\nu \prod_{i=1}^{(n-k)} q_{n-k+i,2(n-k)+i} \prod_{i=1}^{k} p_{k+i,2k+i}]$$

5. PERFECT SWAP AND TRANSFER OF ARBITRARY QUANTUM STATES

5.1 Introduction

Faithful quantum state swapping and transferring is an indispensable element of salable quantum information and quantum communication processes. In fact, in most of quantum technologies the need for transferring a quantum state to different element of a quantum network is inevitable. Therefore, developing reliable of quantum architecture which can enable high fidelity swap and transfer of quantum information is a pivotal task for quantum technologies.

In realistic scenario of quantum state swapping, if the ith subsystem of a quantum network is prepared in state $|\Psi\rangle$ and the the jth subsystem in the state $|\Phi\rangle$, after swapping the quantum states, the first subsystem should end up in the final states $|\Phi\rangle$ and the second subsystem in the $|\Psi\rangle$. In most of quantum state swapping protocols, however, the final states are not swapped faithfully. One main restriction can be traced to the role of decoherence on the states that are being swapped. However, even when the decoherence is not taken into account, the faithful swapping of two unknown quantum states is not a trivial task. In fact, after the protocol is carried out on the system, the final states does not necessarily are the same as the input states.

In this chapter, we find a physically feasible unitary transformation that can swap any given quantum state such that for any given pair of quantum states $|\psi_1\rangle$ $|\psi_2\rangle$, the faithful transformation $|\psi_1\rangle \otimes |\psi_2\rangle \rightarrow |\psi_2\rangle \otimes |\psi_1\rangle$ can be obtained. As we demonstrate, a resonator–qubit system consisting of three resonators and two qubits enable a perfect swap of two unknown quantum states between two of the resonators, providing an experimentally feasible mechanism for universal swap operation in photonics systems. The architecture can faithfully transfer an unknown quantum state from one of the resonators to the other, proving a universal swap operation in Hilbert spaces of any dimensions for the photonic system.

5.2 Swap and transfer of quantum states between resonators

We consider a system of three quantum resonators that interact with two two-level systems (see Fig. 5.1). The Hamiltonian can be given as $H = H_0 + H_1$, such that

$$H_0 = \hbar \sum_{i=1}^{3} \omega_i a_i^\dagger a_i + \hbar \frac{\omega_0}{2} \sigma_{z1} + \hbar \frac{\omega_0}{2} \sigma_{z2}, \tag{5.1}$$

is the free Hamiltonian of our system, while $a_i^\dagger$, and a_i are the raising and the lowering operators associated to the ith resonator. $\sigma_{z1} = |e\rangle_1\langle e| - |g\rangle_1\langle g|$ and $\sigma_{z2} = |e\rangle_2\langle e| - |g\rangle_2\langle g|$ provide the z-component of the Pauli operators of the qubit 1 and 2, respectively. Furthermore, ω_i is the frequency of the ith cavity, and ω_0 is the frequency of the two-level system, respectively. Furthermore, the interaction Hamiltonian of the system can be written as

$$H_1 = \hbar g_1 \sigma_1^+ (a_1 + a_2) + h.c + \hbar g_2 \sigma_2^+ (a_1 + a_3) + h.c., \tag{5.2}$$

in which, σ_1^+ and σ_2^+ are the raising Pauli operators of the atoms 1 and 2 respectively. g_1 and g_2 are the coupling coefficients among the qubits and the interacting resonators. We assume a scenario where the resonators are periodically modulated such that $\omega_j = \omega_0 + \delta \sin(\nu t + \varphi_j)$. This periodic modulation can experimentally be achieved in superconducting circuits. By choosing ν and δ, so that $\omega_0 \gg \zeta = \delta/\nu$, we apply the rotating-wave approximation (RWA) to degenerate the Hamiltonian of the system to

$$\begin{aligned} \mathcal{H}_I = \hbar g_1 (\sigma_1^+ (\hat{a}_1 + \hat{a}_2) e^{i\zeta \cos(\nu t + \varphi_1)}) + h.c. \\ + \hbar g_2 (\sigma_2^+ (\hat{a}_1 + \hat{a}_3) e^{i\zeta \cos(\nu t + \varphi_2)}) + h.c. \end{aligned}$$

Using the previously introduced identity identity $e^{i\zeta \cos(\nu t + \varphi_j)} = \sum_{n=-\infty}^{\infty} J_n(\zeta) e^{in(\nu t + \varphi_j)}$, with $J_n(\zeta)$ being the nth-order Bessel function of the first kind, the Hamiltonian could be reduced to a Floquet Hamiltonian. Hence, the Hamiltonian can be expressed as $\mathcal{H}_I = \mathcal{H}_0 + \sum_{n=1}^{\infty} \mathcal{H}_n e^{in\nu t}$,

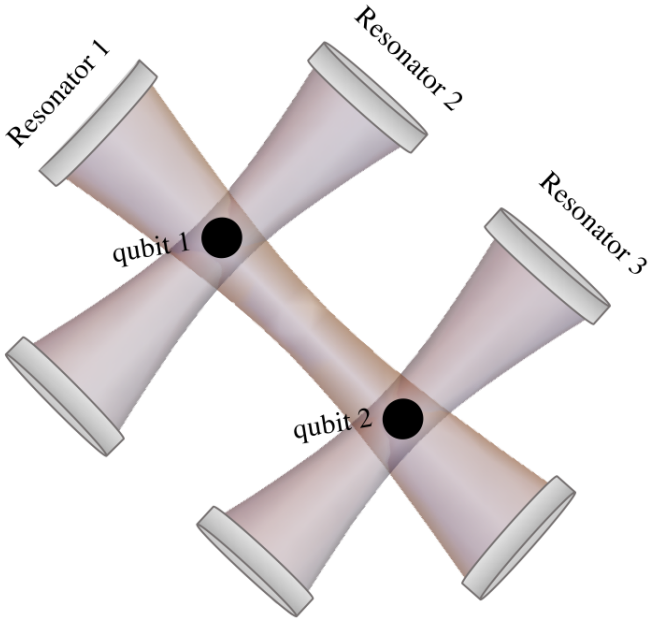

Figure 5.1: The architecture of quantum swapping scheme. Three resonators interact with two qubits. The quantum state transferring and swapping is performed between the second and the third resonators.

where

$$\mathcal{H}_0 = \hbar g_1 J_0(\zeta)[\sigma_1^+(\hat{a}_1 + \hat{a}_2) + (\hat{a}_1^\dagger + \hat{a}_2^\dagger)\sigma_1^-]$$
$$+\hbar g_2 J_0(\zeta)[\sigma_2^+(\hat{a}_1 + \hat{a}_3) + (\hat{a}_1^\dagger + \hat{a}_3^\dagger)\sigma_2^-].$$

and

$$\mathcal{H}_n = \hbar g_1 \sum_{j=1,2} i^n J_n(\zeta)(\sigma_1^+ \hat{a}_j + (-1)^n \hat{a}_j^\dagger \sigma_1^-) e^{in\varphi_j}$$
$$+\hbar g_2 \sum_{j=1,3} i^n J_n(\zeta)(\sigma_2^+ \hat{a}_j + (-1)^n \hat{a}_j^\dagger \sigma_2^-) e^{in\varphi_j}$$

This interaction Hamiltonian can be replaced by the effective Hamiltonian

$$\mathcal{H}_{\text{eff}} = \mathcal{H}_0 + \sum_{n=1}^{\infty} [\mathcal{H}_n, \mathcal{H}_{-n}]/(n\hbar\nu)$$

as

$$\mathcal{H}_{\text{eff}} = \mathcal{H}_0 - i\hbar k_1 \sigma_{z1}(\hat{a}_2^\dagger \hat{a}_1 - \hat{a}_1^\dagger \hat{a}_2) - i\hbar k_2 \sigma_{z2}(\hat{a}_3^\dagger \hat{a}_1 - \hat{a}_1^\dagger \hat{a}_3). \tag{5.3}$$

Where, $k_1 = g_1^2 \chi_2/\nu$ and $k_2 = g_2^2 \chi_3/\nu$ are the coupling coefficients with

$$\chi_2 = \sum_{n=1}^{\infty} 2J_n(\zeta)^2 \sin(n(\varphi_1 - \varphi_2))/n,$$

and

$$\chi_3 = \sum_{n=1}^{\infty} 2J_n(\zeta)^2 \sin(n(\varphi_1 - \varphi_3))/n.$$

Setting $\zeta = 2.40$ ($J_0(2.40) = 0$) and $\varphi_2 \neq \varphi_1$ we find the effective interaction Hamiltonian

$$\mathcal{H}_{\text{eff}} = -i\hbar k_1 \sigma_{z1}(\hat{a}_2^\dagger \hat{a}_1 - \hat{a}_1^\dagger \hat{a}_2) - i\hbar k_2 \sigma_{z2}(\hat{a}_3^\dagger \hat{a}_1 - \hat{a}_1^\dagger \hat{a}_3). \tag{5.4}$$

We note that when $\zeta = 2.40$, if we choose the phase difference $\varphi_1 - \varphi_2 = -\pi/3 = -(\varphi_1 - \varphi_3)$,

we have $\chi_3 = -\chi_2 \simeq 0.628$. We are going to consider the same coupling coefficients which results in $k_1 = -k = -k_2$.

The evolution of the wave function $|\psi(0)\rangle$ of this scheme could be attained by applying the time evolution operator $U(t) = e^{-i\mathcal{H}_{\text{eff}}t/\hbar}$ to the initial state $|\psi(0)\rangle$. We assume the qubits to be kept in their ground states $|\Psi\rangle_{12} = |g\rangle|g\rangle$ during the dynamics of the entire systems. This means that the resonators are passively coupled, due to the presence of the atoms, and the atom subspaces are decoupled from the resonators.

To show an example of the quantum state transfer, let us consider the first and the third resonators prepared in their ground states, while the second resonator containing n photons. Therefore, the cavities are prepared in the state $|\Psi\rangle_R = |0\rangle|n\rangle|0\rangle$. The dynamics of the initial state is given by

$$|\Psi(t)\rangle_R \otimes |\Psi\rangle_{12} = e^{-i\mathcal{H}_{\text{eff}}t/\hbar}|\Psi(0)\rangle_R \otimes |\Psi\rangle_{12}.$$

The qubit subspace will be separable from the resonator, and their states will remain unchanged. hence, once can focus on the resonators subspace which gives

$$|\Psi(t)\rangle_R = \sum_{i=0}^{n}\sum_{j=0}^{n-i}\left(\frac{n!}{(n-i-j)!i!j!}\right)^{1/2}(\frac{-1}{\sqrt{2}}\sin(\sqrt{2}kt))^{(n-i-j)} \tag{5.5}$$

$$\times(\frac{1}{2}[1+\cos(\sqrt{2}kt))])^i(\frac{1}{2}[1-\cos(\sqrt{2}kt))])^j|n-i-j,i,j\rangle_R \tag{5.6}$$

Interestingly, for the case $\sqrt{2}kt = \pi$ the quantum state of the cavities reduces to $|\Psi\rangle_R = |0\rangle|0\rangle|n\rangle$, which means that all of the photons are transferred from the second cavity to the third one, i.e., $|n\rangle_2|0\rangle_3 \rightarrow |0\rangle_2|n\rangle_3$.

As a matter of fact, taking the qubits in their ground states, one can focus on the Hilbert space of the resonators with the Hamiltonian

$$H_{\text{eff}} = -i\hbar k(\hat{a}_2^\dagger\hat{a}_1 - \hat{a}_1^\dagger\hat{a}_2) + i\hbar k(\hat{a}_3^\dagger\hat{a}_1 - \hat{a}_1^\dagger\hat{a}_3). \tag{5.7}$$

By considering the dynamics of the operators with the unitary evolution $U(t) = e^{-iH_{\text{eff}}t/\hbar}$, once

can obtain the time dependence of the operators. For the time passage T given by $T = \pi/\sqrt{2}k$, we attain the transformation $\hat{a}_2(0) \rightarrow \hat{a}_3(T)$ and $\hat{a}_3(0) \rightarrow \hat{a}_2(T)$, i.e., the operator of the second cavity mode at initial time $t = 0$ is mapped to the third cavity mode operator at final time $t = T$. This transformation shows that the states prepared in these two resonators could be swapped after the time passage with the time interval T, so that that we achieve the transformation

$$|\psi\rangle_2|\varphi\rangle_3 \rightarrow |\varphi\rangle_2|\psi\rangle_3.$$

To see this, we write the general form of the any photon state of the second cavity, having d_1 levels, as

$$|\psi\rangle = \sum_{n=0}^{d_1} b_n|n\rangle_2$$

and the quantum state of the third cavity, with d_2 levels, as

$$|\varphi\rangle = \sum_{m=0}^{d_2} c_m|m\rangle_3.$$

It is notable that d_1 and d_2 are arbitrary numbers, which dimension the states in the Fock bases. These numbers can be finite or infinite, in which the later corresponds to the infinite dimensional superposition of Fock bases. By considering the relation

$$|k\rangle_i = \sum_{j=0}^{k} \frac{(\hat{a}_i^\dagger)^j}{\sqrt{n!}}|0\rangle_i,$$

the initial state of the two cavities could be expressed as

$$|\psi\rangle|\varphi\rangle = \sum_{n}^{d_1}\sum_{m}^{d_2} \frac{b_n c_m}{\sqrt{n!m!}}(a^\dagger(0)_2)^n(a^\dagger(0)_3)^m|0\rangle_2|0\rangle_3. \tag{5.8}$$

Hence, after the time evolution $U(t) = e^{-iH_{\text{eff}}t/\hbar}$, for $t = T$, we have

$$|\psi\rangle|\varphi\rangle \to \sum_{n}^{d_1}\sum_{m}^{d_2} \frac{b_n c_m}{\sqrt{n!m!}} (a^\dagger(T)_2)^n (a^\dagger(T)_3)^m |0\rangle_2 |0\rangle_3$$
$$= \sum_{n}^{d_1}\sum_{m}^{d_2} \frac{b_n c_m}{\sqrt{n!m!}} (a^\dagger(0)_3)^n (a^\dagger(0)_2)^m |0\rangle_2 |0\rangle_3 = |\varphi\rangle|\psi\rangle.$$

Hence, an arbitrary photon state superposition of d_1 Fock bases, that is prepared initially in the second cavity can be swapped by an arbitrary photon superposition of d_2 Fock bases of the third cavity. This is true without any restriction on the state of the first cavity, that provides the swap operation for arbitrary quantum states.

To have a better insight into the dynamical properties of the scheme we can define the current operators for the photons. For the cavity j we define

$$I_j = \langle \partial_t n_j \rangle = I_{in} - I_{out}$$

where $n_j = \hat{a}_j^\dagger \hat{a}_j$, for $j = 1, 2, 3$. Since

$$\partial_t n_j = \frac{i}{\hbar}[\mathcal{H}_{\text{eff}}, n_j]$$

we attain the equations for the currents of photons in the cavities as

$$\partial_t n_1 = -\partial_t n_2 - \partial_t n_3, \tag{5.9}$$
$$\partial_t n_2 = k_1 \sigma_{z1} (\hat{a}_2^\dagger \hat{a}_1 + \hat{a}_1^\dagger \hat{a}_2), \tag{5.10}$$
$$\partial_t n_3 = k_2 \sigma_{z2} (\hat{a}_3^\dagger \hat{a}_1 + \hat{a}_1^\dagger \hat{a}_3). \tag{5.11}$$

Obviously,

$$I_1 + I_2 + I_3 = 0$$

which shows that the total photon number is constant in the system.

Starting with a single photon in the second cavity, i.e.,

$$|\Psi(0)\rangle_R = |0,1,0\rangle,$$

the currents can be obtained as

$$I_1 = \sin(2\sqrt{2}kt)$$

$$I_2 = -\frac{1}{\sqrt{2}}\sin(\sqrt{2}kt)[1+\cos(\sqrt{2}kt)]$$

and

$$I_3 = \frac{1}{\sqrt{2}}\sin(\sqrt{2}kt)[1-\cos(\sqrt{2}kt)].$$

We present the time evolution of the currents in the system in Fig. 5.2. The current of the second cavity starts from zero and reduces to below zero due to the fact that the current flows from the second cavity feeds into the other cavities. Hence, as is expected, the other cavities start from zero and attain positive currents. The minimum of the current I_2 could be seen at $\sqrt{2}kt = \pi/3$, in which the cavity has the maximum rate for the population loss. This maximum rate is $(I_2)_{min} = -\sqrt{27/32} \approx -0.92$. The first cavity has a large positive population change for small enough time t, where the third cavity starts slowly to gain population. At $\sqrt{2}kt = \pi/2$, the first cavity also starts to attain negative current that implies that it feeds photons to the other cavities. In the region $\sqrt{2}kt \in (\pi/2, \pi)$, the currents in cavities 1 and 2 are below zero and I_3 is above zero, indicating that the overall population gets fed into the third cavity. The first maximum of I_3 occurs at $\sqrt{2}kt = 2\pi/3$, in which the cavity has the maximum population gain rate that is given by $(I_3)_{max} = \sqrt{27/32} \approx 0.92$. The currents become zero at $\sqrt{2}kt = \pi$, in which the photons are all in the third cavity, and the other cavities are completely depleted.

Now, if we start with n photons in the second resonator having the state $|\Psi(0)\rangle_R = |0,n,0\rangle$,

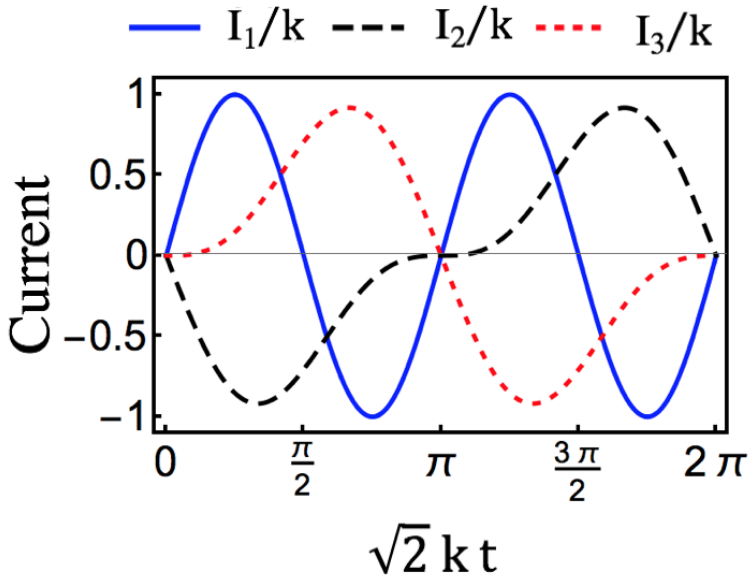

Figure 5.2: The photon currents of the resonators when a single photon is placed in the second resonator and the two other resonators have no photons. At $\sqrt{2}kt = \pi$, the single photon is transferred from the second resonator to the third one.

the current shall be given by

$$I_2 = 2\sum_{i=0}^{n}\sum_{j=0}^{n-i}\left(\frac{n!}{(n-i-j-1)!i!j!}\right)(\frac{-1}{\sqrt{2}}\sin(\sqrt{2}kt))^{2(n-i-j)-1} \tag{5.12}$$

$$\times(\frac{1}{2}[1+\cos(\sqrt{2}kt))])^{2i+1}(\frac{1}{2}[1-\cos(\sqrt{2}kt))])^{2j}, \tag{5.13}$$

which reduces to

$$I_2 = -n\frac{k}{\sqrt{2}}\sin(\sqrt{2}kt)[1+\cos(\sqrt{2}kt)].$$

Interestingly, this current is n times of the current of a single photon. Similarly, the currents of the other cavities provide

$$I_3 = n\frac{1}{\sqrt{2}}\sin(\sqrt{2}kt)[1-\cos(\sqrt{2}kt)]$$

and

$$I_1 = n\sin(2\sqrt{2}kt).$$

Having the current of the n photon Fock state input attained, we can consider current of various quantum states. To this aim, let us consider the coherent state transfer procedure and find the currents flow in the scheme. Hence, starting from the input state $|\Psi(0)\rangle_R = |0, \alpha, 0\rangle$, at $t = T$, the coherent state will transfer to the third cavity, i.e., $|\Psi(T)\rangle_R = |0, 0, \alpha\rangle$. For a coherent state we have

$$I_2 = -2k \exp[-|\alpha|^2] \sum_{n=0}^{\infty} \sum_{i=0}^{n} \sum_{j=0}^{n-i} \frac{|\alpha|^{2n}}{n!} \left(\frac{n!}{(n-i-j-1)!i!j!} \right) (\frac{1}{\sqrt{2}} \sin(\sqrt{2}kt))^{2(n-i-j)-1} \times (\frac{1}{2}[1 + \cos(\sqrt{2}kt))])^{2i+1} (\frac{1}{2}[1 - \cos(\sqrt{2}kt))])^{2j}, \quad (5.14)$$

which reduces to

$$I_2 = -|\alpha|^2 \frac{k}{\sqrt{2}} \sin(\sqrt{2}kt)[1 + \cos(\sqrt{2}kt)].$$

Similarly,

$$I_3 = |\alpha|^2 \frac{k}{\sqrt{2}} \sin(\sqrt{2}kt)[1 - \cos(\sqrt{2}kt)]$$

and

$$I_1 = |\alpha|^2 k \sin(2\sqrt{2}kt).$$

Interestingly, since the value $\bar{n} = |\alpha|^2$ is the average photon number in the coherent state, I_2 takes a similar form as the Fock state that could be written as

$$I_2 = -\bar{n} \frac{k}{\sqrt{2}} \sin(\sqrt{2}kt)[1 + \cos(\sqrt{2}kt)].$$

Thus, the coherent state transfer can be attained by the current dynamics given in Fig. 5.2, where the photon average $|\alpha|^2$ is a overall coefficient.

In fact, for a general input state

$$|\Psi(0)\rangle_R = |0\rangle|\psi\rangle|0\rangle$$

with

$$|\psi\rangle = \sum_{i=0}^{N} c_i |i\rangle$$

the current of the second cavity reduces to

$$I_2 = -\bar{n}\frac{k}{\sqrt{2}}\sin(\sqrt{2}kt)[1+\cos(\sqrt{2}kt)]$$

with

$$\bar{n} = \langle\psi|n|\psi\rangle.$$

Similarly,

$$I_3 = \bar{n}\frac{k}{\sqrt{2}}\sin(\sqrt{2}kt)[1-\cos(\sqrt{2}kt)]$$

and

$$I_1 = \bar{n}k\sin(2\sqrt{2}kt).$$

We note that starting from the initial state in the third cavity will also result in a similar behavior because of the symmetry of the system. Hence, the physics provided here explains the current dynamics of any quantum state transferring in the system.

Now, we investigate a scenario in which the first cavity is populated while the two others are in their ground states. If the first cavity attains n photons and the other cavities have zero photons, i.e., $|\Psi(0)\rangle_R = |n,0,0\rangle$, one can obtain the time evolved state of the system as

$$|\Psi(t)\rangle_R = \sum_{i=0}^{n}\sum_{j=0}^{n-i}\left(\frac{n!}{(n-i-j)!i!j!}\right)^{1/2}(-1)^j \times (\frac{1}{\sqrt{2}}\sin(\sqrt{2}kt))^{i+j}(\cos(\sqrt{2}kt))^{n-i-j}|n-i-j,i,j\rangle_R. \quad (5.15)$$

In this case,

$$I_2 = I_3 = n\frac{k}{\sqrt{2}}\sin(2\sqrt{2}kt)$$

and

$$I_1 = -nk\sqrt{2}\sin(2\sqrt{2}kt).$$

Thus, the photons prepared in the first resonator feeds the second and third resonator with the same rate of population changes, as is evident from the symmetry of the system. The period of the current in the resonators is equal to π , in this case. The maximum current into the cavities is determined by

$$I_2 = I_3 = n\frac{k}{\sqrt{2}}$$

which is fulfilled at $t = 2T$.

Interestingly, for $n = 1$, i.e., $|\Psi(0)\rangle_R = |1, 0, 0\rangle$, the state evolves to the W state

$$|W\rangle = \frac{1}{\sqrt{3}}(|1, 0, 0\rangle + |0, 1, 0\rangle - |0, 0, 1\rangle),$$

when $\tan(\sqrt{2}kt) = 1/\sqrt{2}$.

For a general input state

$$|\Psi(0)\rangle_R = |0\rangle|\psi\rangle|0\rangle$$

with

$$|\psi\rangle = \sum_{i=0}^{N} c_i|i\rangle$$

$$I_2 = I_3 = \bar{n}\frac{k}{\sqrt{2}}\sin(2\sqrt{2}kt)$$

and

$$I_1 = -\bar{n}k\sqrt{2}\sin(2\sqrt{2}kt).$$

The equations imply that the positive flow of population from the first resonator to the others continues until $2\sqrt{2}kt = \pi$. At this point, the sign of the direction of the currents change as the population goes back to the first resonator. Thus, regardless of which resonator is populated at the

initial stage, the current of the first resonator is a periodic with $t = T$.

5.3 Experimental feasibility

Next, we analyze the experimental feasibility of the proposed photonic swapping system. The coupling strength between the qubit and the resonators can be in the order of hundreds of MHz. Specifically, taking the coupling constant $g = 2\pi \times 40$ MHz, with $\nu = 5\chi g$, we obtain $k = g^2\chi/\nu = 2\pi \times 8$ MHz, and for $g = 2\pi \times 200$, we obtain $k = 2\pi \times 40$ MHz, well above the decoherence rates of the resonators, where the rates of less than 1 MHz can be achieved with the current technologies. Thus, with $k = 2\pi \times 8$ MHz, the quantum swap operation time of the system can be $T = \pi/\sqrt{2}k \approx 44$ ns. Which is much shorter than the relaxation time of the resonators. Single photon lifetime of fixed frequency resonators can be in the order of milliseconds. Tunable resonators with kinetic inductance are shown to have a relaxation time as long as 6 μs. To minimize the decoherence resources in our system, both of the qubits can be considered in their ground states. Thus, the dephasing and relaxation of the qubits have no effects on our system. Note that one may choose the modulation parameters such that $k_1 = k_2$, and take one of the qubits in the ground state and the other one in its excited state to relax the condition $k_1\sigma_{z1} = -k_2\sigma_{z2} = -k$, for realizing the Hamiltonian in Eq. (6). However, with the conditions, the decoherence of the exited qubit can be relevant in the process.

The frequency modulation can be efficiently controlled similarly to the recent experiments, where the periodic dynamical modulation of the relevant parameters in quantum systems can be fulfilled.

To investigate the dynamics of the system subjected to the decoherence, we consider the pertinent master equation for the density operator $\hat{\rho}$,

$$\frac{\partial\hat{\rho}}{\partial t} = \sum_j \frac{\gamma_j}{2}(1+\bar{n}_{th})(2\hat{a}_j\hat{\rho}\hat{a}_j^\dagger - \hat{a_j}^\dagger\hat{a}_j\hat{\rho} - \hat{\rho}\hat{a}_j^\dagger\hat{a}_j) + \frac{\gamma_j}{2}\bar{n}_{th}(2\hat{a}_j^\dagger\hat{\rho}\hat{a}_j - \hat{a}_j\hat{a}_j^\dagger\hat{\rho} - \hat{\rho}\hat{a}_j\hat{a}_j^\dagger), \tag{5.16}$$

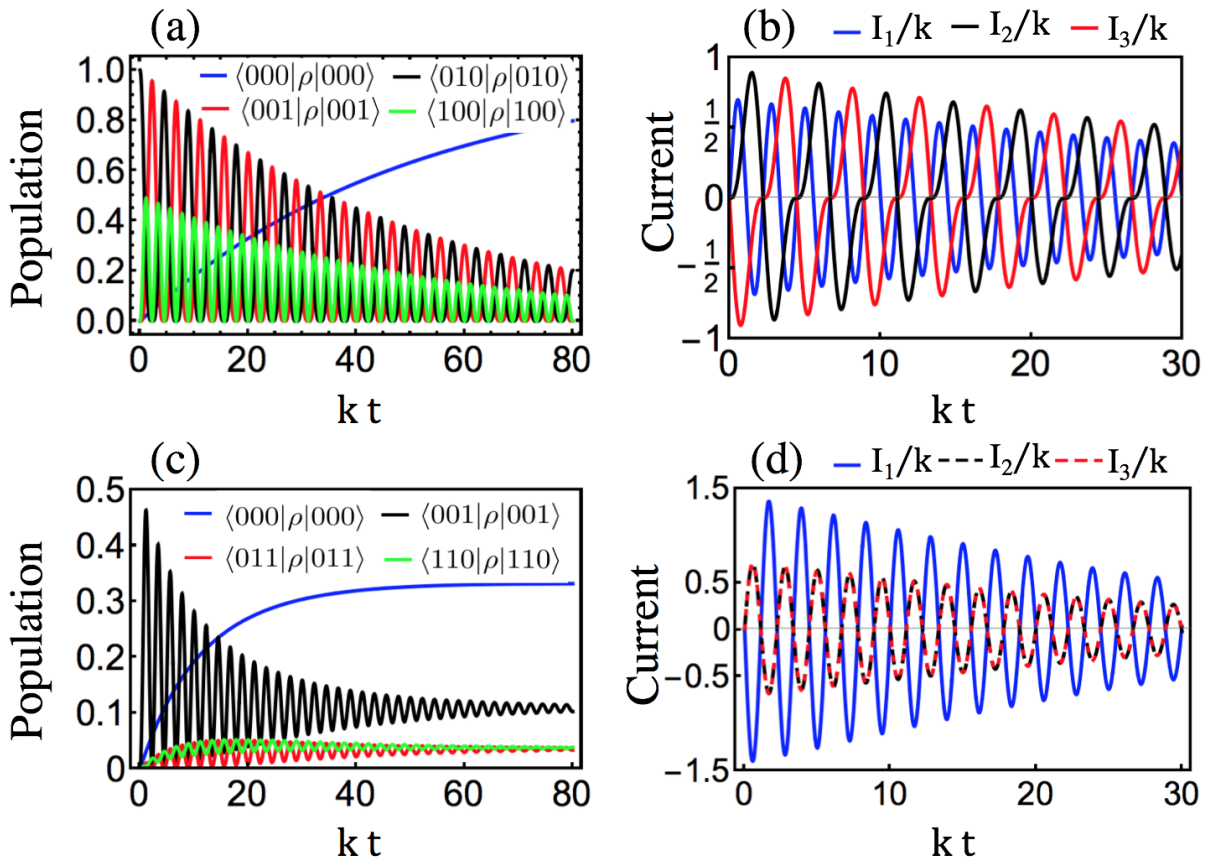

Figure 5.3: Quantum state trasfer in the presence of decoherence with the resonator decay rate $\gamma/k = 0.02$. (a,b) with $\bar{n}_{th} = 0.1$ and the initial state $|0,1,0\rangle$. (c,d) with $\bar{n}_{th} = 0.5$ and the initial state $|1,0,0\rangle$. (a,c) population of the density matrix elements, and (b,d) dynamics of the photon currents in the resonators.

where j = 1, 2,3, γ_i is the decoherence rate of the ith resonator, and $\bar{n}_{th} = [\exp(\hbar\omega/k_B\tau)-1]^{-1}$ is the thermal photon average at temperature τ with the frequency ω of the resonators. We consider the configuration of similar resonators with the same decoherence rate of γ.

The dynamics of the system, in the presence of damping in the resonators, is depicted in Fig. 5.3, where we have assumed the damping rate of $\gamma/k = 0.02$. This rate is quite feasible with the current technologies. Fig. 5.3(a)&(b) present the dynamical evolution of the single photon when transferred from the second resonator with the initial state $|0,1,0\rangle$ to the third resonator. As can be seen from Fig. 5.3 (a), the population of the second resonator drops from 1 as time increases from $t = 0$ until the photon is transferred to the third resonator at the $t = T$. The first resonator

is also gets populated in this process; however, it feeds its population to the third resonator at $t = T$. The increase in the density matrix element $\langle 0,0,0|\rho(t)|0,0,0\rangle$, demonstrates the buildup of the loss in the system. The target density matrix element $\langle 0,0,1|\rho(t)|0,0,1\rangle$, demonstrates the fidelity of the quantum state transfer to the third resonator. As Fig. 5.3 (a) demonstrates even with a relatively large ratio of the loss, the fidelity of the information transfer is about 94% at the first maxima, which demonstrates the robustness of our scheme to decoherence. Note that this fidelity can efficiently be improved by decreasing the thermal photon average $\bar{n}_{th}$ or using high finesse resonator with an ultrastrong coupling to the field, where a faithful quantum state transfer and be achieved. For instance, with $\gamma/k = 0.005$ and $\bar{n}_{th} = 0.01$, the fidelity of $\approx 99\%$ can be achieved. Fig. 5.3(b) demonstrates the currents in the resonators with the parameters the same as for Fig. 5.3(a). Accordingly, the currents still demonstrate periodic characteristics, except the amplitude of the currents decreases due to the loss in the resonators. For a sufficiently long time, all the currents approach zero as the system approaches its steady state. In Fig. 5.3(c)&(d), we have considered the thermal photon average $\bar{n}_{th} = 0.5$, when the single photon is prepared in the first resonator, with the initial state $|1,0,0\rangle$. In this scenario, the photon from the first resonator feeds the second and the third resonators with the same rate, thus, $\langle 0,0,1|\rho(t)|0,0,1\rangle = \langle 0,1,0|\rho(t)|0,1,0\rangle$. At a very long time scale, the system approaches the steady state, where the populations in the resonators approach to some fixed values. Fig. 5.3(d), demonstrates the current of the resonators with the parameters same as Fig. 5.3(c). Accordingly, the currents of the second and the third resonators are the same, when the population is prepared only in the first resonator. First, the current in the first resonator becomes negative as the population is fed to the other resonators, then it becomes zero where it has lost the maximum of its population and starts to gain populations from the other resonators beyond this point. This cyclic behavior is repeated as time increases, except the amplitudes of the currents decrease due to the loss in the resonators.

6. CONCLUSION AND OUTLOOK

Quantum entanglement is the cornerstone of various quantum technologies and is an indispensable ingredient of quantum information processing. These make the generation, characterization and quantification of entangled states very important in quantum information studies, beside all their fundamental importance. As a particular example of such applications one may consider quantum metrolgy, in which, quantum entanglement is shown to have a remarkable role for suppressing the classical limits. However, generation, characterization and quantification of desirable entangled states are not easy most of the times.

We introduced new deciplins for engineering multipartite entangled states that are shown to be useful for quantum information processing and quantum metrology applications. In particular, we introduced new methods which could be used for generating N00N states, as one of the most challenging states to generate, which enables realization of such states in both photonic and spintronic architectures. We outlined a rather generic quantum circuit, for the N00N state generation, that could be realized in various quantum systems. Furthermore, we extended this platform for the generation of states beyond the N00N state. Typical examples of such sates could be entangled coherent or squeezed states, for instance. Furthermore, we extended the protocol for the multimode scenario. Also, we demonstrated that attaining the ultimate sensitivity in phase estimation is not an exclusive property of the N00N states. As a result, we found a large class of entangled states that could provide us with the ultimate sensitivity achieved by the N00N state.

As a part of our investigations for the N00N state generation, we developed a new scheme where N00N states could be realized in two ensembles of nitrogen–vacancy centers in diamond. This could be interesting by noting the fact that NV centers in diamonds provide a remarkably long coherence time, even at the room temperature. This opens up new possibilities for protecting N00N states against decoherence.

Moreover, having the long coherence time of the ensembles of the NV centers, we showed that a hybrid quantum system consisting of three ensembles of NV centers coupled to a superconducting

device enables the generation of controllable macroscopic multipartite entangled states, which could be used as a building block for quantum networks.

Furthermore, we investigated entanglement of nonorthogonal states in details, and more spesifically, we derived a closed-form analytical expression for the entanglement degree of a multipartite qutrit state, offering a quantitative measure for entanglement within the class of n-mode nonorthogonal qutrit states with an arbitrary n.

Finally, we introduced a new configuration where any pair of quantum states can perfectly be swapped between two quantum resonators enabling a realization of a universal swap operation in photonics systems.

REFERENCES

[1] V. Vedral, *Introduction to quantum information science*. Oxford University Press on Demand, 2006.

[2] D. Petz, *Quantum Information Theory and Quantum Statistics*. Springer-Verlag Berlin Heidelberg, 2008.

[3] M.A. Nielsen and I. L. Chuang, *Quantum Computation and Quantum Information*. Cambridge University Press 2002.

[4] C. H. Bennett, G. Brassard, C. Crepeau, R. Jozsa, A. Peres, W. K. Wootters, "Teleporting an unknown quantum state via dual classical and Einstein-Podolsky-Rosen channels," Phys. Rev. Lett. **70**, 1895, 1993.

[5] C. H. Bennett, S. J. Wiesner, "Communication via one- and two-particle operators on Einstein-Podolsky-Rosen states," Phys. Rev. Lett. **69**, 2881 1992.

[6] A. K. Ekert, "Quantum cryptography based on Bells theorem," Phys. Rev. Lett. **67**, 661, 1991.

[7] S. Y. Lee, C. W. Lee, H. Nha, D. Kaszlikowski, Quantum phase estimation using a multi-headed cat state, J. Opt. Soc. Am. B, **32**, 1186-1192 (2015).

[8] T. D. Ladd, F. Jelezko, R. Laflamme, Y. Nakamura, C. Monroe, and J. L. OBrien, Quantum computers, Nature **464** 45-53 (2010).

[9] M. Hillery, M. S. Zubairy, Entanglement conditions for two-mode states: Applications, Phys. Rev. A, **74**, 032333 (2006).

[10] J. Li, G. Li, J. M. Wang, S. Y. Zhu, and T. C. Zhang, A comparison of two nonclassical measures, entanglement potential and the negativity of the Wigner function, J. Phys. B: At. Mol. Opt. Phys. **43**, 085504 (2010).

[11] V. Coffman, J. Kundu, W. K. Wootters, Distributed entanglement, Phys. Rev. A, **61**, 052306 (2000).

[12] S. J. Akhtarshenas, Concurrence vectors in arbitrary multipartite quantum systems, J. Phys. A: Math. Gen. **38**, 6777 (2005).

[13] W.K. Wootters, Entanglement of Formation of an Arbitrary State of Two Qubits, Phys. Rev. Lett. **80**, 2245 (1998).

[14] N. A. Peters, T. C. Wei, and P. G. Kwiat, Mixed-state sensitivity of several quantum-information benchmarks, Phys. Rev. A, **70**, 052309 (2004).

[15] S.P. Walborn, P.H. Souto Ribeiro, L. Davidovich, F. Mintert and A. Buchleitner, Experimental determination of entanglement with a single measurement, Nature **440**, 1022 (2006).

[16] O. Guhne and G. Toth, Entanglement detection, Phys. Rep. **474**, 1 (2009).

[17] R. Horodecki, P. Horodecki, M. Horodecki, and K. Horodecki, Quantum entanglement, Rev. Mod. Phys. **81** , 865 (2009).

[18] V. Giovannetti, S. Lloyd, and L. Maccone, Nature Photonic **5**, 222 (2011).

[19] P. R. Bevington and D. K. Robinson, Data Reduction and Error Analysis for the Physical Sciences (McGraw-Hill, New York, 2003).

[20] B. Sanders, Phys. Rev. A **40**, 2417 (1989).

[21] A. N. Boto , P. Kok, D. S. Abrams, S. L. Braunstein, C. P. Williams, J. P. Dowling, Phys. Rev. Lett. **85** 2733, (2000).

[22] Y. Maleki and A. M. Zheltikov, Laser Phys. Lett. **15** 056201 (2018).

[23] Y. Maleki, A. M. Zheltikov, "Generating maximally-path-entangled number states in two spin ensembles coupled to a superconducting flux qubit," Physical Review A, **97** 012312, 2018.

[24] P. Cappellaro, J. Emerson, N. Boulant, C. Ramanathan, S. Lloyd, and D. G. Cory, Phys. Rev. Lett. **94,** 020502 (2005).

[25] G. Y. Xiang, B. L. Higgins, D. W. Berry, H. M. Wiseman, G. J. Pryde, Nature Photonic **5**, 43-47 (2011).

[26] I. Afek, O. Ambar, and Y. Silberberg, Science **328**, 879 (2010).

[27] Z.-L. Xiang, S. Ashhab, J. Q. You, F. Nori, Rev. Mod. Physics, **85**, 623(2013).

[28] W. L. Yang, Y. Hu, Z. Q. Yin, Z. J. Deng, M. Feng, Phys. Rev. A **83**, 022302 (2011).

[29] Z.-L. Xiang, X.-Y. Lu, T. F. Li, J. Q. You, F. Nori, Phys. Rev. B **87**, 144516 (2013).

[30] V. Ranjan, G. de Lange, R. Schutjens, T. Debelhoir, J. P. Groen, D. Szombati, D. J. Thoen, T. M. Klapwijk, R. Hanson, and L. DiCarlo, "Probing Dynamics of an Electron-Spin Ensemble via a Superconducting Resonator," Phys. Rev. Lett. **110**, 067004 (2013).

[31] M. G. Raizen, R. J. Thompson, R. J. Brecha, H. J. Kimble, and H.J. Carmichael, "Normal-mode splitting and linewidth averaging for two-state atoms in an optical cavity," Phys. Rev. Lett. **63**, 240 (1989).

[32] B. P. Abbott et al., Phys. Rev. Lett. **116**, 061102 (2016).

[33] N. Bar-Gill, L.M. Pham, A. Jarmola, D. Budker, R.L. Walsworth, Nat. Commun. **4**, 1743 (2013).

[34] M. Reagor, W. Pfaff, C. Axline, R. W. Heeres, N. Ofek, K. Sliwa, E. Holland, C. Wang, J. Blumoff, K. Chou, M. J. Hatridge, L. Frunzio, M. H. Devoret, L. Jiang, R. J. Schoelkopf, Phys. Rev. B **94**, 014506 (2016).

[35] T. Liu, Q. -P. Su, S. -J. Xiong, J. -M. Liu, C. -P. Yang, F. Nori, Sci. Rep. **6**, 32004 (2016).

[36] H. Wang, M. Mariantoni, R. C. Bialczak, M. Lenander, E. Lucero, M. Neeley, A. D. O'Connell, D. Sank, M. Weides, J. Wenner, T. Yamamoto, Y. Yin, J. Zhao, J. M. Martinis, A. N. Cleland, Phys. Rev. Lett. **106**, 060401 (2011).

[37] Q. -P. Su, C. -P. Yang, S. -B. Zheng, Sci. Rep. **4**, 3898 (2014).

[38] D. Marcos, M. Wubs, J. M. Taylor, R. Aguado, M. D. Lukin, and A. S. Sørensen, Phys. Rev. Lett. **105**, 210501 (2010).

[39] X. Zhu, S. Saito, A. Kemp, K. Kakuyanagi, S. Karimoto, H. Nakano, W. J. Munro, Y. Tokura, M. S. Everitt, K. Nemoto, M. Kasu, N. Mizuochi, and K. Semba, Nature (London) 221-224 **478**,221 (2011).

[40] Y. Maleki, A. M. Zheltikov, "A high-N00N output of harmonically driven cavity QED," Scientific Reports, **9** 16780, 2019.

[41] Y. Maleki, A. M. Zheltikov, "Spin cat-state family for Heisenberg-limit metrology," JOSA B, **37** 1021–1026, 2020.

[42] L. Childress, M. V. G. Dutt, J. M. Taylor, A. S. Zibrov, F. Jelezko, J. Wrachtrup, P. R. Hemmer, and M. D. Lukin, Science **314**, 281 (2006).

[43] M. G. Dutt, L. Childress, L. Jiang, E. Togan, J. Maze, F. Jelezko, A. S. Zibrov, P. R. Hemmer, and M. D. Lukin, Science **316**, 1312 (2007).

[44] Da-Wei Wang, Han Cai, Ren-Bao Liu, Marlan O. Scully, Phys. Rev. Lett. 116, 220502 (2016) .

[45] D.-W. Wang, H. Cai, L. Yuan, S.-Y. Zhu, and R.-B. Liu, Optica **2**, 712 (2015).

[46] N. Goldman and J. Dalibard, Phys. Rev. X **4**, 031027 (2014).

[47] G. Jotzu, M. Messer, R. Desbuquois, M. Lebrat, T. Uehlinger, D. Greif, T. Esslinger, Nature **515**, 237 (2014).

[48] W. Song, Z. Yin, W. Yang, X. Zhu, F. Zhou, M. Feng, Sci. Rep. **5**, 7755 (2015).

[49] K. Hammerer, A. S. Søensen, E. S. Polzik, Rev. Mod. Phys. **82**, 1041 (2010).

[50] X. -Y. Lü, Z. -L. Xiang, W. Cui, J. Q. You, F. Nori, Phys. Rev. A **88** 012329 (2013).

[51] M. O. Scully and M. S. Zubairy, Quantum Optics (Cambridge University Press, Cambridge, 1997).

[52] G. S. Agarwal, Quantum Optics, Cambridge University Press (2013).

[53] J. Joo, W. J. Munro, and T. P. Spiller, Phys. Rev.Lett. **107**, 083601 (2011).

[54] W. K. Wootters, "Entanglement of Formation of an Arbitrary State of Two Qubits," Phys. Rev. Lett. **80**, 2245 (1998).

[55] Su, Q.P., Zhu, H.H., Yu, L., Zhang, Y., Xiong, S.J., Liu, J.M. and Yang, C.P., 2017. Generating double NOON states of photons in circuit QED. Physical Review A, 95(2), p.022339.

[56] B. C. Sanders and C. C. Gerry, Phys. Rev. A **90**, 045804 (2014).

[57] M. Al-Amri, M.O. Scully, and M.S. Zubairy, J. Phys. B **44**, 165509 (2013).

[58] Y. S. Kim, J.-C. Lee, O. Kwon, Y.-H. Kim, Nature Physics **8**, 117–120 (2012).

[59] Z. Liao, M. Al-Amri, and M.S. Zubairy, J. Phys. B **36**, 145501 (2013).

[60] X. Zeng, M. A.-Amri, S. Zhu, M. S. Zubairy, Phys. Rev. A, **93**, 053826 (2016).

[61] S.S. Esfahani, Z. Liao, and M.S. Zubairy, J. Phys. B **49**, 155501 (2016).

[62] A. H. Zeng, L. M. Kuang, Influence of quantum entanglement on quantum tunnelling between two atomic Bose–Einstein condensates, Phys. Lett. A **338**, 323 (2005).

[63] J. Huang, M. Zhuang, B. Lu, Y. Ke, C. Lee, Phys. Rev. A 98, 012129 (2018).

[64] Y Maleki, A. M. Zheltikov, Optics Express 26 (14), 17849-17858 (2018).

[65] Y Maleki, A. M. Zheltikov, "Macroscopic tripartite entanglement of nitrogen-vacancy centers in diamond coupled to a superconducting resonator," JOSA B 36 (2), 443-450 (2019).

[66] M. Horodecki, P. Horodecki, and R. Horodecki, "Separability of mixed states: necessary and sufficient conditions," Phys. Lett. A **223**, 1 (1996).

[67] N. Ganguly, S. Adhikari, A. S. Majumdar, and J. Chatterjee, "Entanglement Witness Operator for Quantum Teleportation", Phys. Rev. Lett. **107**, 270501 (2011).

[68] M. Barbieri, F. D. Martini, G. D. Nepi, P. Mataloni, G. M. DÁriano, and C. Macchiavello,"Detection of Entanglement with Polarized Photons: Experimental Realization of an Entanglement Witness," Phys. Rev. Lett. **91**, 227901 (2003).

[69] Yimin Liu, Jiabin You, and Qizhe Hou, "Entanglement dynamics of Nitrogen-vacancy centers spin ensembles coupled to a superconducting resonator," Sci. Rep. **6**, 21775 (2016).

[70] T. Astner, S. Nevlacsil, N. Peterschofsky, A. Angerer, S. Rotter, S. Putz, J. Schmiedmayer, and J. Majer, "Coherent Coupling of Remote Spin Ensembles via a Cavity Bus", Phys. Rev. Lett. **118**, 140502 (2017).

[71] B. Vlastakis, G. Kirchmair, Z. Leghtas, S. E. Nigg, L. Frunzio, S. M. Girvin, M. Mirrahimi, M. H. Devoret, and R. J. Schoelkopf, "Deterministically encoding quantum information using 100-photon schrödinger cat states," Science **342**, 607–610 (2013).

[72] A. Acin, D. Brus, M. Lewenstein, A. Sanpera, "Classification of Mixed Three-Qubit States," Phys. Rev. Lett. **87**, 040401 (2001).

[73] M. Bourennance, M. Eibl, C. Kurtsiefer, S. Gaertner, H. Weinfurter, O. Guhne, P. Hyllus, D. Brus, M. Lewenstein, and A. Sanpera, "Experimental Detection of Multipartite Entanglement using Witness Operators," Phys. Rev. Lett. **92**, 087902 (2004).

[74] Y. -C. Ou , H. Fan, "Monogamy inequality in terms of negativity for three-qubit states," Phys. Rev. A **75** 062308 (2007).

[75] R. J. Glauber, Coherent and Incoherent States of the Radiation Field, Phys. Rev. A, **131**, 2766 (1963).

[76] H. Fu, X. Wang, and A.I. Solomon, Maximal entanglement of nonorthogonal states: classification, Physics Letters A, **291**, 73-76 (2001).

[77] Y. Maleki, F. Khashami, Y. Mousavi, Entanglement of Three-Spin States in the Context of SU(2) Coherent States, Int. J. Theor. Phys. **54**, 210 (2015).

[78] L.Y. Hu and Z.M. Zhang, Statistical properties of coherent photon-added two-mode squeezed vacuum and its inseparability, J. Opt. Soc. Am. B, 30 , 518-519 (2011).

[79] G. Najarbashi, Y. Maleki, Maximal Entanglement of Two-Qubit States Constructed by Linearly Independent Coherent States, Int. J. Theor. Phys. **50**, 2601 (2011).

[80] Y. maleki, A. Maleki, Entangled multimode spin coherent states of trapped ions, JOSA B **35**, 1211–1217 (2018).

[81] Y. maleki, Generation and entanglement of multi-dimensional multi-mode coherent fields in cavity QED, Quantum Information Processing **15**, 4537–4562 (2016).

[82] Y. maleki, Entanglement and decoherence in two-dimensional coherent state superpositions, International Journal of Theoretical Physics **56**, 757–770 (2017).

[83] Y Maleki, B Ahansaz, Quantum correlations in qutrit-like superposition of spin coherent states, Laser Physics Letters **16**,075205 (2019).

[84] M. Paternostro, M. S. Kim, B. S. Ham, Generation of entangled coherent states via cross-phase-modulation in a double electromagnetically induced transparency regime, Phys. Rev. A,**67** 023811 (2003).

[85] S. Glancy, H. M. Vasconcelos, and T. C. Ralph, Transmission of optical coherent-state qubits, Phys. Rev. A, **70** 022317 (2004).

[86] S.J. van Enk and O. Hirota, Entangled coherent states: Teleportation and decoherence, Phys. Rev. A **64** 022313 (2001).

[87] M. Fujiwara et al., Exceeding the Classical Capacity Limit in a Quantum Optical Channel, Phys. Rev. Lett. **90**, 167906 (2003).

[88] W. Chuan, F.-G. Deng, Y.-S. Liu and G. L. Long, Quantum secure direct communication with high-dimension quantum superdense coding, Phys. Rev. A **71** 044305 (2005).

[89] N. K. Langford, et al., Measuring Entangled Qutrits and Their Use for Quantum Bit Commitment, Phys. Rev. Lett. **93**, 053601 (2004).

[90] D. Bruss and C. Macchiavello, Optimal Eavesdropping in Cryptography with Three-Dimensional Quantum States, Phys. Rev. Lett. **88** 127901 (2002).

[91] L. Sheridan and V. Scarani, Security proof for quantum key distribution using qudit systems, Phys. Rev. A **82** 030301 (2010).

[92] M. L. Almeida, S. Pironio, J. Barrett, G. Toth, and A. Acin, Noise Robustness of the Nonlocality of Entangled Quantum States, Phys. Rev. Lett. **99** 040403 (2007).

[93] S. Bose, K. Jacobs, and P. L. Knight, Preparation of nonclassical states in cavities with a moving mirror, Phys. Rev. A **56** 4175 (1997).

[94] Aspelmeyer, Markus and Kippenberg, Tobias J and Marquardt, Florian, Cavity optomechanics, Reviews of Modern Physics, **86**, 1391, (2014).

[95] J. D. Teufel, D. Li, M. S. Allman, K. Cicak, A. J. Sirois, J. D. Whittaker, and R. W. Simmonds, Nature (London) 471, 204 (2011).

[96] Y. Maleki, A. M. Zheltikov, "Linear entropy of multiqutrit nonorthogonal states," Optics express 27 (6), 8291-8307 (2019).

[97] M. H. Devoret, R. J. Schoelkopf, Superconducting Circuits for Quantum Information: An Outlook, Science **339**(6124), 1169-1174 (2013).